A THESIS

FOR THE DEGREE OF DOCTOR OF PHILOSOPHY

Printed Memristive Devices for Electrical Switching and Memory Applications

Muhammad Naeem Awais

Department of Mechatronics Engineering

GRADUATE SCHOOL

JEJU NATIONAL UNIVERSITY

August, 2013

Printed Memristive Devices for Electrical Switching and Memory Applications

Muhammad Naeem Awais

(Supervised by Professor Kyung Hyun Choi)

A thesis submitted in partial fulfillment of the requirement for the degree of Doctor of Philosophy

2013. 08

The thesis has been examined and approved.

Chul Ung Kang

Thesis director, Chul Ung Kang, Professor, Department of Mechatronics Engineering

Ki Rin Kwon

Ki Rin Kwon, Professor, Department of Mechanical Engineering

Jin Ho Bae

Jin Ho Bae, Professor, Department of Ocean System Engineering

Jeongdai Jo

Jeongdai Jo, Director, Korea Institute of Machinery & Materials

Kyung Hyun Choi, Professor, Department of Mechatronics Engineering

June 3, 2013

Date

Department of Mechatronics Engineering
GRADUATE SCHOOL
JEJU NATIONAL UNIVERSITY
REPUBLIC OF KOREA

To

My Parents and Family

Acknowledgements

Alhamdulillaah e Rabbil-aalameen. Wassalatu Wassalamu alaa Sayyad-il-Mursaleen. Amma baad fa-Aauzo Billaahi Minash Shaitaan Nir Rajim. Bismillaah Hir Rehman Nir Rahim.

I would like to present my humble gratitude to Almighty Allah Who bestow me courage and skill by virtue of Rasoolullah Hazrat Muhammad Sallahu alaihe wa-alahe wasalam to complete the doctoral studies with quite satisfaction and contentment.

The day I joined Advanced Micro-Mechatronics (AMM) Lab, I was nothing now the day I am leaving, I am feeling that I leant a lot during my stay in AMM Lab to start my career in research and technology and can exercise my potential for the welfare of mankind. This is all about the schooling of Prof. Kyung Hyun Choi who polished my skills with novel ideas and innovative thoughts. I would like to pay my heartiest thanks with best regards to Prof. Kyung Hyun Choi, who put his full efforts to give me confidence, access over all the resources in the laboratory and hire external resources as well to accomplish the task. During my Ph.D. studies Prof. Choi provided me shelter against all kind of crisis from morally depraved conditions to financial problems. I would also like to thank Prof. Jinho Bae who gave me valuable suggestions and ideas to pursue the fruitful end of my research work.

In my life, I think if there is any sort of good thing in me is because of my colleagues and friends. I would like to thanks my colleagues in AMM Lab and friends in the Jeju University as well. Few of the names are coming in my mind including Navaneethan, Maria, Adnan, Zubair, Kamran, Murtuza, Sridharan, Hyung Chan Kim, Jeong Beom Ko, Hyun Woo Dang, Jae Hee Park, Hu Kyun Chang, Shoaib, Zahid, Safdar, Rasheed, Farrukh, Jameel, Junaid, Shahid, and Waqar. I am also pleased to thanks my former colleagues who helped me a lot during their stay in AMM Lab and in the Jeju University as Dr. Ahsan, Dr. Khalid, Dr. Nauman, Dr. Ganesh, Saleem, and Arshid. I am especially grateful to Dr. Ahsan who introduced me to AMM Lab.

My whole world, my complete life and whatever you name it, is my family. I would love to present my tribute to my humble Father, loving Mother, Sister, Brothers, Wife, and Son (Muhammad Husnain Naeem). All of my family has always been a source of appreciation and admiration throughout my life either in my professional career or student life. I would like to disclose that Almighty Allah bestowed me such a noble and dominating figures in my life, without whom I could not have predicted myself to accomplish this task.

In the end, I would like to acknowledge and promise myself to be bind by the golden tips of life as positive thinking, hard work and consistency in execution of the idea.

Abbreviations and Notations

CC	Compliance Current
DCB	Di-cholorobenzene
DMF	N,N-dimethyl-formamide
EHDP	Electrohydrodynamic Patterning
FESEM	Field Emission Scanning Electron Microscope
FIB	Focused Ionic Beam
FORS	Full Organic Resistive Switch
HRS	High Resistance State
ITO	Indium Tin Oxide
I-V	Current-Voltage
LRS	Low Resistance State
MEH:PPV	Poly[2-methoxy-5-(2'-ethylhexyloxy)–(*p*-phenylenevinylene)]
Memristor	Memory Resistor
MIM	Metal Insulator Metal
MOSFET	Metal Oxide Semiconductor Field Effect Transistor
NDR	Negative Differential Resistance
NP	Nanoparticle
OLED	Organic Light Emitting Diode
PEDOT:PSS	Poly(3,4-ethylenedioxythiophene):poly(styrenesulfonate)
PET	Polyethylene terephthalate
PI	Polyimide
PVP	Poly(4-vinylphenol)
ReRAM	Resistive Random Access Memory
SCLC	Space Charge Limited Current
STDP	Spike Timing Dependent Plasticity
TCLC	Trap Charge Limited Current

TFT	Thin Film Transistors
WORM	Write Once Read Many
XPS	X-ray Photoelectron Spectroscopy
XRD	X-ray Diffraction
ZrO_2	Zirconium Dioxide
μ	Electronic Mobility
A^*	Effective Richardson Constant
C	Capacitance
d	Thickness
e	Electron
E	Electric Field
H_b	Density of Traps at the Edge of Valance Band
k	Boltzmann Constant
L	Inductance
l	Distribution of Traps in the Band Gap
M	Memristance
n_0	Density of Free Carriers
N_v	Effective Density of State
R	Resistance
R_{OFF}	High Resistance State
R_{ON}	Low Resistance State
T	Absolute Temperature
V_{TH}	Threshold Voltage
β	Schottky Coefficient
E	Dielectric Constant
ε_0	Permittivity of the Free Space
Θ	Trapping Fraction
λ	Wavelength
φ_B	Barrier Height
j	Current Density
i	Electric Current
q	Electric Charge

v	Voltage
φ	Flux

Contents

List of Figures

List of Tables

Abstract

The research work reveals the engineering of ZrO_2 & polymer-based sandwiched structures for resistive switching applications. The fabrication of devices was performed by electrohydrodynamic printing (EHDP) and spin coating techniques. The jetting mode of the EHDP was used for the patterning of bottom and top electrodes. The atomization mode of EDHP and spin coating techniques were used for the deposition of thin sandwiched layers between bottom and top electrodes. Fabrication of the resistive switches was done on glass, polyethylene Terephthalate (PET), and polyimide (PI) substrates. Electrically conducting material including indium tin oxide (ITO) and silver (Ag) were used as electrodes, while zirconium dioxide (ZrO_2), poly(4-vinylphenol) (PVP), poly(3,4-ethylenedioxythiophene):poly(styrenesulfonate) (PEDOT:PSS) and poly[2-methoxy-5-(2'-ethylhexyloxy)–(*p*-phenylenevinylene)] (MEH:PPV) were used for the deposition of sandwiched layers between bottom and top electrodes. Full organic resistive switches (FORS) were also fabricated with the sandwiched structure of PEDOT:PSS/PVP/PEDOT:PSS on a PI substrate. The fabricated resistive switches were morphologically characterized with field emission scanning electron microscope (FESEM) and focused ionic beam (FIB) techniques. Chemically composition was confirmed using x-ray diffraction (XRD) and x-ray photoelectron spectroscopy (XPS) techniques. Electrically characterization of the fabricated devices was done using semiconductor device analyzer. The sandwiched structures exhibited at least two distinct states when were being forced with opposite polarity at its electrodes. The change in the resistance was then exploited for the electrical

switching and memory applications. Characterization results showed high degree of uniformity in deposited structures. The fabricated devices performed exceptionally well in bipolar resistive switching regime with a reasonable high OFF/ON ratio, endurance test, and retention time. Effect of compliance current was examined to measure the electrical switching capability of the fabricated resistive devices. Resistive switching mechanisms were also investigated for reliable application of the fabricated devices in printed electronics. The obtained results show the promising feasibility of the fabricated switches for electrical switching and memory applications in printed electronics. Current conduction mechanisms in the fabricated resistive switches were concluded based on slope calculation and were supported with the governing physical current conduction laws.

1. Introduction

Electronic industry is growing day by day. It is progressing not only in its processing capability, but also in device density per area. Electrical switching is one of the most important phenomena for data process in all the processing units. After the processing of data, the results must be saved to be used for further calculations. In current semiconductor technology, transistors have been employed as the basic instrumental part of the circuit design for the electrical switching. Transistors have been used for designing processing units and flash-memory/capacitors have been employed for storing the information. So, two different kinds of devices are being needed for performing two different tasks.

All the processing and storage capabilities in modern electronic devices are still based on elementary charge. When the feature size continues to shrink, charge leakages would become prominent in transistor-based processing units and capacitor-based memory devices. Nevertheless, according to the Moore's law, the number of transistors doubles almost every two years. So, the current semiconductor technology is approaching its limits. To overcome the forthcoming challenges and bottlenecks, engineers and scientists have always been looking for some cutting-edge technologies and alternative devices.

1.1 Resistive Switching

Resistance-based processing and storage technique is the only hope to counteract the upfront challenges to the electronic industry. Resistive switches considered as a justified replacement for the memory devices and electrical switching elements have been researched productively for many years (Asamitsu et al. 1997, Beck et al. 2000, Schindler et al. 2007, Strukov et al. 2008, Chua 2011, and Wang et al. 2011). Solid electrolyte sandwiched between two electrodes is considered to be the preeminent composition to elucidate the reversible resistive switching characteristics. The sandwiched structures exhibit at least two distinct states when are being forced with opposite polarity at its electrodes. The change in the resistance is then exploited for the electrical switching and memory applications. The resistive switching devices are fabricated by simply sandwiching some metal oxide, polymer-based material,

perovskite material, or even a vacuum nano-gap etc between two conducting electrodes as shown in figure 1.1. So, it is a simple capacitor type or metal-insulator-metal (MIM) type structure.

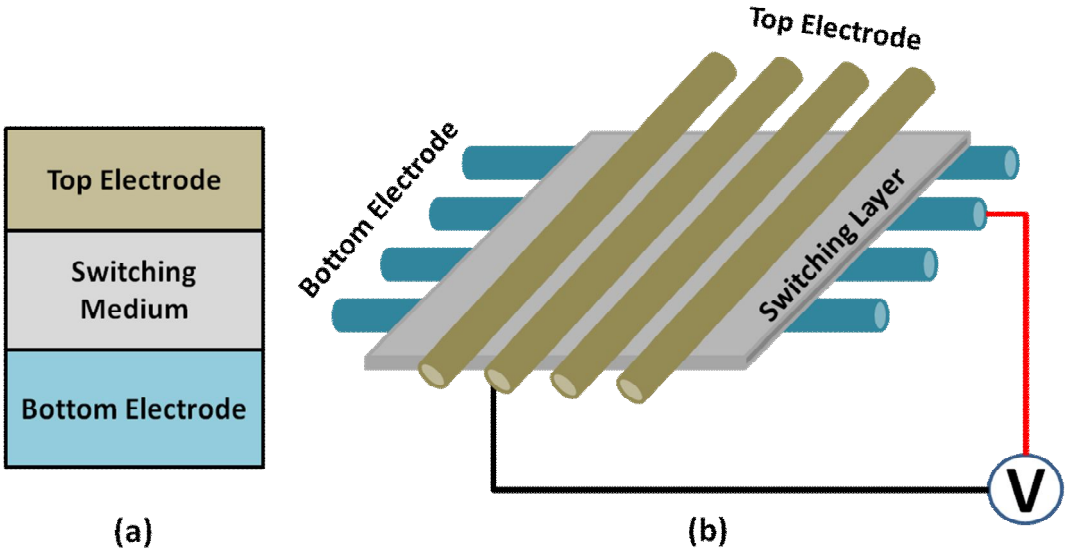

Figure 1.1 Resistive switching device structures: (a) Simple device (b) Cross-bar array.

Resistive switching device is known with many names in literature, for example resistive switch, memory resistor, memristor etc. The basic phenomenon behind the resistive switching function is negative differential resistance (NDR) effect. NDR switching has been reported since 1962 in many oxides in a sandwiched MIM structure (Hickmott 1962).The NDR switching in the sandwiched structures has attracted much attention, for its application in resistive random access memory (ReRAM) devices. Different switching layers including polymeric and non-polymeric materials have been employed to fabricate NDR switching devices through different deposition techniques (Bozano et al. 2004, Du et al. 2012, and Shang et al. 2006). In fact two groups of researchers are working on this device with different nomenclatures as shown in figure 1.2.

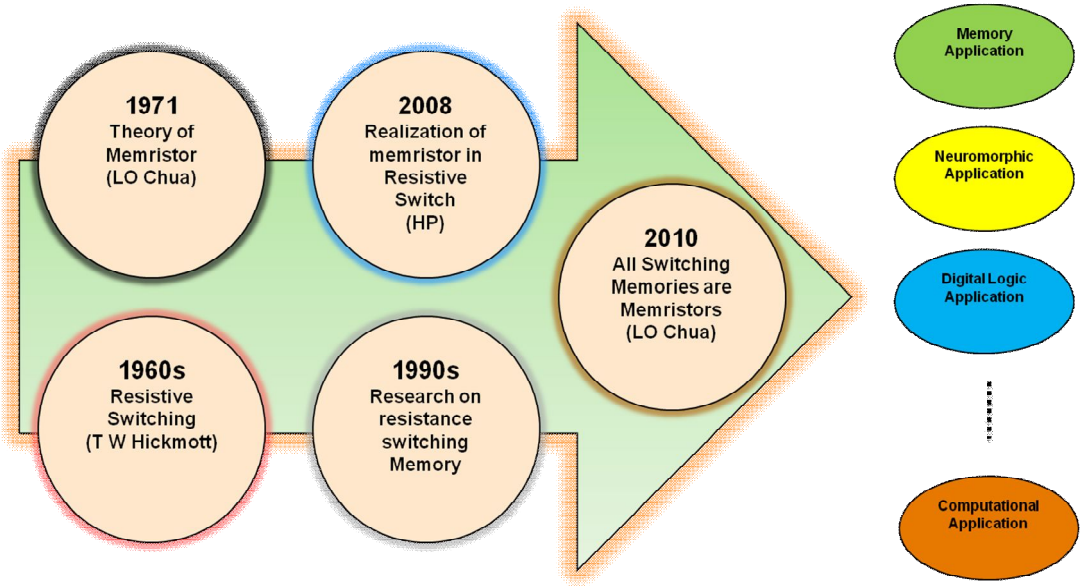

Figure 1.2 History of resistive switching devices.

One group is working on this device with the name of resistive switch/resistive switching memory and the other group is working on this device with the name of memristor (memory resistor). The former group is older than the later one. The latter group is lead by Professor Leon Chua. The concept of memristor was found in 1971 by Leon Chua (Chua 1971). He argued that there are four fundamental variables (current, voltage, charge and flux). So, there should be six possible relationships among these four fundamental variables. Five out of six relationships have already been sorted out. The 6^{th} relationship was yet to be discovered before 1971. He hypothesized that the only missing relationship was between charge and flux as shown in figure 1.3.

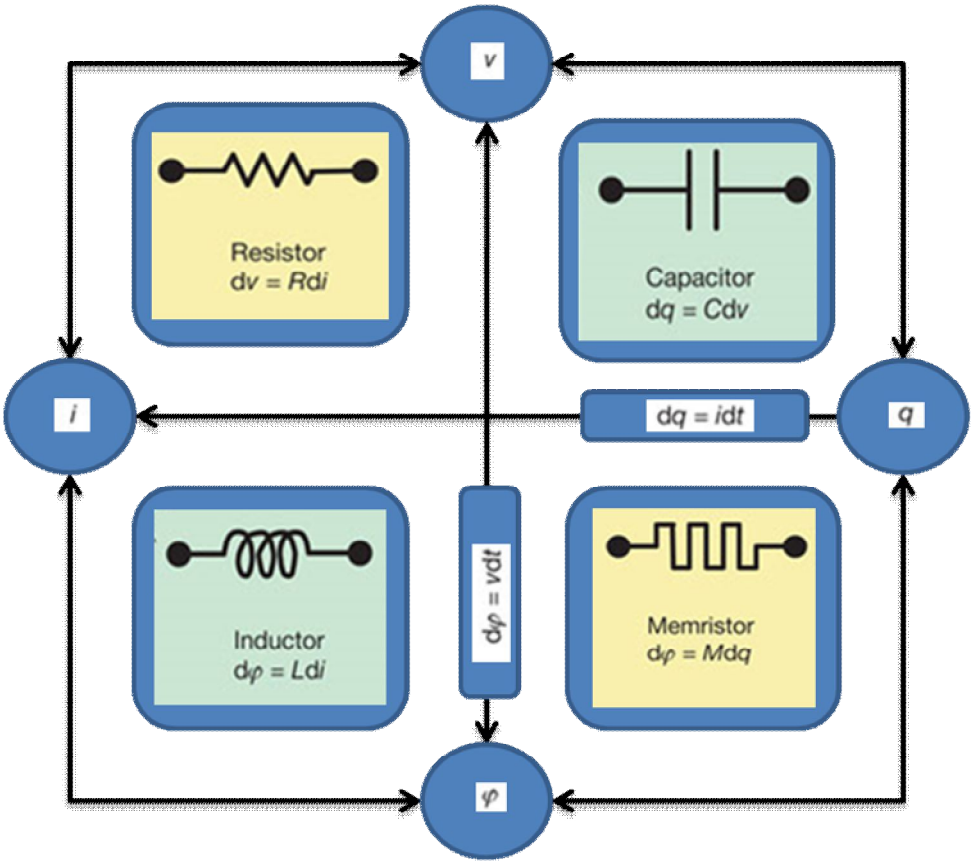

Figure 1.3 Hypothetical concept of Memristor by Leon Chua.

So, memristor is a 4th mystery passive two-terminal circuit element that maintains a functional relationship between the time integrals of current and voltage.

$$d\varphi = M dq \quad | \quad M = \frac{d\varphi}{dq} \qquad (1.1)$$

Where M is the memristance of the system.

(1.2)

And (1.3)

The device shares many properties of resistor and shares the same unit as Ohms (Ω). In an ordinary resistor, the resistance of the device is fixed but in contrast to an ordinary resistor, the resistance of the resistive switching device/memory resistor/memristor can be programmed and switched to some specific value based on the history of the applied voltage. So, it is just like a variable resistor or programmable resistor whose resistance changes over time based on the amount of current that has passed through it. If *M* is a constant then it is identical to resistance but if it is a function of q then it yields a nonlinear element because no RLC (Resistor (R), Inductor (L) and Capacitor (C)) circuit can duplicate the behavior of memristor. At higher frequencies, memristor behaves like a resistor but at lower frequencies it just behaves like a nonlinear resistor.

The resistive switch provides great data storage density due to its simple device structure. The sandwiched type structures are more reliable because these devices are resistance based so they keep their state unchanged even when the power is interrupted in data centers. They combine the job of processing unit and memory in a single unit. These devices use less energy so produce less heat. Conventional devices work on only 0 and 1, these devices can use anything between 0 and 1 (0.1, 0.2. 0.3 etc) so capable of performing both analog and digital electronic functions depending on the particular switching material. It is also possible to change the behavior of these devices by just changing the speed and strength of the current. Transistor is three-terminal device but resistive switch is a two-terminal device. It is scale able by just reducing its thickness of the switching material between two counter electrodes.

1.2 Types of Resistive Switching

As mentioned in the previous section that in contrast to an ordinary resistor, memory resistor can be programmed or switched to different/specific resistance state based upon the history of the voltage signal applied to the device. This phenomenon can be understood in a current-voltage (I-V) graph. Resistive switching are categories into two types based upon the voltage polarity needed to derive the device operation. The two types of resistive switching are listed below:

1.2.1 Unipolar Resistive Switching

If switching of the resistive switch is independent of the polarity of the voltage/current source and is dependent on the amplitude of the voltage/current then the switching is categorized as unipolar resistive switching as shown in figure 1.4. As noticed in the I-V graph, setting and resetting of the device is happening irrespective of the polarity of forcing node. A device in an OFF-state/high resistance state (HRS)/R_{OFF} can be switched to ON-state/low resistance state (LRS)/R_{ON} by a threshold voltage (V_{TH}) and the current is limited by compliance current (CC) to avoid hard break down in the switching layer of the device. Resetting back to ON-state happens at a same polarity below its V_{TH}. A much higher current can be observed in retting state of the device. Application of CC in not needed in retting of the device. So, both the transition of setting and resetting are possible on both sides of the polarity.

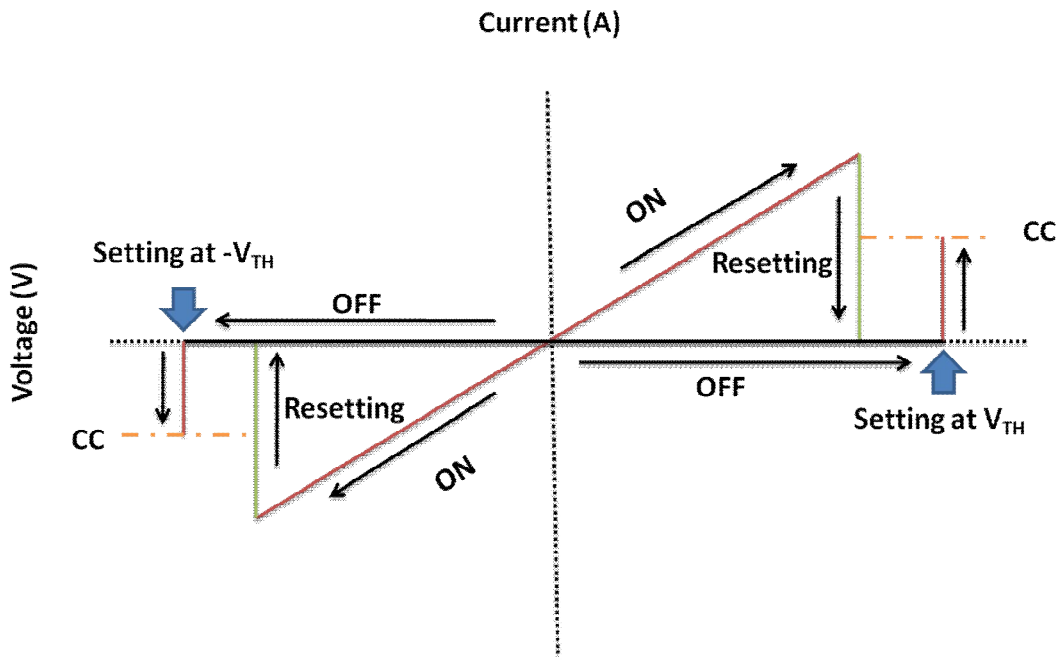

Figure 1.4 Amplitude dependent unipolar resistive switching.

1.2.2 Bipolar Resistive Switching

The behavior of the device in which setting and retting of the device appeared at different sides of the polarity is termed as bipolar resistive switching. In this type of resistive switching, ON-state of the device occurs at some V_{TH} and OFF-state of the

device occurs at some specific V_{TH} on the opposite side of the voltage polarity as shown in figure 1.5. Bipolar resistive switching is also called polarity dependent resistive switching. Current observes in bipolar resistive is much lower as compared to that of unipolar resistive switching.

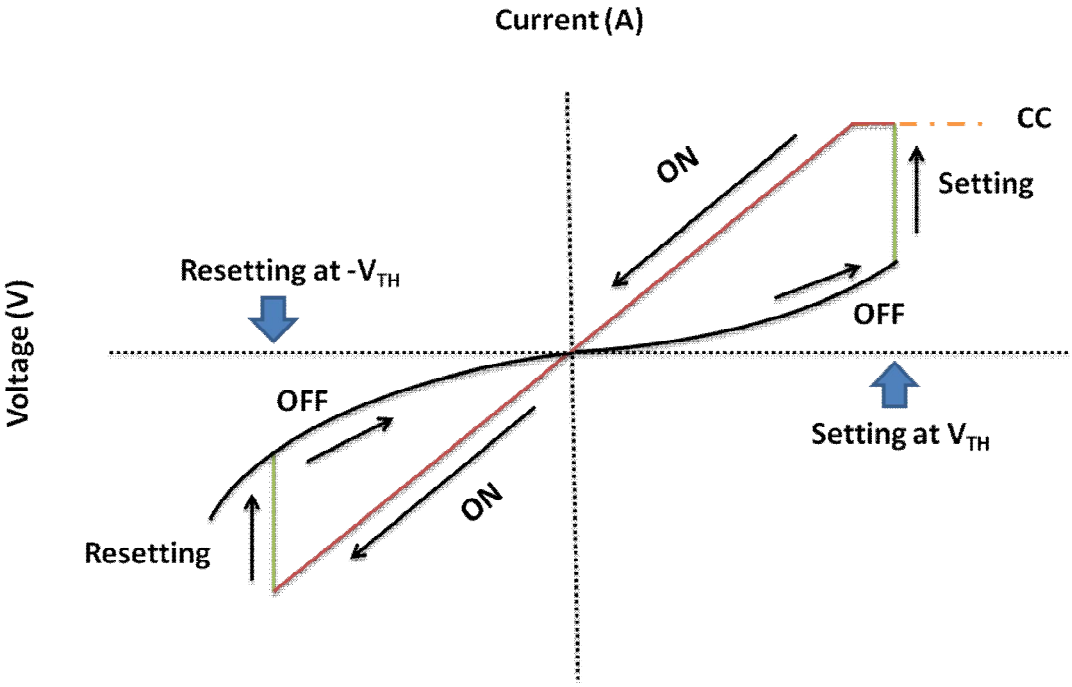

Figure 1.5 Polarity dependent bipolar resistive switching.

1.3 Resistive Switching Mechanisms

Several studies have been conducted for resistive switching mechanisms involved in metal oxides and polymers based sandwiched structures (Waser and Aono 2007, Sawa 2008, Akinaga and Shima 2010, Lee and Chen 2012, Cho et al. 2011, and Ling et al. 2008). Broadly, the purposed mechanisms are categories into two classes: the bulk effect and the interface effect.

1.3.1 Bulk Effect

The resistive switching effect that is caused by formation and rupturing of the conductive filaments due to joule heating in the sandwiched material between the two electrodes is termed as bulk effect or thermal effect. Bulk effect is observed common in unipolar resistive switching devices. Forming voltage is usually needed in these types of resistive switching. The filaments are formed by the voltage induced

partial dielectric breakdown. These filaments may be composed of electrode material transported into the sandwiched layer, local degradation of the organic film or decomposed insulator material such as sub-oxides. During the resetting state of the device, the filaments are undergone into the rupturing phase hence the device change its LRS into HRS.

1.3.2 Interface Effect

Interface effect is common in bipolar devices. Different models are involved to explain the interface effect in bipolar resistive switching devices. Some common models are explained with the charge injection and trapping of charges in the traps in the insulator/oxide switching material. Traps play important rule when the interface between metallic/conducting electrode and insulator/oxide is schottky. When external potential is provided then the injected charges are trapped in the interface between conducting electrode and insulator. When sufficient number of charges are gathered in the trap site eventually the scenario overcomes the barrier between metal-insulator interface and large current starts to flow through the interface. Contrary when the biasing is reversed then again the schottky barrier establishes and changes the device state to its original HRS.

1.3.3 Redox Process Induced Cation Migration

This model is based on the redox reaction of the metallic electrode. When one of the electrodes is chemically reactive while the other conducting electrode is inert then cations migrate in the ionic conductor. Chemically reactive electrode (Ag or Cu etc) undergoes oxidation reaction when force with some potential. The drift of cations (such as Ag^{+} or Cu^{+} etc) in the ion-conducting layer and their discharge at the counter electrode form a highly conductive path results in setting the device into the ON state. When the polarity is reversed, the conductive path undergoes into the electrochemical dissolution and resetting the device into the OFF state.

1.3.4 Redox Process induced Anion Migration

Anion migration model is based on the chemical redox reaction of insulator/oxide. This is the mechanism in which resistive switching takes place by the migration of anion/oxygen ion towards anode or better described by the migration of oxygen

vacancies towards cathode. This model is also termed as oxygen vacancy migration resistive switching model. The migration of anion (oxygen ion) or oxygen vacancy leads to the change in stoichiometry and a valance change of the cation sublattice. Eventually the state of the device changes to the LRS by the change in the electronic conductivity of the oxide/insulator.

1.3.5 Formation and Disruption of Metal Oxide

In some of the reports, the resistive switching effect was attributed to the formation and disruption of the metal oxide between the metallic electrode and oxide interface. When a potential is applied to the device, metal oxide formed due to the electrochemical reaction between the electrode material and sandwiched layer.

1.4 Research Goal

Resistive switches have vigorously been researched for many applications including random access memory, electrical switching, neouromorphic applications, digital logic application, and computational applications etc. The resistive switches are well thought-out to be the realistic replacement of MOSFET (metal oxide semiconductor field effect transistor) in electronics industry due to their fast switching speed, small size, and simple device structure. Nevertheless, these devices combine the job of working memory and hard drives into one tiny device thus having the ability to create computers that never has to boot up.

Printed electronics has revolutionized the world and is leading to new innovations on a quasi-daily basis. The term “printed electronics” refers to the application of printing techniques for the fabrication of electronic structures, devices, and circuits by using a variety of functional materials (printing inks) and substrates. It bestows many advantages of cost-effectiveness, mechanical flexibility, and low fabrication cost over their semiconductor technology counterpart.

The motivation of this research is to realize the magic characteristics of the resistive switch with printed electronics techniques. So, the fabrication of resistive switches has been done by using two printing techniques including EHDP (electrohydrodynamic printing) and spin coating. The switching materials used in

this research work are zirconium dioxide (ZrO_2), poly(4-vinylphenol) (PVP), poly(3,4-ethylenedioxythiophene):poly(styrenesulfonate) (PEDOT:PSS), and poly[2-methoxy-5-(2'-ethylhexyloxy)–(*p*-phenylenevinylene)] (MEH:PPV). The conducting materials used for the fabrication of the resistive switches are indium tin oxide (ITO) and silver (Ag). The substrates used for the fabrication of the devices are glass, polyethylene terephthalate (PET), and polyimide (PI). The fabricated devices were characterized morphologically with field emission scanning electron microscope (FESEM) and focused ionic beam (FIB) techniques. Chemically composition was confirmed using X-ray diffraction (XRD) and X-ray photoelectron spectroscopy (XPS) techniques. Electrically characterization of the fabricated devices was done using semiconductor device analyzer. The resistive switches were checked with different robustness tests, mechanical flexibility tests, and endurance tests. The fabricated sandwiched structures were also characterized with different CCs to elucidate their behavior for electrical switching purposes. The devices showed excellent feasibility to be used in random access memory and electrical switching applications with high OFF/ON ratio. Resistive switching and current conduction mechanisms were investigated by the analysis of I-V curves.

The thesis is organized into five chapters as under:

Chapter 2 deals with the fabrication of ZrO_2-based resistive switches on ITO-coated PET, glass and PI substrates with EHDP technique. Resistive switching properties and resistive switching mechanism are investigated in the fabricated devices. This chapter also describes the fabrication of flexible resistive switch.

Chapter 3 deals with the realization of the organic resistive switches with the printing techniques. The organic materials used for the fabrication of sandwiched structures are PVP, PDOT:PSS, and MEH:PPV. The last section of this chapter deals with the fabrication of full organic resistive switch and its current conduction mechanism.

Chapter 4 presents the executive summary of the thesis work and Chapter 5 concludes the research work with future suggestions.

2. Resistive Switching in ZrO_2

ZrO_2 (Zirconium Dioxide) is one of the best switching metal oxides that has meticulously been researched for resistive switching characteristics. Resistive switching has been observed in ZrO_2 for many years (Wu et al. 2007, Guan et al.2008, Chen et al. 2010, Long et al. 2011, Liu et al. 2005, Lin et al. 2007, Lin et al. 2012, Lin et al. 2006, Liu et al. 2008, Guan et al. 2007, Wang et al. 2011, Choi and Awais 2012, Awais et al. 2013, and Awais et al. 2013) due to its unique properties: including high ionic conductivity, multiple stable oxidation states, low electron affinity, work compatibility at high temperature, and fabrication friendliness. In this chapter, the realization of ZrO_2–based resistive switches has been discussed on different substrates using printing technology. The fabricated devices were characterized to elucidate their reversible resistive switching characteristics.

2.1 Fabrication of Printed ZrO_2 Resistive Switches on ITO-coated PET

Nano-fabrication of ZrO_2 (Zirconium Dioxide) thin film as an insulating layer has been researched in the MIM (Metal-Insulator-Metal) sandwich for the scalabity of the resistive switches. Resistive switching device was explored that memristive (resistive) switching is more prominent as the thickness of the insulting region shrink to nano-scales (Strukov et al. 2008). So scalabity of the memristor depends a lot on the nano-fabrication of the insulating region. Different nano-fabrication technologies are available for the insulating region in the MIM sandwich like atomic layer deposition (Choi et al. 2005), sputtering (Yang et al. 2009), sol-gel method (Hackett et al. 2009), and anodization (Miller et al. 2010). Some fabrication technologies are matured and some are being researched nowadays. Apart from the deposition of high quality insulating layer they have some inherent limitations like high capital cost, high temperature environment, infeasible for mass production, radiation effects on human life and long fabrication time (Mitzi et al. 2009, Muhammad et al. 2011, and Prodromakis et al. 2010). The need of a nano-fabrication technology has been felt to deposit a high quality thin film for the MIM sandwich.

EHDA (Electrohydrodynamic Atomization) is a cost effective, ambient temperature deposition, feasible for mass production, free of harmful radiation and short

fabrication time deposition technique. EHDA printing technology is an emerging direct printing and deposition technology in which the ink is pumped through a nozzle at some appropriate flow rate with the positive potential at the nozzle and grounding the substrate. The induction of the surface charges on the pendent meniscus emerging at the nozzle outlet, results in an electric stress over the liquid surface. If the electric field and flow rate are in some operating range then this will overcome the surface tension stress over the liquid surface and results in deformation of the droplet at the orifice of the nozzle into a conical shape. Due to the tangential electric field acting on the surface of the liquid cone, a thin jet emanates at the cone apex which further breaks up into a number of small droplets under the effect of coulomb forces. Different spraying modes exit in EHDA technology like dripping, microdripping, spindle, cone-jet and multi-jet mode but stable cone-jet is most important spraying mode because of the generation of the monodispersed droplets with few micrometer diameters (Muhammad et al. 2011). A complete detail and phenomenon of the EHDA process can be explored in (Hartman 1998 and Jaworek 2007). Thin film deposition through EHDA has been researched for a lot of applications. The EHDA technique has been used for the deposition of the CIS absorber layer [13]. Gold films have been deposited with the EHDA on silicon wafer substrate (Samarasinghe et al. 2008). High quality zinc-oxide layers have been successfully deposited by EHDA for printed electronics application (Muhammad et al. 2012).

EHDA has been deployed in this work to electrohydrodynmically atomize the ZrO_2 layer on the ITO PET and discuss its operating envelope under different flow rates and voltages. This research work also describes the resistive switching in the deposited ZrO_2 film with ITO as a bottom electrode and Ag as a top electrode. No one else has used the said technique to show the memristive behavior in the electrohydrodynamically atomized layer of ZrO_2 on the ITO coated PET substrate. The technique deployed in the current research work provides the cost-effective, rapid processing and friendly environment fabrication of the memristive devices. The deposited thin film has been characterized through SEM, XRD and XPS analysis. Electrical characterization has been done with semiconductor analyzer to show the reversible resistive switching through deposited ZrO_2 thin film.

2.1.1 Experimental Details

The experimental setup used for the ZrO_2 layer deposition is shown in the figure 2.1. The equipment consist of metallic capillary, high-voltage power supply, ink supply section, X-Y stage control, Z-axis control for nozzle, high speed camera and light source.

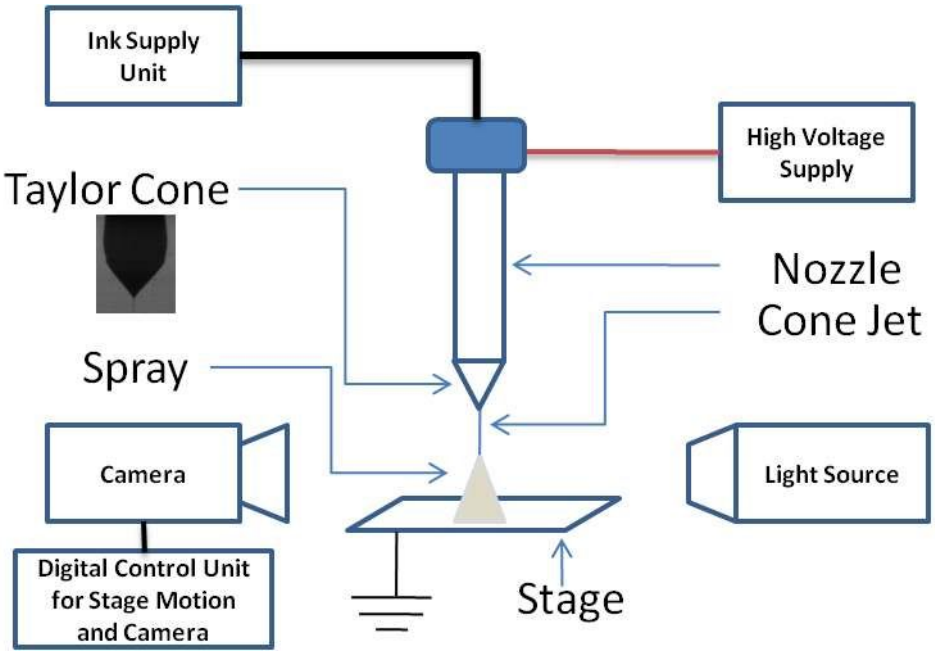

Figure 2.1 Experimental Setup for EHDA Printing Technology.

For electrohydrodynamic atomization of ZrO_2, the ink containing nanoparticles (Sigma Aldrich) is pumped through a nozzle at some appropriate flow rate with the positive potential at the nozzle and grounding the substrate. The movement of the substrate is controlled through the X-Y stage control and Z-axis control is used to control the nozzle to substrate distance. The high speed camera with the light source is used to observe the EHDA phenomena during the cone jet mode. The experiment was performed at standard room temperature and pressure.

ITO (Indium-Tin Oxide) coated PET (Polyethylene Terephthalate-Sigma Aldrich) was used as a substrate for the deposition of the ZrO_2 layer. ITO was used as a bottom electrode for the MIM structure. The substrate was rinsed with ethanol and processed with ultraviolet light for around 10 minutes. Prior to the deposition process, 5% weight ratio ZrO_2 (Sigma Aldrich) dispersion containing nanoparticles less than

100 nm was mixed in ethanol with 1 : 1 volume ratio. After mixing, the nanoparticle solution was sonicated for 15 minutes and no segmentation was observed for a longer period of time than the experiment time. To deposit oxide layer, ZrO_2 dispersion was pumped to a metallic nozzle having the inner diameter 110 μm and outer diameter 210 μm. Atomization of the ZrO_2 was attempted with the flow rate from 25 μl/hr to 100 μl/hr. Different spraying modes were observed by varying the voltage during the experiment. Dripping mode, unstable cone jet mode, stable cone jet mode and muti-cone jet mode are shown in the figure 2.2 as observed during the ZrO_2 deposition process.

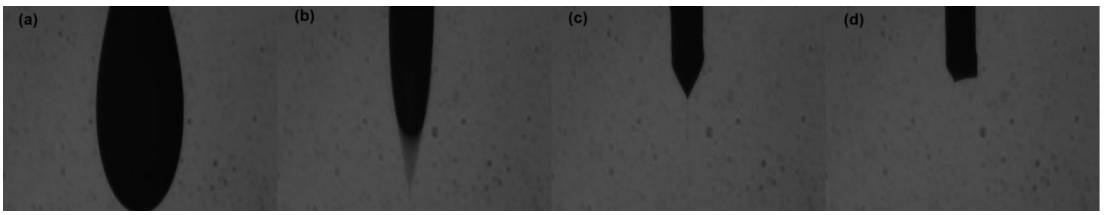

Figure 2.2 Different Spraying Modes in the EHDA of ZrO_2: (a) Dripping (b) Unstable cone-jet (c) Stable cone-jet (c) Multi cone-jet.

Figure 2.3 shows the operating envelope of each mode observed during the experimental process.

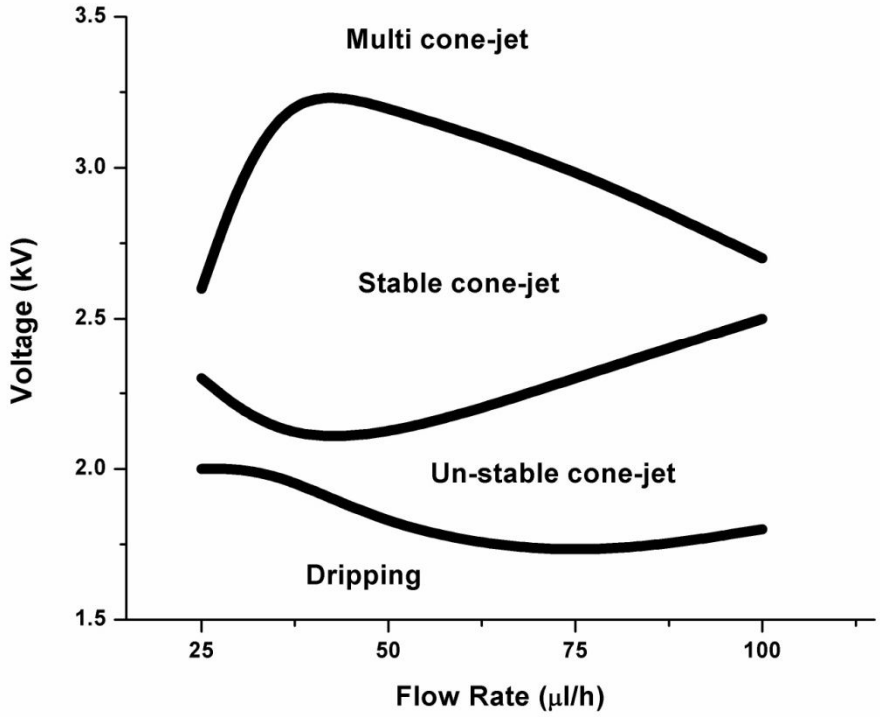

Figure 2.3 Operating Envelope of the EHDA of ZrO_2 on the ITO Coated PET.

The experiments were performed with the nozzle to substrate distance as around 1.5 mm. The reported ZrO_2 layer was deposited during the stable cone jet mode with the flow rate of 50 μl/hr and with the applied voltage of 3.09 kV. The substrate speed was kept as 2.6 mm/s throughout the experiment. After the deposition of the ZrO_2 layer the sample was cured at 135 °C for 1.5 hours. Ag drop was used to make the top electrode to complete the structure for the MIM sandwich.

2.1.2 Layer Characterization of ZrO_2 Resistive Switches

To check the surface morphology the sample was analyzed with a scanning electron microscope (SEM), Jeol JSM-7600F. The average grain size was observed to be 45 nm as shown in the figure 2.4.

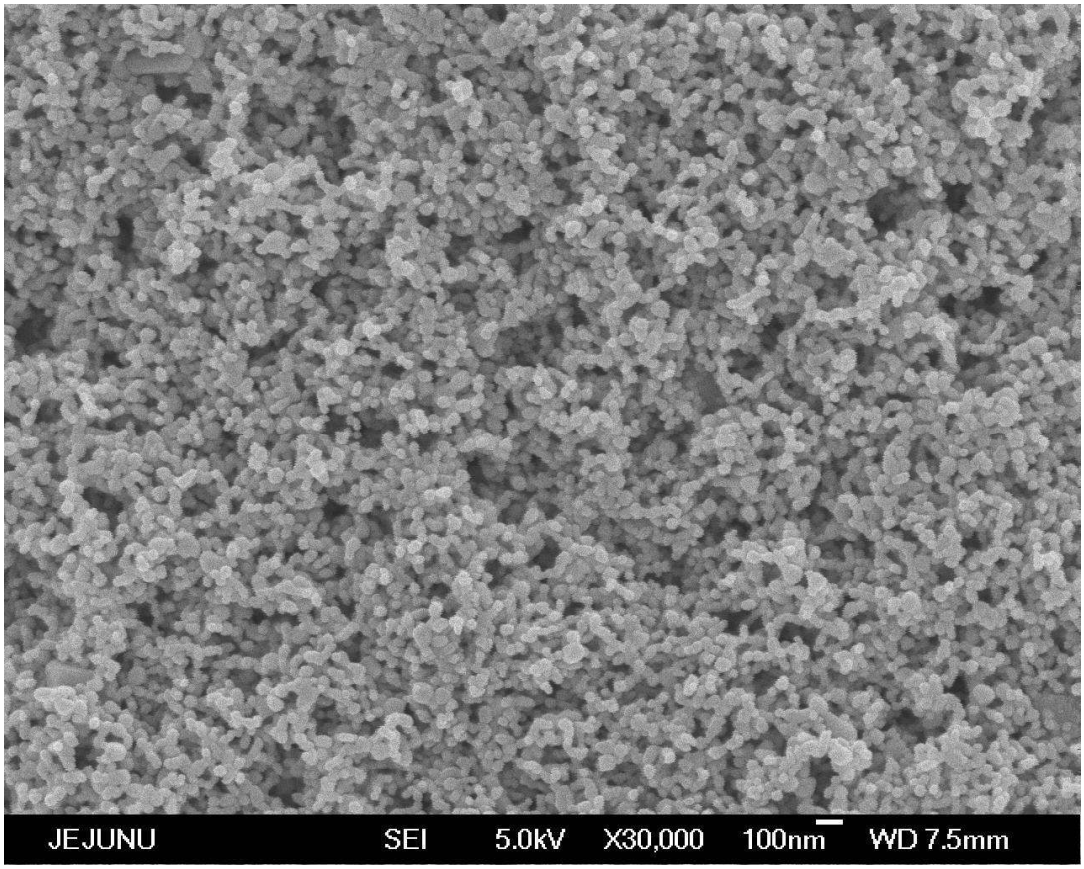

Figure 2.4 SEM Image of ZrO_2 Layer Deposited through EHDA.

Film thickness plays a vital role in memristive behavior. Different samples were prepared to check the optimum film thickness for the memristive behavior. The film thickness can be varied by varying the spray time by adjusting the substrate speed. The small substrate speed has more deposition time, consequently thick layer could be obtained and large substrate speed provides small deposition time so thin layer will be obtained in this case. The film thickness was measured with the thin film thickness measurement system K-MAC ST4000-DLX and was observed to be around 67 nm. This was the optimum film thickness achieved through our experiments showing consistent bipolar reversible resistive switching.

The X-ray diffraction pattern (XRD) analysis of ZrO_2 nanoparticles was also carried out as shown in the figure 2.5. All the diffraction peaks of the pattern could be indexed to monoclinic or tetragonal phase of zirconium oxide.

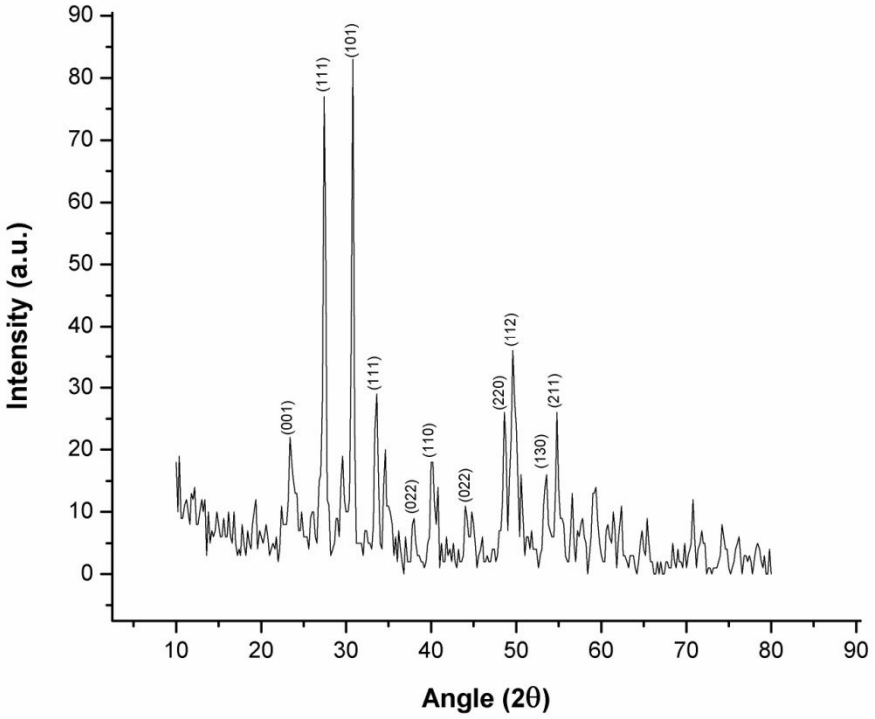

Figure 2.5 XRD Analysis of ZrO_2 Nanoparticles.

Figure 2.6 shows the x-ray photoelectron spectroscope (XPS) graph of ZrO_2 film. All the peaks in the graph indicate the presence of Zr and O elements. The presence of C peak in the graph is attributed to the environmental contamination.

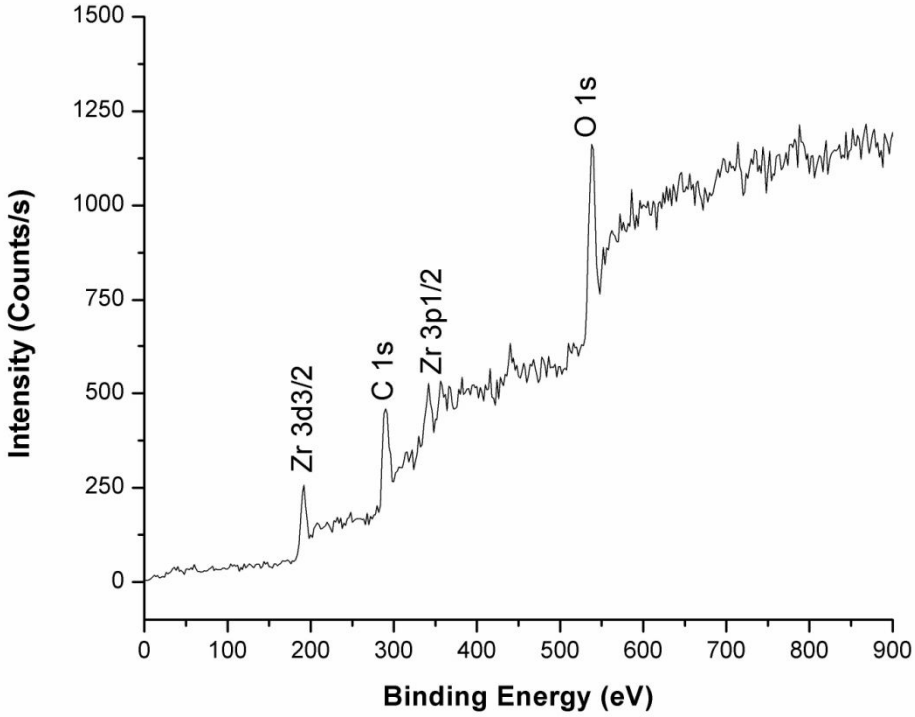

Figure 2.6 XPS Analysis of ZrO_2 Film.

2.1.3 Resistive Switching Characterization

Agilent B1500A Semiconductor Device Analyzer was used to carry out all the electrical characterization of the samples. The voltage was applied on the Ag top electrode and grounding the ITO bottom electrode in all the measurements. Polarity dependent bipolar switching was used to characterize the memristive behavior. Double voltage sweeps were applied from +3 V to -3 V with different current compliances initially from 100 μA to 1 mA and then up to 5 mA. Before starting resistive switching operation in a virgin sample an appropriate positive or negative voltage was applied to establish the conducting paths and to get a soft breakdown which is necessary for the stable reversible resistive switching operations (Choi et al. 2005, Yang et al. 2009, and Hackett et al. 2009). The sample was electroformed and soft breakdown was occurred at around 5 V in our experiment.

After initial electroforming process the sample was biased with a double voltage sweep from +3 V to -3 V with a current compliance of 100 μA. The sample showed a

lissajous figure '8' with two distinct states: R_{ON} and R_{OFF} as shown in figure 2.7 which can be exploited to use the fabricated switch for binary switching purposes.

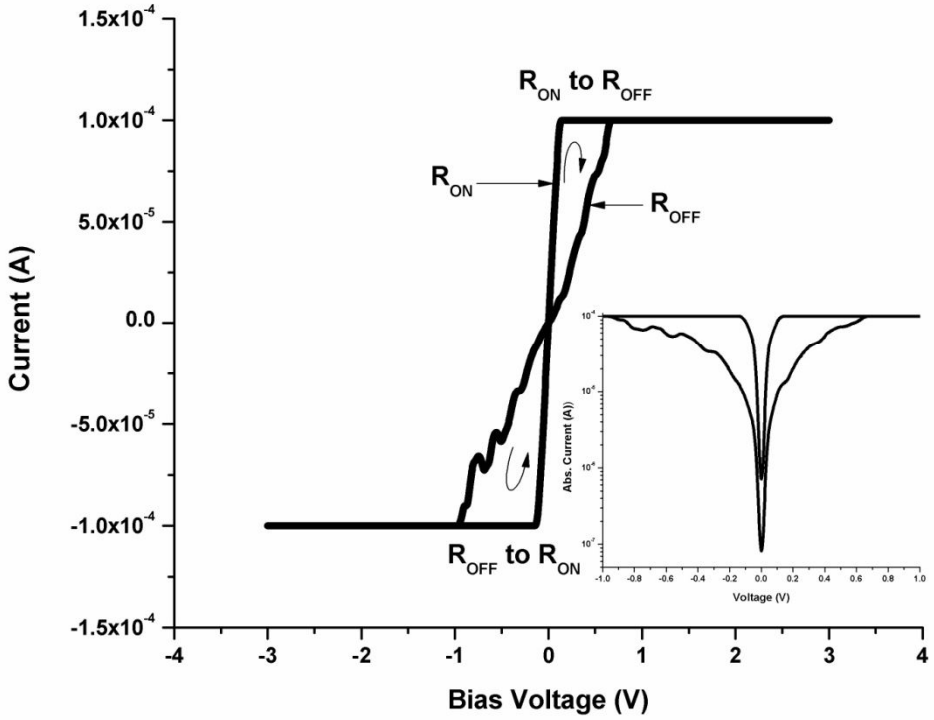

Figure 2.7 Resistive Switch (Memristor) IV Curve with Current Compliance: 100 µA.

The R_{ON} state shows the resistive switch in low resistance state and R_{OFF} state shows the switch in high resistance state. The upper loop of the figure '8' indicates the transition of the resistive switch from R_{ON} to R_{OFF} and lower loop illustrates the transition state from R_{OFF} to R_{ON}. The device can be used in binary switching around ±1 V. The fabricated switch started operating in R_{OFF} state from +1 V to -1 V and from -1 V to +1 V it switched to R_{ON} state. The resistance during the ON state of the device was observed to be around 1.07×10^3 Ω and during the OFF state it was observed to be around 1.59×10^4 Ω. The reading voltage of ±0.12 V could be used for measuring high or low state of the resistive switch. The inset of the figure 2.7 shows the ON to OFF ratio of the device that is more than 1 : 10. This ratio is quite reasonable to distinguish between the two states of the device.

The sample was further analyzed with different current compliances from 200 µA to 1mA. It was observed that with the increase of the current compliance the voltage requirement, to observe the bipolar resistive switching, increased and provided more reading voltage range in the IV curve of the switching device as shown in figure 2.8.

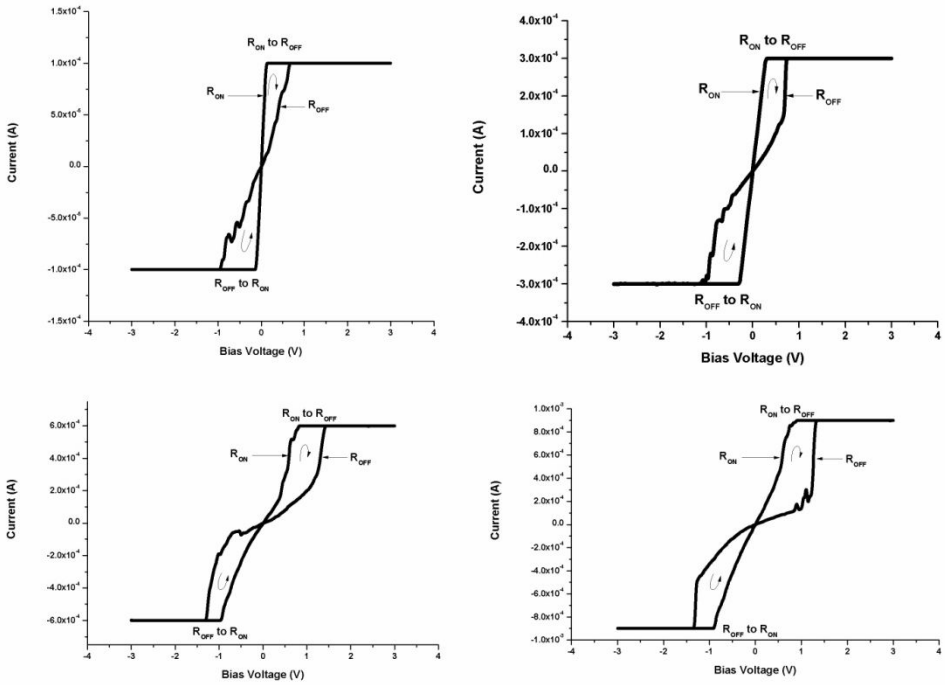

Figure 2.8 Resistive Switch (Memristor) IV Behavior during Different Current Compliances.

The variation in resistance was also measured for the current compliance from 100 µA to 1 mA: in the high/ON state of the switch, the variation in resistance was measured to be less than 3 Ω and in the low/OFF state of the device, it was measured to be less than 5 Ω. The resistance distribution in the OFF state is little bit larger than that in the ON state of the resistive switch. Restricting the operation of the device at different current compliances has two reasons: one is to switch a wide range of electrical circuit elements with different current compliances, second is to avoid hard breakdown of the resistive switch. Just above 1 mA current compliance, bipolar reversible resistive switching collapsed and simple ohmic behavior appeared. But

when the device was tested with the current compliance of 5 mA, the device showed stable bipolar resistive switching with high ON/OFF ratio as shown in the figure 2.9.

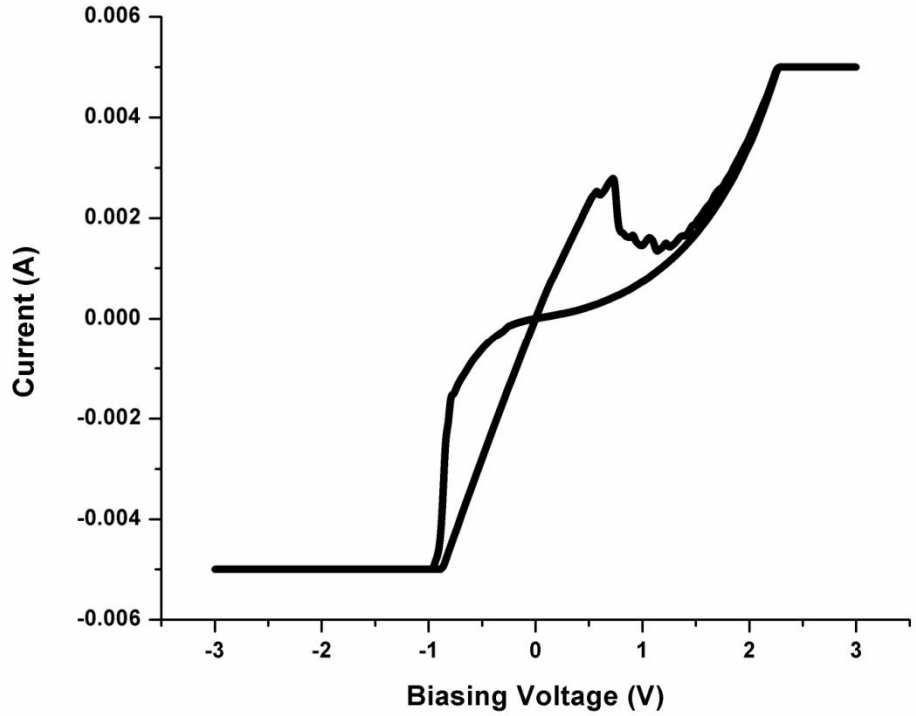

Figure 2.9 Resistive Switch (Memristor) IV Curve with Current Compliance: 5 mA.

The average resistance during the ON state of the device was measured to be 224 Ω and during the OFF state, the average resistance of the device was 2558 Ω at 5 mA current compliance. Such sort of resistive switches could be used as switching elements in the printed electronics in place of transistor or with memristor-transistor/diode hybrid integrated circuits. The resistive switch was tested under multiple voltage sweeps as shown in the figure 2.10.

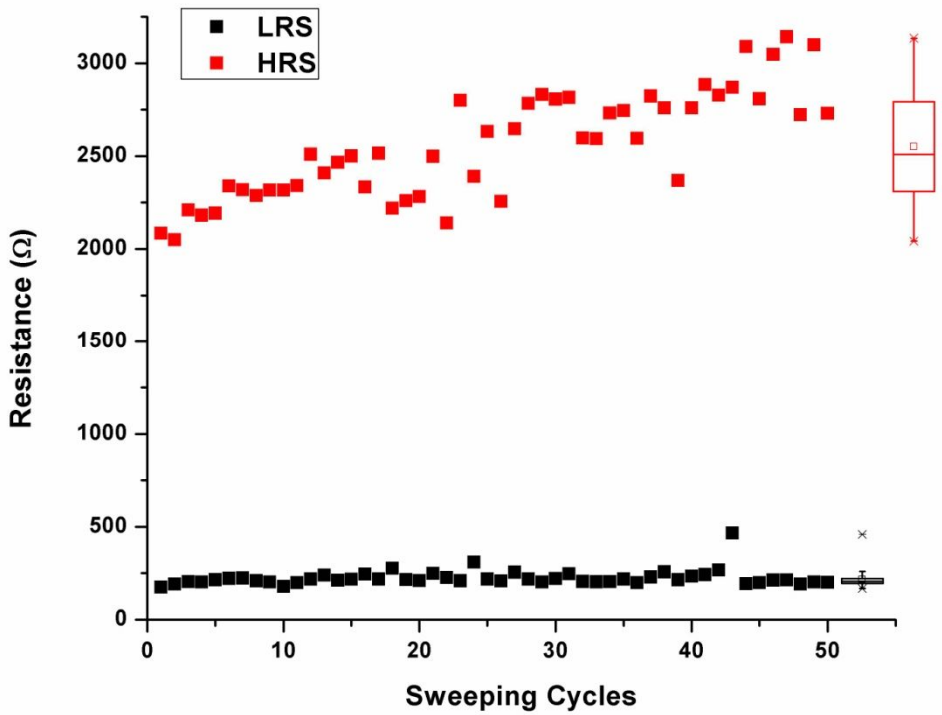

Figure 2.10 Resistance Vs Multiple Voltage Sweeps for the Printed Resistive Switch.

Stable ON/OFF ratio of more than 1 : 10 was observed. The reading voltage of 0.12 V has been used for measuring the current. It was observed that the resistance during the ON state was more stable than that of the OFF state because of the wide distribution of the OFF state of the device. The resistance during the ON state was changed from 176 Ω to 467 Ω and the resistance change in OFF state was observed from 2050 Ω to 3141 Ω. The cumulative probability of the HRS/R_{OFF} and LRS/R_{ON} of the fabricated switch for 50 cycles has been depicted in figure 2.11.

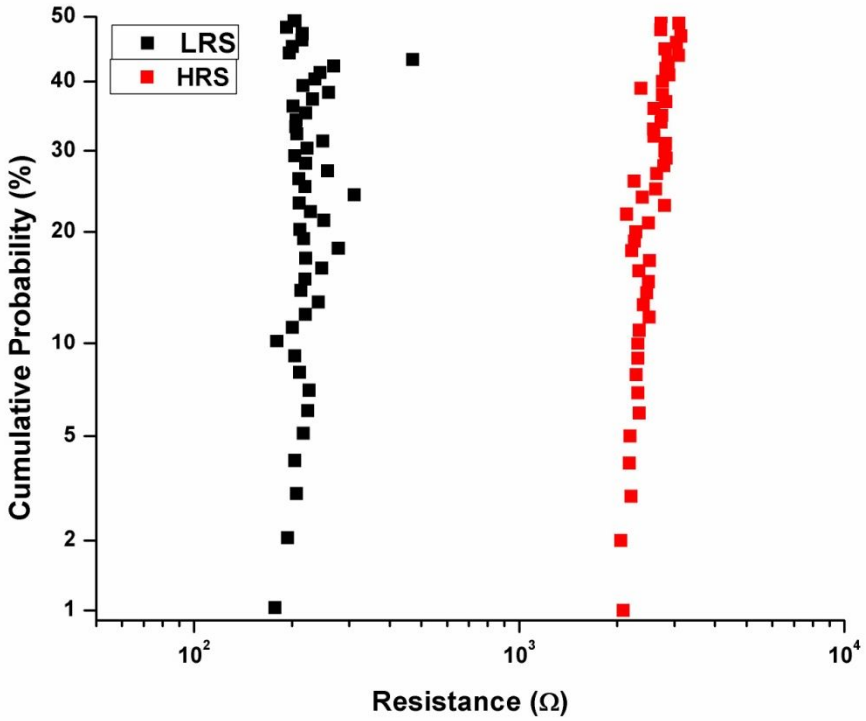

Figure 2.11 Cumulative Probability of HRS/ROFF and LRS/RON of the Cell for 50 Switching Cycles.

Both the switching states are properly distinguishable as evident from the graph. The data presented in the graph proves the feasibility of the EHDA technique by the distribution of the resistance in HRS and LRS against different switching cycles. Moreover it was also concluded that at some low current compliances, from 100 µA to 500 µA in our devices, almost linear conduction was observed during the ON state of the device that depicts the Ohmic or electronic conduction during the high state of the device and nonlinear conduction was observed during the OFF state of the device showing ionic conduction during low state of the device. In contrast to the low current compliance, setting high current compliances, above 500 µA in our devices, leaded to the non-linear or ionic conduction during both the high and low states of the device but at the current compliance of 5 mA linear conduction was observed in the ON state of the device and non-linear conduction was observed during the OFF state of the device. So both electronic and ionic conductions exist in the fabricated

device during its switching operations. Further analysis is required, which is in progress, to deeply investigate the switching mechanism of the fabricated devices.

The retention endurance of ZrO_2 resistive switches were measured over 10^6 seconds as shown in the figure 2.12.

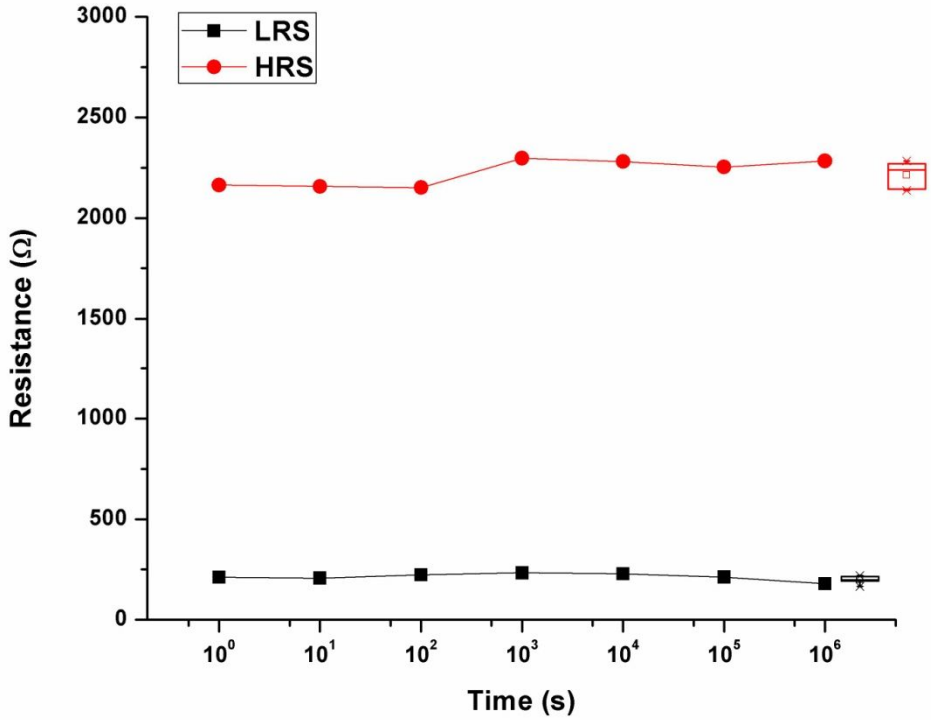

Figure 2.12 Retention time: Resistance Vs Time Stresses for the Printed Resistive Switch.

The resistive switches keep their ON/OFF ratio constant with no significant change in the resistance of the ON and OFF states of the device. The resistance distribution in both the ON and OFF states is depicted in the figure 2.11 as well. It was observed that the ON state was more stable than the OFF state of the resistive switch.

More than 30 devices were fabricated in consecutive two experiments; over 90% devices showed bipolar resistive switching. As mentioned earlier 67 nm thickness of ZrO_2 showed stable reversible resistive switching. This is due to the large particle size around 45 nm. Devices having less than 67 nm switching-layer thickness get short and larger than this thickness collapsed their resistive switching operation after

small number of voltage sweeps. So the operational probability of devices with the switching layer thickness of 67 nm is maximum.

2.1.4 Resistive Switching Mechanism in the Fabricated Switches

The switching characteristics among these sandwich structures are commonly attributed to the formation and dissolution of the active material bridges in the solid electrode. The reliable resistive switching characteristics in the ZrO_2 electrochemical cells have been contributed to a wide range depending upon chemical nature of electrode material, compliance current and stoichiometric properties of ZrO_2 layer. Different switching mechanisms have been suggested for the reversible transition behavior of ZrO_2 between its high resistance state (HRS) and low resistance state (LRS). Reproducible unipolar resistance switching in stoichiometric ZrO_2 films is ascribed to the contribution of the joule heating effect by the external current (Wu et al. 2007). Formation and rupturing of the reactive electrode is one of the popular mechanisms nominated to the stable bipolar resistive switching of ZrO_2-based resistive switches (Guan et al. 2008, Chen et al. 2010, Long et al. 2011, and Lin et al. 2012). Resistive switching memory effect of ZrO_2 films with Zr^+ implanted is explained by the trap-controlled space charge limited conduction (Liu et al. 2008). Charge trapping in the inherent defects of the ZrO_2 is also the admired mechanism operating these switches to show reversible resistive characteristics (Guan et al. 2007). ZrO_2 electrochemical cells are also researched being exhibiting reversible characteristics based on ohmic conduction and Frenkel-Poole emission (Lin et al. 2012, Liu et al. 2008, Guan et al. 2007, Liu et al. 2005, and Lin et al. 2006). Sufficient work has been done for this metal oxide to investigate its reversible resistive switching characteristics but quite a few co-relationships have been made among the concluded mechanisms with the chemical reactions take place inside the switching layer, modulation of electrical contacts with respect to the transition from one state to another and physical current conduction laws governing the charge transportation inside the solid electrolytes among different states of the device.

In this research work, resistive switching mechanism of the Ag/ZrO_2/ITO resistive switches have been analytically concluded and correlated with the electro-chemo-physic phenomenon behind its transition from one state to the other. Reversible

resistive switching of the Ag/ZrO_2/ITO devices has successfully been revealed in our previous work (Awais et al. 2013). The Ag/ZrO_2/ITO resistive switches were engineered by depositing the ZrO_2 switching layer with the thickness of 67 nm on the indium tin oxide (ITO) coated polyethylene terephthalate (PET) through electrohydrodynamic-atomization (EHDA) technique and the top electrode was established through Ag with the diameter of around 500 µm.

The fabricated devices showed reversible bipolar resistive switching behavior when biased the top Ag electrode of the device with the forcing node and grounding the bottom ITO electrode. Figure 2.13 shows the current voltage (IV) switching characteristics of the device with the double sweeping voltage of -3 to +3 with a current compliance of 5 mA.

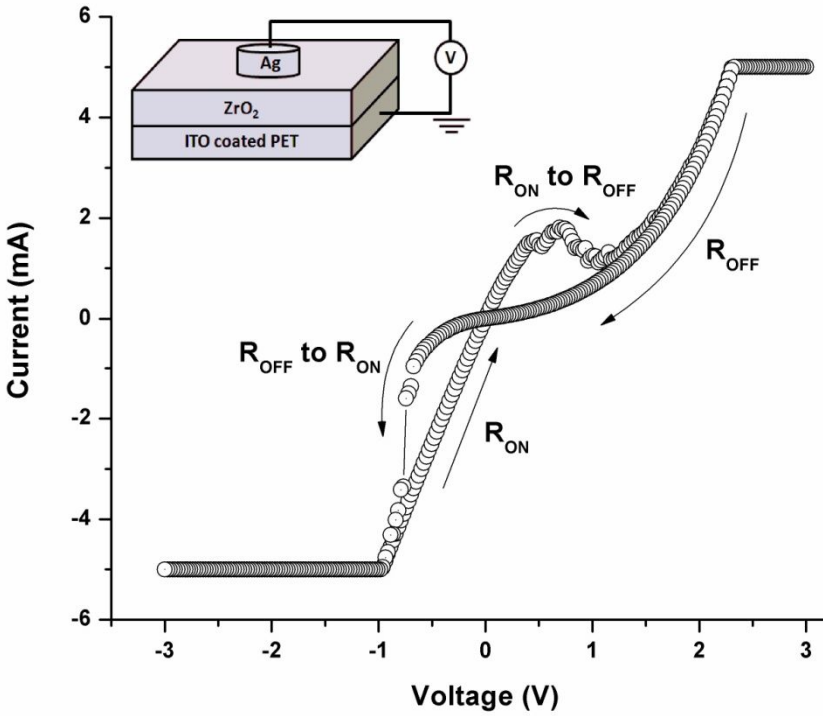

Figure 2.13 IV curve of the Ag/ZrO_2/ITO resistive switching device during the double voltage sweep of -3 V → +3 V. The inset shows the biasing of the device.

The pristine devices showed low resistance state when biased with the voltage source. The low resistance of the fabricated devices is attributed to the diffusion of the Ag

metallic electrode into ZrO_2 switching layer due to the annealing process of the device after the deposition of the top electrode. When the voltage was swept from -3 V to +3 V, the device initiated resetting around +0.5 V and completely changed its high state to low state about at +1 V as shown in figure 2.14.

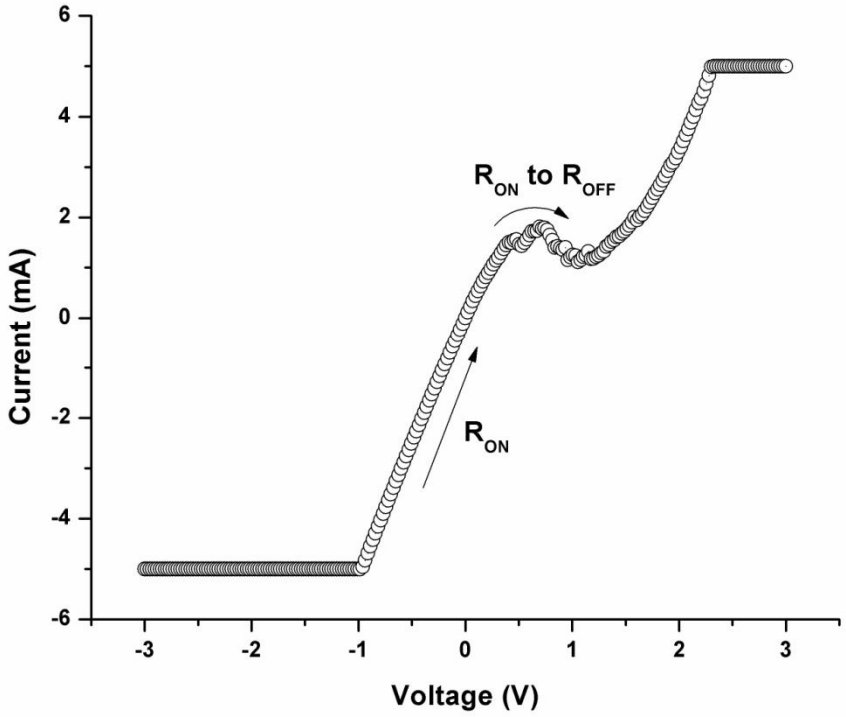

Figure 2.14 IV curve of the Ag/ZrO_2/ITO resistive switch during the voltage sweep of -3 V → +3 V.

The resetting process of the fabricated switch is attributed to the electrochemical dissolution of the diffused Ag particles into the ZrO_2 switching layer. The rupturing process started in the Ag metallic bridge into the weak points near ITO bottom electrode due to the chemically reactive nature of the Ag metal. Chemically the dissolution of the Ag filament can be described by the following oxidation process:

$$Ag \rightarrow Ag^{+} + e^{-} \qquad (2.1)$$

The Ag^{+} cations produced during the oxidation reaction remain there near the rupturing zone into the ZrO_2 layer. During the voltage sweep from -3 V → +3 V,

before around +0.5 V, the current was passing through the Ag metallic particles diffused into ZrO_2 layer that contributed the ohmic contact between top Ag electrode and bottom ITO electrode. But as the voltage exceeded +0.5 V towards positive side, electrochemical dissolution of the Ag filament occurred and eventually modulating the ohmic conduction into schottky conduction between of the electrodes. As the voltage was swept reversibly from +3 V → -3 V, schottky behavior continued to appear until around -0.7 V as depicted in figure 2.15.

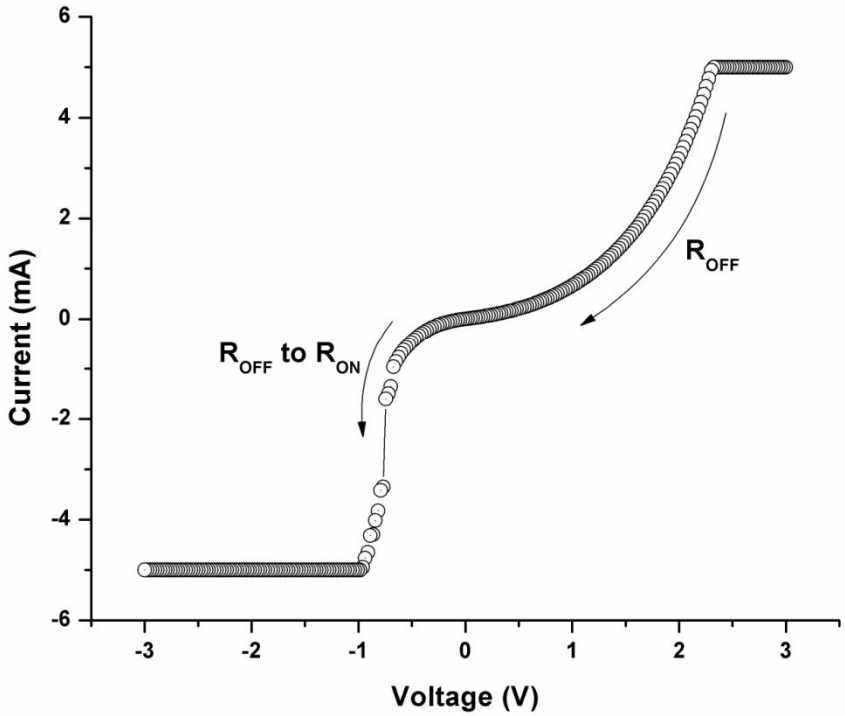

Figure 2.15 IV curve of the Ag/ZrO_2/ITO resistive switching device during the voltage sweep of +3 V → -3 V.

After -0.7 V the setting process appeared changing the HRS of the device into the LRS. The setting process came into picture by virtue of the reduction of the of the Ag^+ cations induced during the earlier oxidation reaction and now hosted through the electrons by the forcing (negative potential) node on the top electrode. The Ag^+ cations went through a reduction process eventually reforming Ag conducting filament in the ZrO_2 switching layer according to the following chemical reaction:

$$Ag^{+} + e^{-} \rightarrow Ag \qquad (2.2)$$

In this way the complete cycle of resetting and setting of the resistive switch accomplished. In the LRS state of the device, the conduction is through the Ag filament thus forming ohmic contact between top and bottom electrodes. While in the case of HRS of the fabricated device, the charge conduction is dissimilar to that of the LRS of device involving ZrO_2 nanolayer apart from the electrode material.

The analysis revealed that the HRS of the device is more complex desiring more intuitive insight to research the mysteries hidden in it. The schottky behavior exhibited by the device is different in the positive side of the voltage polarity as well as negative polarity on the top electrode. The asymmetric schottky conduction on both sides of the voltage polarity concluded that the rupturing of the Ag filament occurred only near the weak area at ITO bottom electrode. Electrochemical dissolution of the Ag conducting bridge should have led to a symmetric schottky conduction either in the case of rupturing in any point in the middle of Ag filament or between the Ag top electrode and filament itself. Thus electrochemical damage in the Ag filament modulated the ohmic contact into two opposite schottky barriers inside the ZrO_2 layer: one with Ag top electrode and ZrO_2 layer while the other between ITO bottom electrode and ZrO_2 layer. Thus asymmetric schottky behaviors on both sides of the polarity in the high resistance state led two opposite schottky barriers. The impendence of the reverse biased barrier dominated in the whole sweep from +3 V → -3 V. The above discussion directed to the schottky conduction above +1 V and in the reverse direction of the voltage polarity as well until reformation of the Ag conduction bridge between both electrodes.

2.1.5 Current Conduction Mechanism

The concluded current conduction mechanisms are validated through straight line fittings in IV graphs.

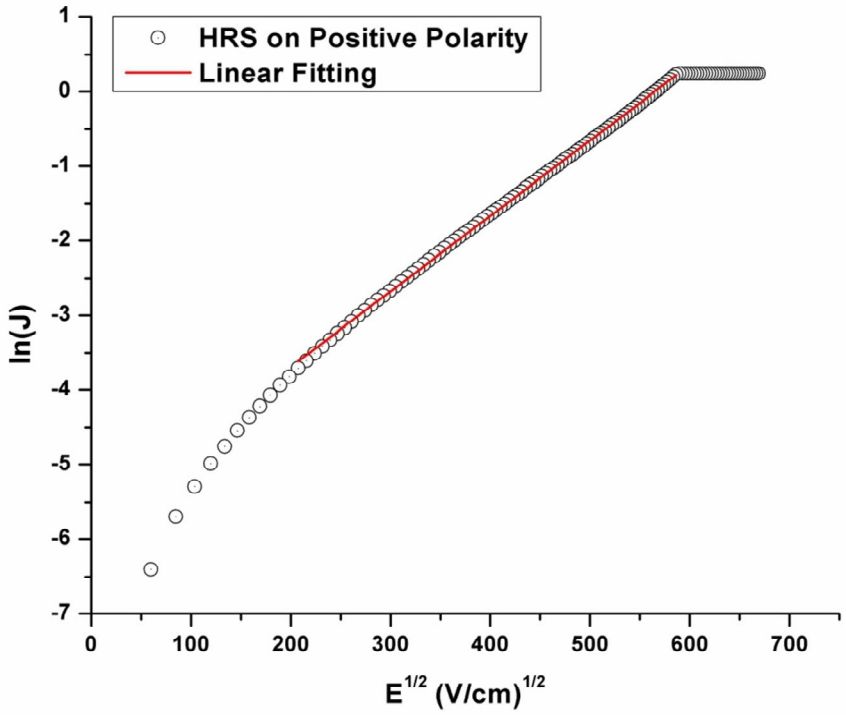

Figure 2.16 ln(J) vs. $E^{1/2}$ graph showing schottky emission in the HRS of the device during positive polarity.

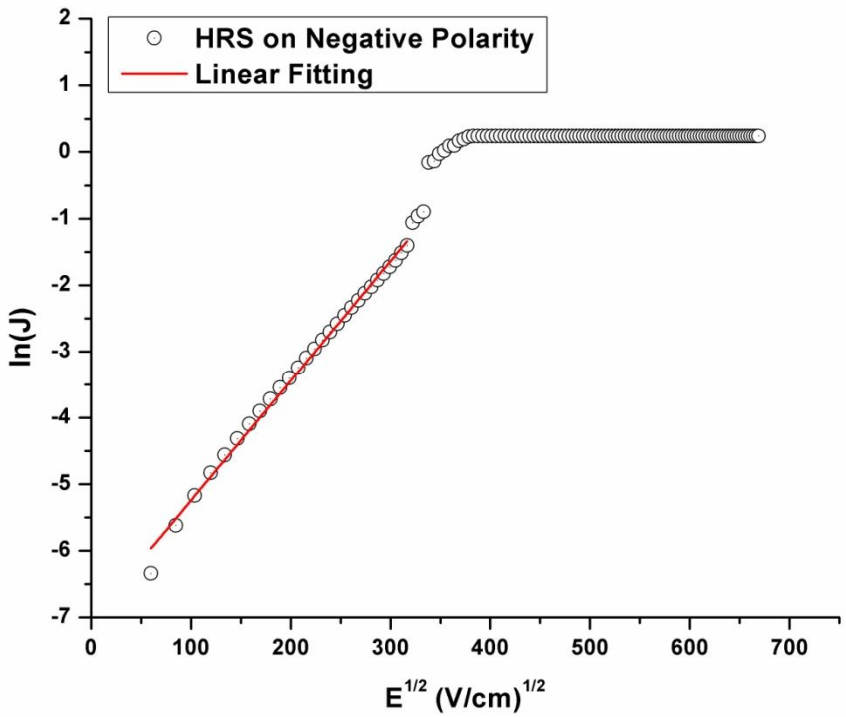

Figure 2.17 ln(J) vs. $E^{1/2}$ graph showing schottky emission in the HRS of the device during negative polarity.

Figure 2.16 and figure 2.17 show the HRS of device in positive and negative polarity respectively, almost fitted with straight lines through schottky emission model as follows described by the equation (2.3):

$$J = A^{\uparrow} \cdot T^{\uparrow 2} \exp[(-q(\varphi_{\downarrow}B - \beta E))/kT] \quad (2.3)$$

Where J is the current density, A^* is the effective Richardson constant, T is the absolute temperature, q is the electronic charge, φ_B is the barrier height, β is the schottky coefficient, E is the electric field and k is the Boltzmann constant. The graph between ln(J) vs. $E^{1/2}$ exhibited a linear relationship in the HRS of the device showing that the conduction mechanism in the HRS is governed by the Schottky emission model reinforceing the concluded conduction mechanism as described above.

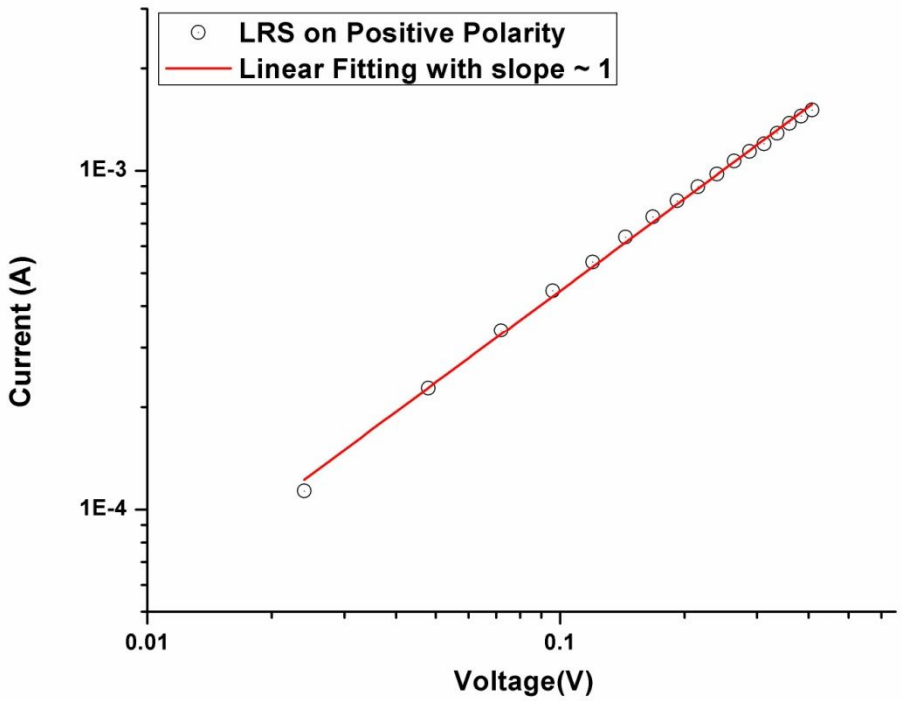

Figure 2.18 IV graph in double logarithmic scales showing ohmic current conduction in the LRS of the device during positive polarity.

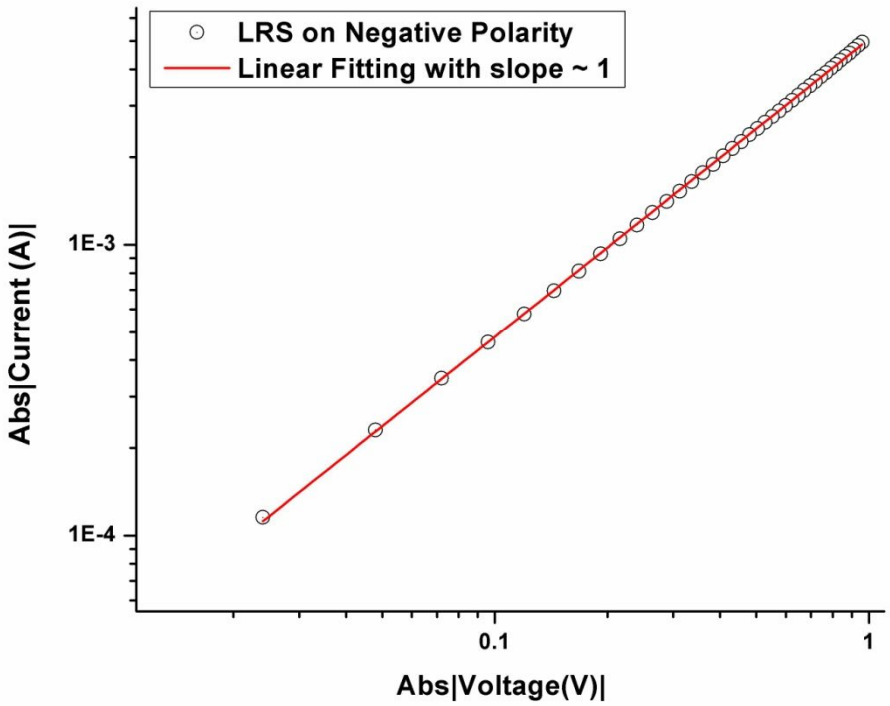

Figure 2.19 IV graph in double logarithmic scales showing ohmic current conduction in the LRS of the device during negative polarity.

Figure 2.18 and figure 2.19 elaborate the IV graphs in double logarithmic scales in the LRS of the device in positive and negative polarity respectively. Slope measurements remain around 1 through straight line fitting indicates the ohmic conductions as concluded above. The ohmic current conduction in the LRS of the device is due to the thermally excited electrons hopping from one isolated state to the next. In high state of the device, the current density J can be described by the following equation (2.4):

$$J = \frac{qn_0\mu V}{d} \qquad (2.4)$$

Where J is the current density due to Ohm's law, q is the electronic charge of the carriers, n_0 is the density of free carriers in thermal equilibrium, μ is the electronic mobility in the oxide, V is the applied voltage and d is the thickness of the switching layer.

2.2 ZrO_2 - Resistive Switches on Glass Substrate

Miniaturization of the electrode dimensions of resistive switch is as important as its thickness for the scalability of the device. A number of electrode deposition techniques, such as standard photolithography, focused ion beam nano-machining, electron-beam lithography and nano-imprint lithography, etc. are reported in the literature (Jung et al. 2004, Prodromakis et al. 2010, Li et al. 2003). Apart from the better performance of the existing technologies, they have some inherent limitations such as high fabrication cost, lack of suitable for mass production, long fabrication time and destruction of the molecules in organic and biological entities (Prodromakis et al. 2010, Xu et al. 2004, and Samarasinghe et al. 2009). Thus, a cost-effective fabrication technology is needed to address the shortcomings for the deposition of electrodes for crossbar resistive switching devices.

Electrohydrodynamic (EHD) printing is a direct writing deposition technique that takes short time to cover large area substrates at room temperature. EHD printing is capable of depositing high resolution patterns without complex processing of wet etching and harmful chemical processing. EHD printing requires the pumping of the liquid by the ink supply section through a nozzle. The nozzle is forced with the positive potential and the substrate is grounded. Pendent emerges at the orifice of the nozzle due to the continuous flow of liquid. The electrical stresses between the nozzle and substrate overcome the surface tension of the liquid. The pendent appearing at the orifice of the nozzle deforms into a conical shape and consequently a thin jet emerges at the orifice of the conical shape. EHD printing can be used in different printing modes: dripping, micro-dripping, spindle, multi-spindle, cone-jet and multi-cone jet etc but stable cone-jet mode is the most useful mode among the all. Printing in a cone jet or taylor-cone mode provides large neck down ratio which can be exploited to achieve nano-scale device dimension without miniaturization of the nozzle diameter. By adjusting the distance between nozzle to substrate, the jet emanating at the cone apex can be disintegrated into a number of small droplets under the effect of coulomb forces. The purpose of increasing the distance between nozzle to substrate fulfills two advantages: one is to the breakage of the jet into small droplets and other is to provide sufficient flight time to the small droplets so that

most of their solvent be evaporated before collected at the substrate. This feature of EHD technique could be used to atomize nano-layer over wide area. EHD printing is a versatile deposition technology that could be used for high resolution patterns and thin film deposition as well.

EHD jetting has successfully been used to deposit Ag electrodes for the memristor (Choi et al. 2011) in our previous work, but the feasibility of its use for the fabrication of the memristor-electrode with other conducting materials like ITO, Pt, Au, Al etc. for the fabrication of resistive switches (memristors) and for the fabrication of crossbar resistive switches with a structure of ITO/ZrO_2/Ag on a glass substrate has not been proven. This research work elucidates the engineering of a low-cost resistive switching device (memristor) with a structure of ITO/ZrO_2/Ag on a glass substrate by EHD printing. A colloidal solution containing ITO nanoparticles was used to deposit the ITO bottom electrode with EHD jetting because ITO is one of the promising candidates for a memristor-electrode conducting materials due to its transparent nature in visible light, improved reproducible functionality, reversible non-volatile memory characteristics and sensor application (Kavehei et al. 2011). ZrO_2 has been atomized with EHD printing as an active layer for resistive switching operations. Finally, a colloidal solution containing Ag nanoparticles was used to pattern the top electrode with EHD jetting to complete the crossbar memristive device.

The surface and morphology characterizations were carried out through microscopic images and SEM (scanning electron microscope) analyses. A B1500A Semiconductor Device Analyzer was used for the IV measurements. The fabricated device could be operated at different voltage levels less than ± 10 V with an excellent high ON/OFF ratio of 100000:1.

2.2.1 Experimental Details

The setup for EHD printing is shown in figure 2.20.

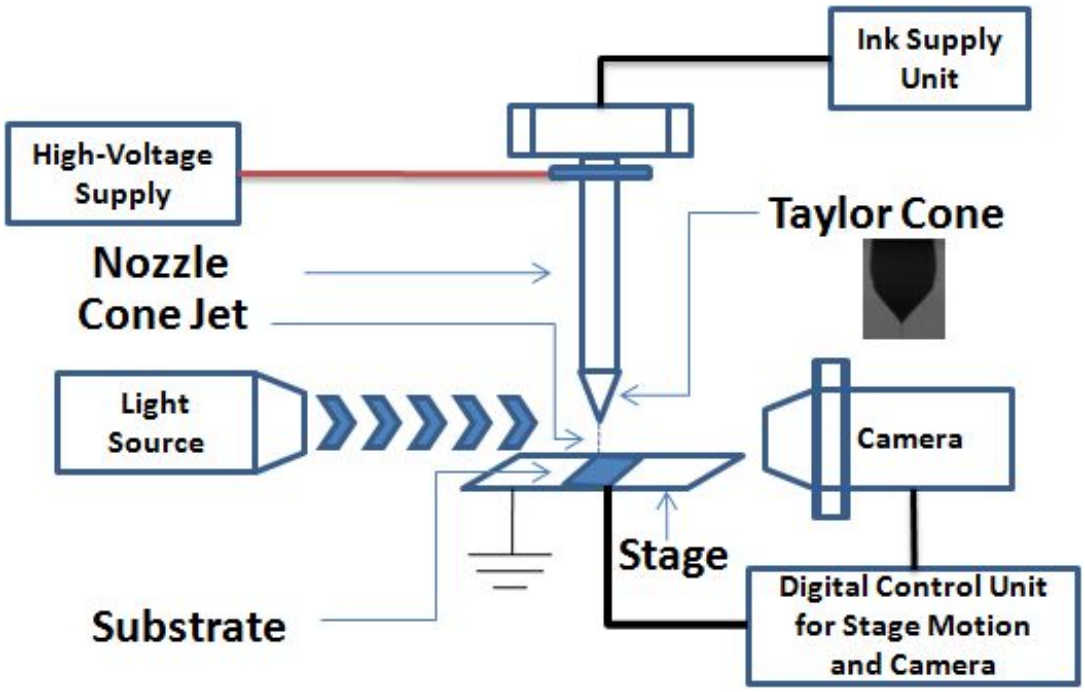

Figure 2.20 Experimental setup for EHD printing technology.

The setup includes a metallic capillary, a high-voltage power supply, an ink supply section, an X-Y stage control, a Z-axis control for the nozzle, a high-speed camera, a light source and a digital control unit to control and monitor all the operations [19, 33, 34]. ITO (in-lab developed) and commercially available Ag (NPK 02) nanoparticle-based inks were used for the bottom and the top electrodes respectively. A ZrO_2 colloidal solution, 5%, containing nanoparticles of less than 100 nm in size available at SigmaAldrich was used for the deposition of the active layer for the MIM structure. The ITO bottom and the Ag top electrodes were deposited through EHD jetting, and the active layer of ZrO_2, sandwiched between the electrodes, was deposited through an EHD atomization technique at normal room conditions.

The device fabrication process started with the pre-processing of the glass substrate with acetone, ethanol, followed by UV treatment for 5 minutes. First of all, the ITO bottom electrode was deposited on the glass substrate with EHD jetting; then, the ZrO_2 layer was atomized with an EHD atomization technique. Lastly, the Ag top electrode was patterned over the already-deposited ITO/ZrO_2 layers in a crossbar fashion. Curing was done after the deposition of each layer. To deposit each of the three layers for the crossbar memristive device, we put ink-containing nanoparticles in the ink supply unit (Hamilton, Model 1001 GASTIGHT syringe), and we pumped

the ink through a Teflon tubing to a metallic nozzle (Harvard 33G - internal diameter of 110 µm and outer diameter of 210 µm) by using a Harvard PHD2000 infusion pump. High voltage was applied on the metallic nozzle by using a NanoNC power supply, and the substrate was grounded throughout the experiment. A stage was used for the X-Y movement of the substrate, and a camera and light source were used to capture and monitor all the operations during the deposition processes. A digital control unit was used to control the X-Y movement of the stage and the image capturing and processing during the experiment. The pendent generated at the orifice of the nozzle deformed into a conical shape, called a taylor cone, due to the electric field between the tip of the nozzle and the substrate, and a thin jet emerged at the apex of the metallic capillary. To deposit ITO and Ag solutions for the bottom and the top electrodes, respectively, the jet was collected on the substrate before it disintegrated into small droplets, but to deposit an active layer of ZrO_2, the electrified jet was first disintegrated into small droplets by increasing the distance between the nozzle and the substrate so that small droplets containing nanoparticles were collected on the substrates. The experimental parameters are listed in Table 1.

The device fabricated using the experimental parameters given in table 2.1 in the current research work has larger physical dimensions due to the limitations of the experimental setup available to us.

Table 2.1 Experimental parameters for spraying the active layer and patterning the top & the bottom electrodes.

Parameters	**Printing (ITO)**	**Spraying (ZrO_2)**	**Printing (Ag)**
Flow Rate	**35 µl/h**	**35 µl/h**	**15 µl/h**
Voltage	**1.7 kV**	**2.3 kV**	**1.5 kV**
Nozzle Size	**110 µm**	**110 µm**	**110 µm**
Nozzle-to-Substrate Distance	**500 µm**	**3 mm**	**500 µm**
Curing Temperature	**450 °C**	**120 °C**	**120 °C**

A reduction in the nozzle diameter and a faster stage speed could provide high-resolution patterns (Park et al. 2007).

2.2.2 Layer Characterization of ZrO_2 Resistive Switches

Figure 2.21 shows a microscopic image of the ITO bottom electrode, and the width of the bottom electrode was measured to be around 100 μm.

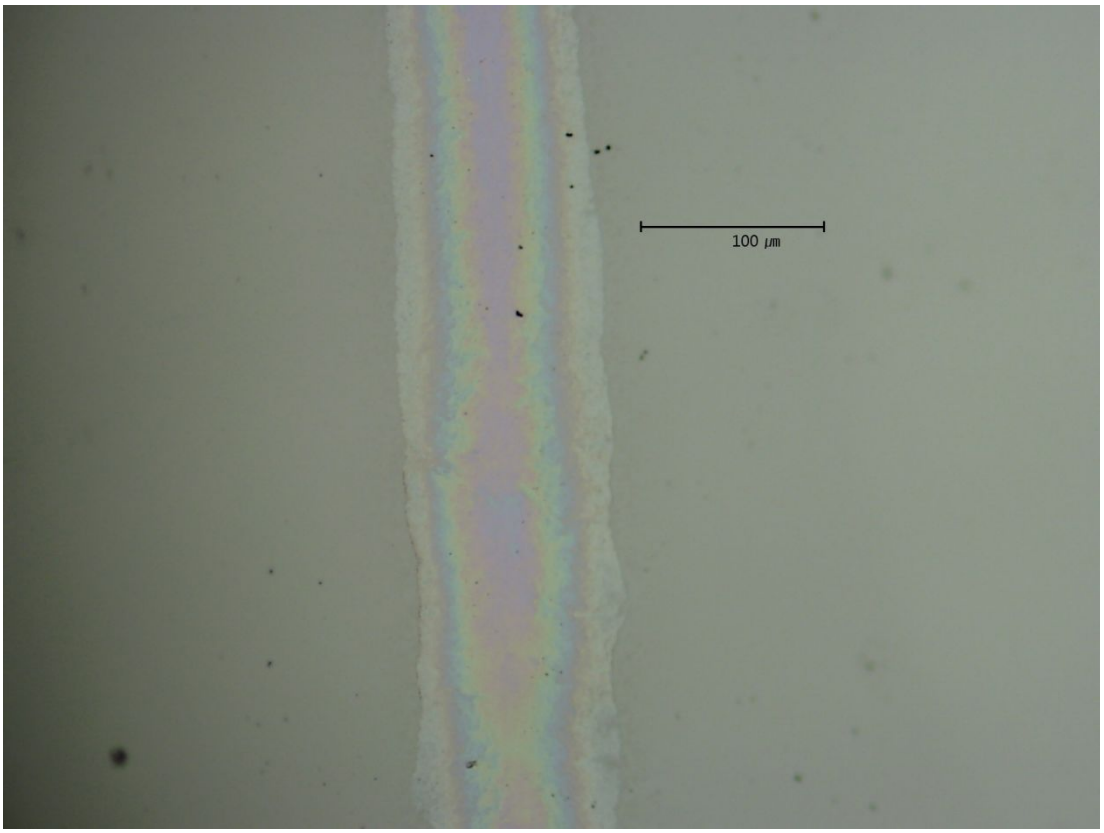

Figure 2.21 Microscopic image of the ITO pattern with a pattern width of around 100 μm.

Figure 2.22 shows a microscopic image of the top electrode, and the Ag top electrode width was measured to be around 100 μm. Both electrodes were quite smooth and sharp. The thickness of the electrode was measured to be around 670 nm.

Figure 2.22 Microscopic image of the Ag pattern with a pattern width of around 100 µm.

The surface morphology of the ZrO_2 layer was analyzed using a scanning electron microscope (SEM, Jeol JSM-7600F), as shown in figure 2.23. The film's thickness was measured by using a non-destructive, thin film-thickness machine (K-MAC ST4000-DLX) to be 110 nm.

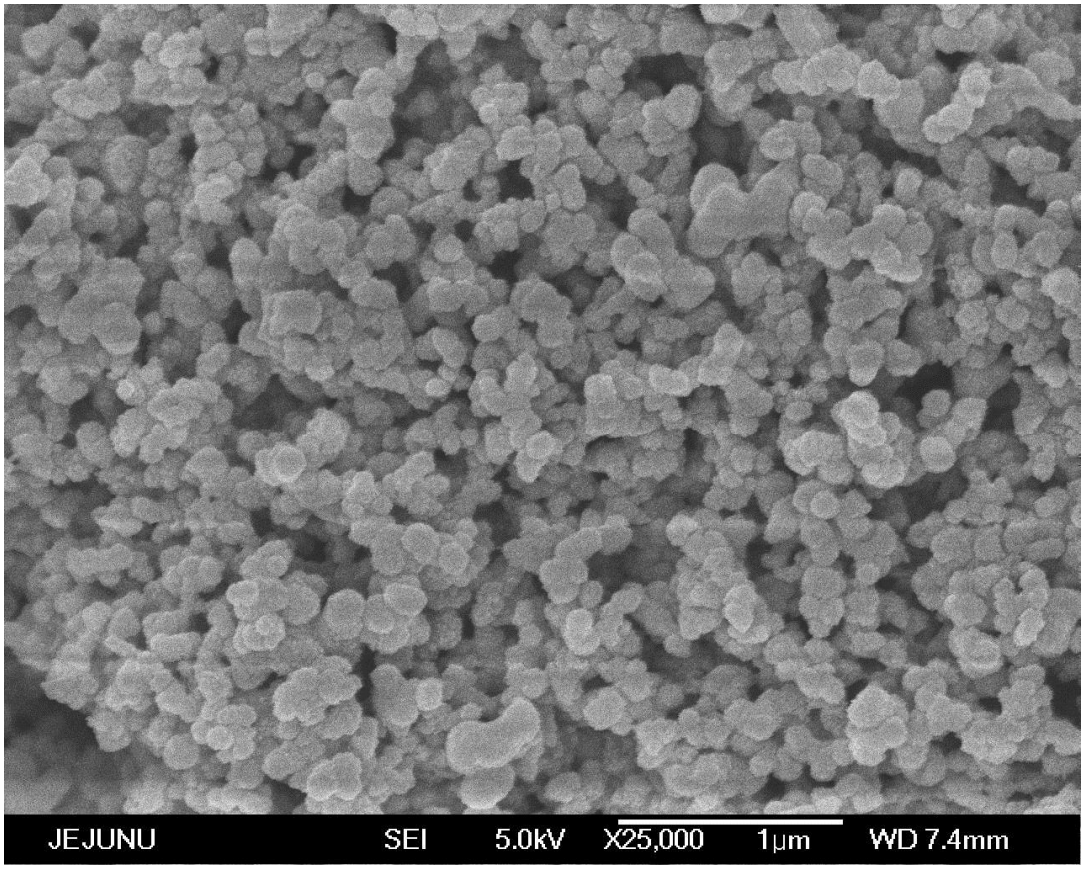

Figure 2.23 SEM image of the ZrO_2 active layer.

2.2.3 Resistive Switching Characterization

The upper inset in figure 2.24 shows the crossbar structure of the fabricated device with a biasing polarity during the IV measurements. A forcing voltage was applied to the top Ag electrode, and the bottom ITO electrode was grounded in all the measurements. Figure 2.24 demonstrates the initial forming process for stable reversible resistive switching as reported in the literature. The device started in a high resistance state (HRS) and electroformed around 10 V to switch into a low resistance state (LRS).

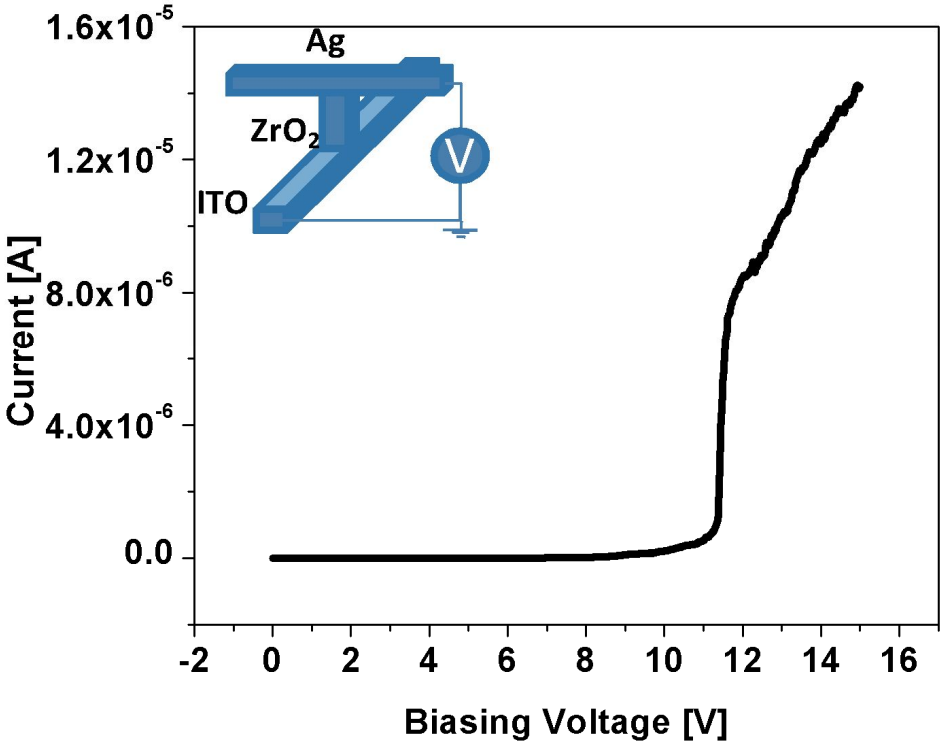

Figure 2.24 Forming IV curve. The sample was electroformed around 10 V. A crossbar device structure is shown in the upper inset with its biasing polarity.

Figure 2.25 shows a single cycle of the IV measurement. Voltage-amplitude-dependent bipolar switching was adopted for the reversible resistive switching for the fabricated device. After the initial electroforming process, the device was operated within ± 8 V. A voltage sweep was applied from + 8 V to – 8 V and was then swept back from - 8 V to + 8 V. During an on-state/LRS of the device, the resistance was measured to be around 1×10^6 Ω, and in an off-state/HRS of the device, the resistance was measured to be around 5×10^{11} Ω.

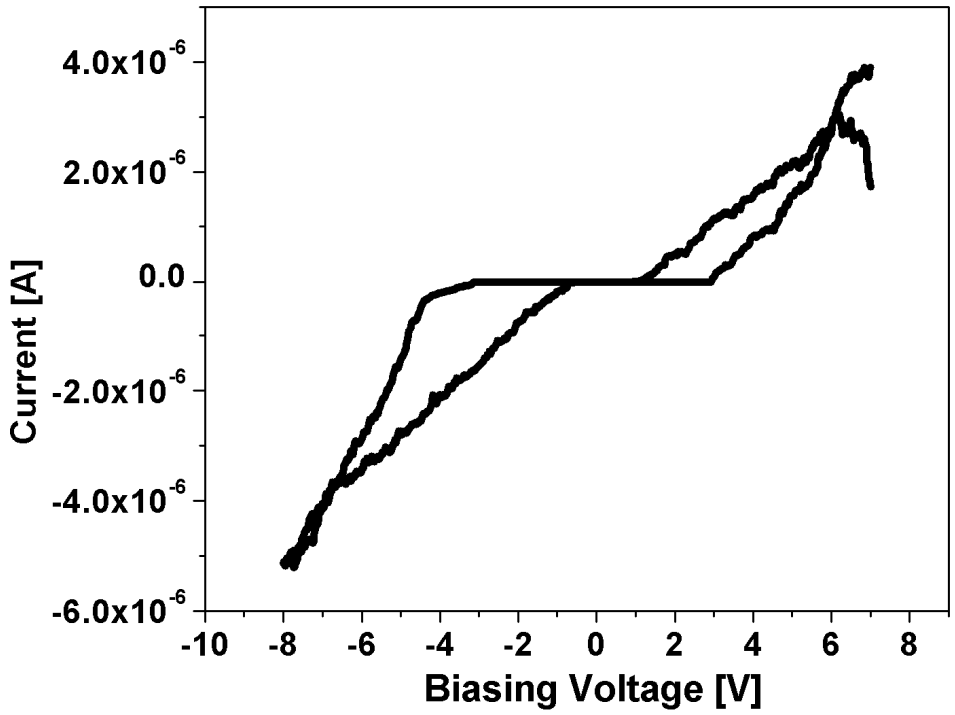

Figure 2.25 One cycle of the IV measurement. A double voltage sweep of + 8 V to - 8 V was applied to the crossbar device.

Figure 2.26 shows another IV measurement of the same sample in which a double voltage sweep of + 4 V to - 4.5 V was applied, and the device was observed to show stable reversible resistive switching. Thus, we can conclude that the device can be operated at multiple voltage levels with stable reversible resistive switching. Multiple voltage sweeps were also taken to check it robustness and consistence. The inset of the figure 2.26 shows consistent resistive switching for multiple voltage sweeps.

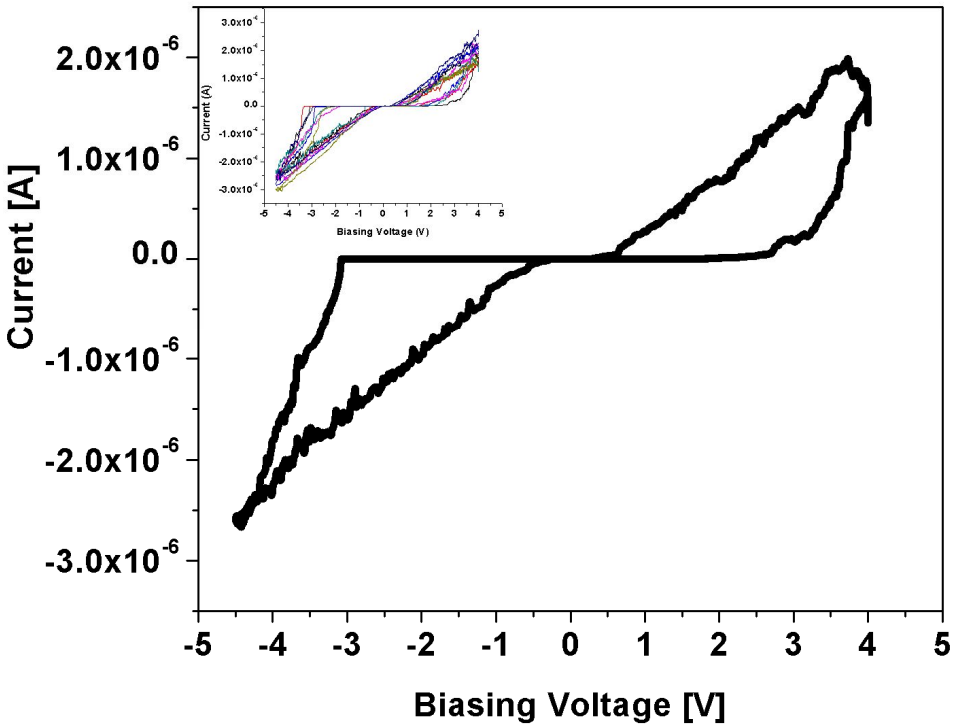

Figure 2.26 One cycle of the IV measurement curve for the same device. A double voltage sweep of + 4 V to – 4.5 V was applied to examine the IV curves. The inset shows multiple, reproducible, reversible, resistive switching cycles.

Figure 2.25 and figure 2.26 show incremental changes in its resistance. The incremental setting (HRS to LRS) and resetting (LRS to HRS) mechanisms in the device offer an incredible advantage in that the device can be used for neuromorphic applications. Such devices can be used in integrated analog memristor-CMOS neuron circuits that can map a number of synaptic functions such as spike timing dependent plasticity (STDP) (Lu et al. 2011 and Jo et al. 2010).

Figure 2.27 shows the resistance in the on- and the off-state of the device versus the number of switching cycles. The plot shows consistent reversible resistive switching behavior with multiple voltage sweeps. The resistance during the on-states of the device was within the range of 2×10^6 Ω to 6×10^6 Ω and during the off-states of the device, it was within 2×10^{11} Ω to 8×10^{11} Ω. The ON/OFF ratio was observed to be around 100000 : 1. This high ON/OFF ratio provides a sufficiently high margin between the on- and the off-state of the device. The device was operated with over

100 multiple voltage sweeps for different voltages and exhibited reproducible resistive switching.

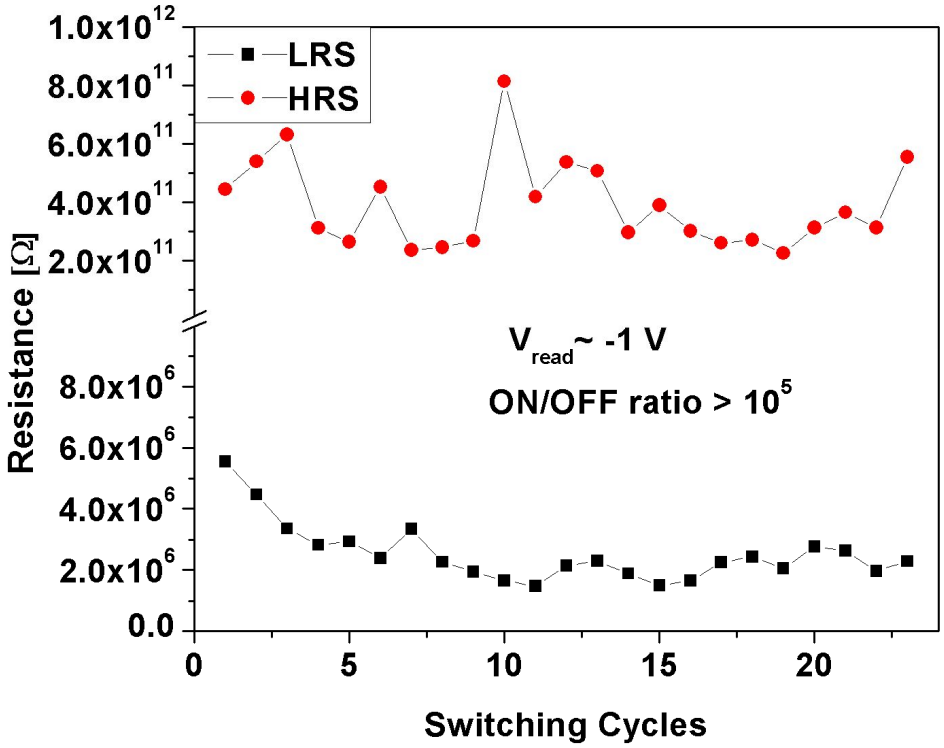

Figure 2.27 Resistance vs switching-cycle graph. The plot indicates a high ON/OFF ratio of 100000 : 1. The reading voltage was around - 1 V for the measurements.

The retention time was measured to be over 3 days, with the device showing unchanged resistance. A reading voltage of around - 1 V was used to measure the resistance of the device in the on- and the off-states.

2.3 ZrO_2 - Resistive Switches on Flexible Substrate

Cost-effectiveness and mechanical flexibility of flexible electronics have opened up new vistas in electronics industry. The role of flexible electronics has been advancing day by day in our daily life replacing its rigid substrate counterparts in some of the applications. Before the invention of memristor (Memory Resistor), transistor was the only basic switching element available with us for flexible electronics applications.

Different fabrication technologies have been used for the fabrication of a flexible memristor or flexible resistive switching memories. Thermal and e-beam evaporation through shadow mask have been used for the deposition of electrodes and for the active layer deposition a number of processes have been deployed including spin-on sol-gel process, radio-frequency magnetron sputtering and spin coating (Hackett et al. 2009, Lee et al. 2009, Jeong et al. 2010, Hong et al. 2010 Wang et al. 2011, and Wang 2012). In some literature device electrodes were deposited using radio-frequency sputtering and lift-off process and the active layer was fabricated by plasma-enhanced atomic layer deposition process (Kim et al. 2011). The previous literature reveals that different fabrication technologies have been employed for the complete fabrication of the flexible device: device electrodes and active layer deposition. Furthermore some processes have inherent limitation: thermal evaporation is a costly process, not suitable for many compounds with poor material usage and requires heat generation in the deposition system thus producing harmful radiation effects where as magnetron sputtering process is also a high capital cost process and requires long time deposition processing. These factors limit the production of less expensive flexible memristors or resistive switch. So a demanding technology is needed and this consequently has opened the gate to explore new technologies for the cost effective memristor fabrication.

The current research work elucidates the engineering of a flexible memristor by using EHD printing technology: jetting mode of EHD printing has been used to deposit top and bottom electrodes and its atomization mode has been deployed for the thin film deposition between the top and bottom electrodes to complete the MIM sandwich structure on a polyimide (PI) substrate. Silver (Ag) metal has been used for both the top and bottom electrodes and ZrO_2 has been used as an active layer for resistive switching operations.

The fabricated device has been morphologically characterized by microscopic images, Scanning Electron Microscope (SEM) and Focused Ionic Beam (FIB) analysis. X-ray Diffraction (XRD) analysis was also carried for the ZrO_2 layer. The device has been electrically characterized with the semiconductor analyzer to evaluate the Current-Voltage (IV) characteristics in order to illustrate the memristive

behavior. Physical endurance of the device has been tested, after being physically flexed, for flexible electronics applications. The researched device can be used in flexible resistive non-volatile random access memories and can be used in binary switching purposes as well. So the current research provides a low cost, low power, portable and flexible non-volatile memory and having the potential to revolutionize the electronic industry regarding switching operations.

2.3.1 Experimental Details

The system used for the device fabrication is shown in figure 2.28. The system includes metallic capillary, high voltage power supply, ink supply section, X-Y stage control, Z-axis control for nozzle, high speed camera, light source and digital control unit to control and monitor all the operations during the fabrication process.

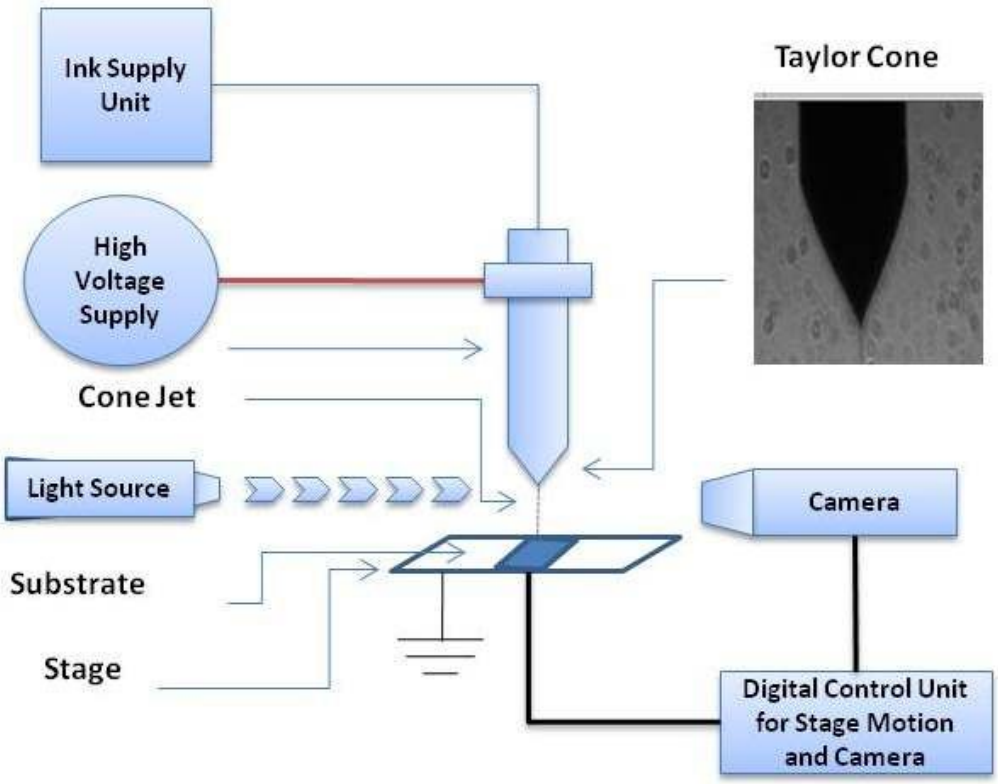

Figure 2.28 Experimental setup for the EHD printing.

The memristor's fabrication process was started with the pre-processing of PI substrate with ethanol and then ultra violet treatment around 5 min. Commercially available Ag nanoparticle based solution from Harima Company (60 wt %) was used

for the top and bottom electrodes and dispersion of ZrO_2 commercially available at Sigmaaldrich (5 wt %) was used to deposit the active layer for the device. The device was fabricated in a three layer cross-bar structure as shown in figure 2.29.

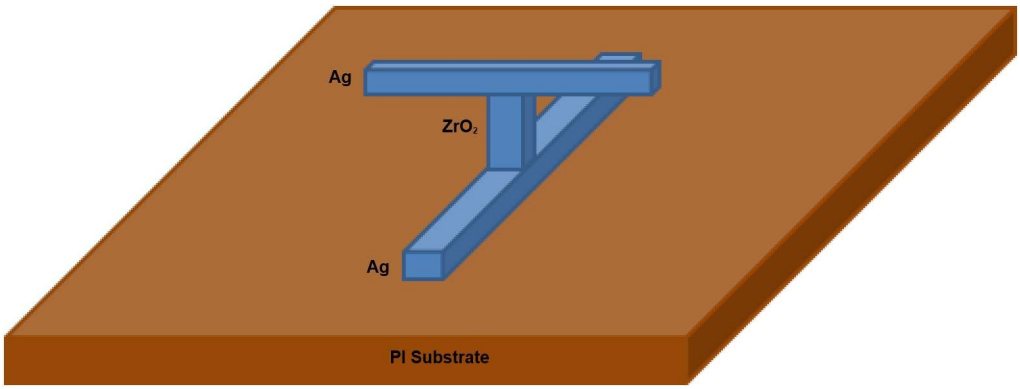

Figure 2.29 Cross-bar structure of Ag/ZrO_2/Ag device on PI substrate.

The Ag bottom electrode was deposited with the jetting of EHD printing in cone jet mode on the PI substrate. To deposit the oxide layer, ZrO_2 was atomized with EHD printing on the bottom electrode. The atomization of the ZrO_2 was done by adjusting the distance between the nozzle and the substrate. Comparatively large distance between the nozzle and the substrate broke the continuous jet into small number of droplets. Most of the solvent in these small droplets was evaporated during their flight time before impinging on the substrate. Consequently a high quality thin layer was deposited on the bottom electrode. Finally the top electrode was deposited through EHD printing (similar to the bottom Ag electrode) on PI/Ag/ZrO_2 in a cross-bar fashion to the bottom Ag electrode to complete the MIM structure as shown in figure 2.29.

The device dimension could be controlled by controlling the width of the bottom and top Ag electrodes and the thickness of the sandwich ZrO_2 layer. The width of electrodes can be increased or decreased with increasing or decreasing the flow rate of the solution containing nanoparticles and stage speed of the system. The thickness of the switching layer can be increased or decreased with increasing or decreasing the spray time. The stage speed during the deposition of both the top and bottom electrodes was 5 mm/s. The spray time for the ZrO_2 layer was around 3 min. The experimental parameters for spraying the active layer with ZrO_2 ink containing

nanoparticles and patterning the bottom and top electrodes with Ag ink containing nanoparticles are given in table 2.2. After the deposition of each layer the sample was subjected to heat treatment.

Table 2.2 Experimental parameters for patterning the top and bottom electrodes (Ag) and spraying the active layer (ZrO_2) for the MIM structure.

Parameters	Bottom Electrode Patterning (Ag)	Active Layer Spraying (ZrO_2)	Top Electrode Patterning (Ag)
Flow Rate/ Pressure	0 kPa	100 µl/h	0.3 kPa
Voltage	1 kV	~ 9 kV	1.25 kV
Nozzle Size	30 µm	410 µm	30 µm
Nozzle to Substrate Distance	~ 200 µm	5 mm	~ 200 µm
Curing Temperature	150 °C	150 °C	150 °C

2.3.2 Layer Characterization of ZrO_2 Resistive Switches

The as-fabricated memristor was characterized to check the dimensions and surface morphology of the device. The deposited width for the conducting electrodes was around 100 µm as analyzed by the microscopic as shown in figure 2.30.

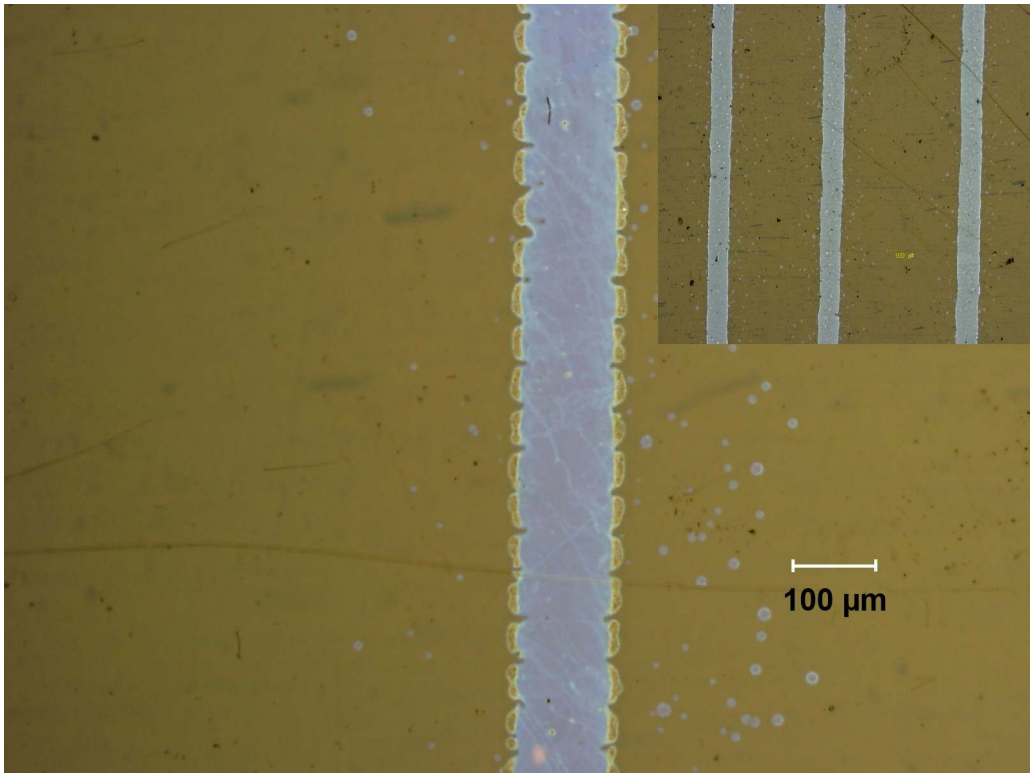

Figure 2.30 Microscopic image of the memristor electrode (Ag) deposited with EHD jetting on PI substrate. The inset of the figure shows the array of 3 Silver patterns.

Small irregular shapes (almost squares) came into sight along the deposited electrode through EHD technique. These shapes are formed due to the basic attributes of the EHD process as the jet impinges a flat surface it undergoes two processes similar to an impinging droplet: initially it spreads to a maximum width and subsequent motion which dissipates the impact inertia by viscous effect and then retracting process emerges resulting from the evaporation of the solvent (Poon 2002 and Kim and Chun 2001). The inset of figure 2.30 shows the array of the Ag electrodes on the flexible substrate that depicts the uniformity of the deployed EHD printing technique. The achieved dimensions of the cross-bar printed device were around 100 µm × 100 µm.

To check the surface morphology of the ZrO_2 layer on the PI flexible substrate, the sample was analyzed through SEM system (JSM-6700F, JEOL Ltd, Japan) with the operating voltage of 40 kV. The SEM analysis shows smooth surface of the deposited ZrO_2 sample after sintering temperature of 150 ºC. The average grain size was observed to be 45 nm as shown in figure 2.31.

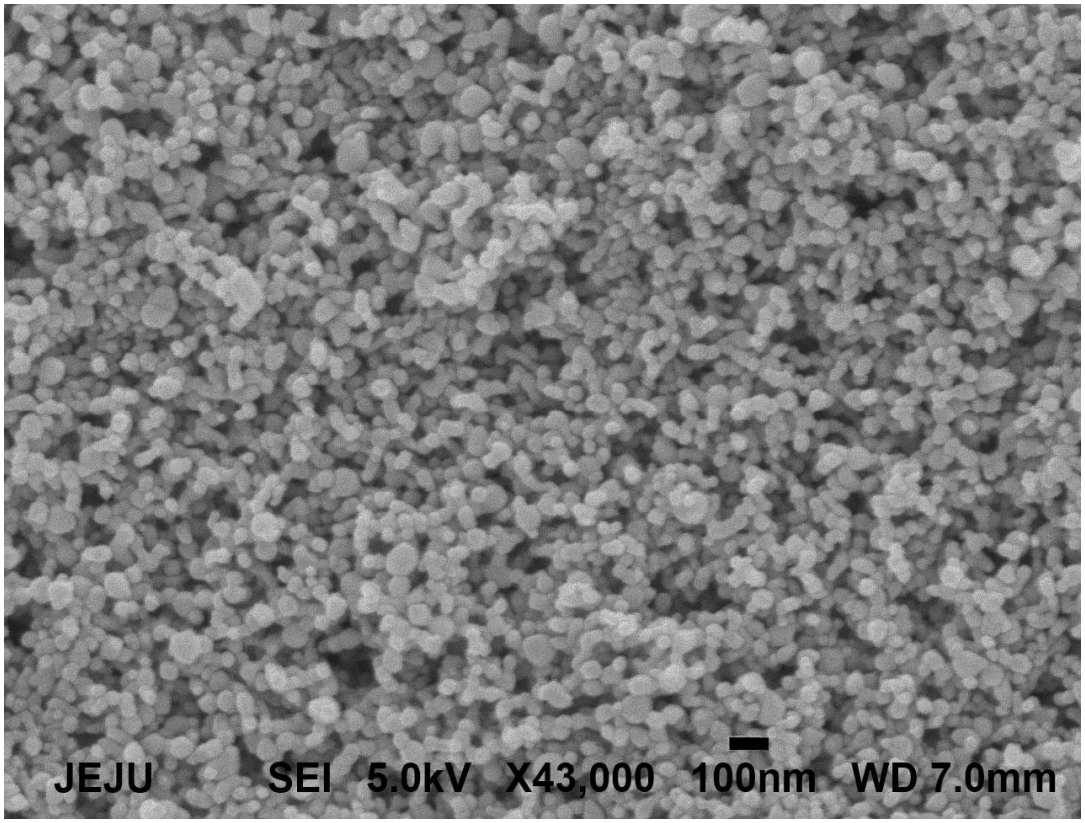

Figure 2.31 SEM image of the ZrO_2 active layer on the PI flexible substrate after sintering temperature of 150 ºC.

The XRD analysis of the deposited sample on the PI substrate was performed with the X-ray diffractometer system (D/MAX 2200H, Bede 200, Rigaku Instruments C, Japan) using a Cu K_α radiation source of wavelength (λ=1.541). All the diffraction peaks of deposited sample after sintering at 150 ºC are indexed to monoclinic and tetragonal phase of zirconium oxide as shown in figure 2.32. The reported diffraction peaks of ZrO_2 are coinciding with the reported literature (Jayakumar et al. 2011). The substrate (PI) peak appears in the angle (2θ) range of 15 to 25.

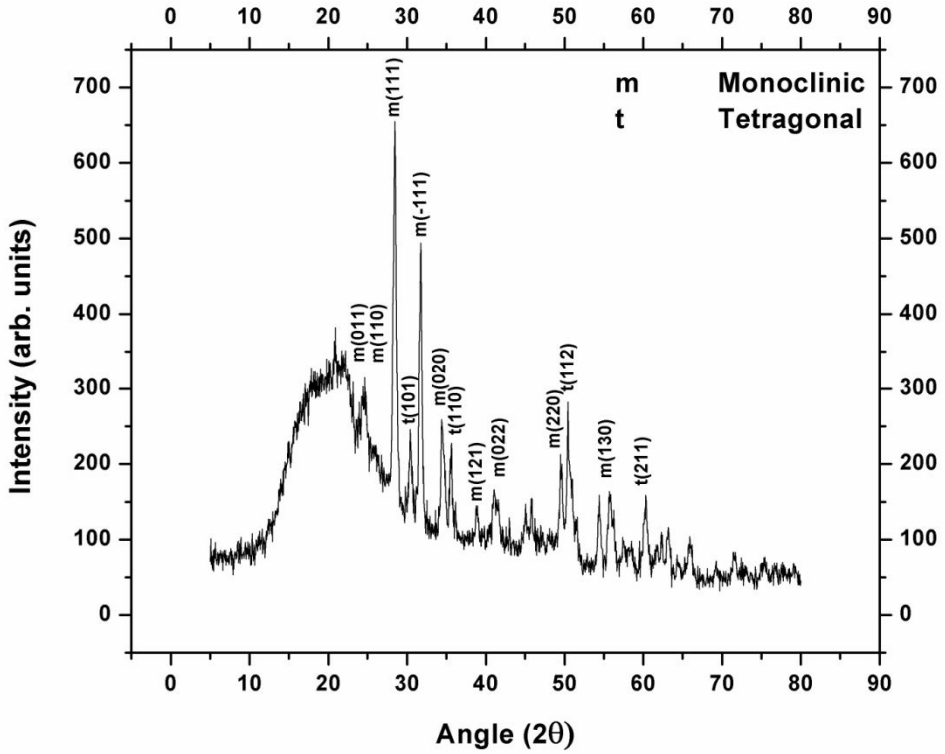

Figure 2.32 XRD analysis of the ZrO_2 active layer on the PI flexible substrate after sintering temperature of 150 ºC.

High Resolution Scanning Ion Microscope SMI2050 Focused Ion Beam System was used to check the cross-sectional view of the device with the main chamber pressure of 1.5×10^{-4} Pa and ion acceleration voltage of 30 kV. FIB process of scanning was deployed by three steps: vapor deposition of carbon particles, slope cutting of the active area at the angle of 45° and lastly etching the active area with gallium ions. FIB image as shown in figure 2.33 shows smooth three layered structure of the device. The average thicknesses of the bottom electrode, sandwich layer and top electrode were around 230 nm, 680 nm and 420 nm respectively.

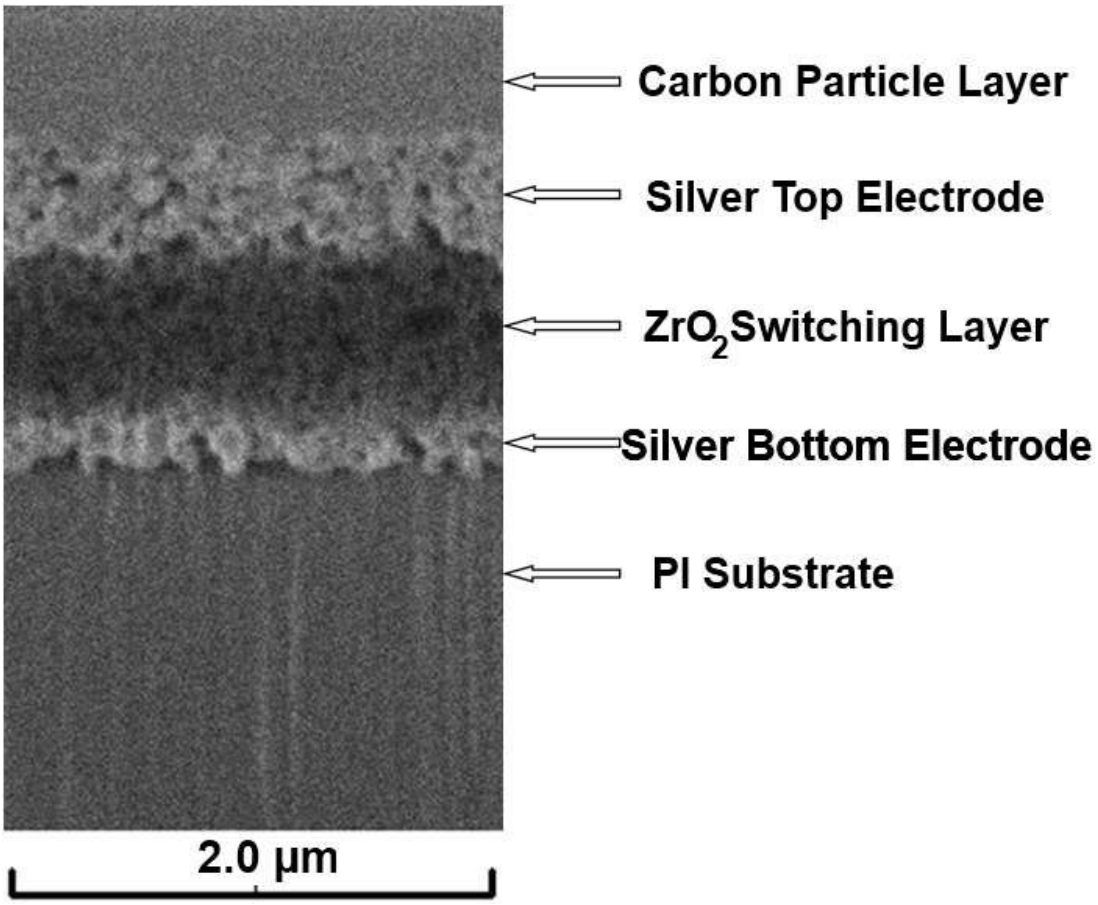

Figure 2.33 Figure shows the FIB image for the cross-sectional view of the MIM structure on PI substrate.

2.3.3 Resistive Switching Characterization

The IV measurements of the depostited sample were performed with Agilent B1500A Semiconductor Device Analyzer. During all the IV measurements the sample was forced with the top electrode while the bottom electrode was grounded as shown in the inset of figure 2.34.

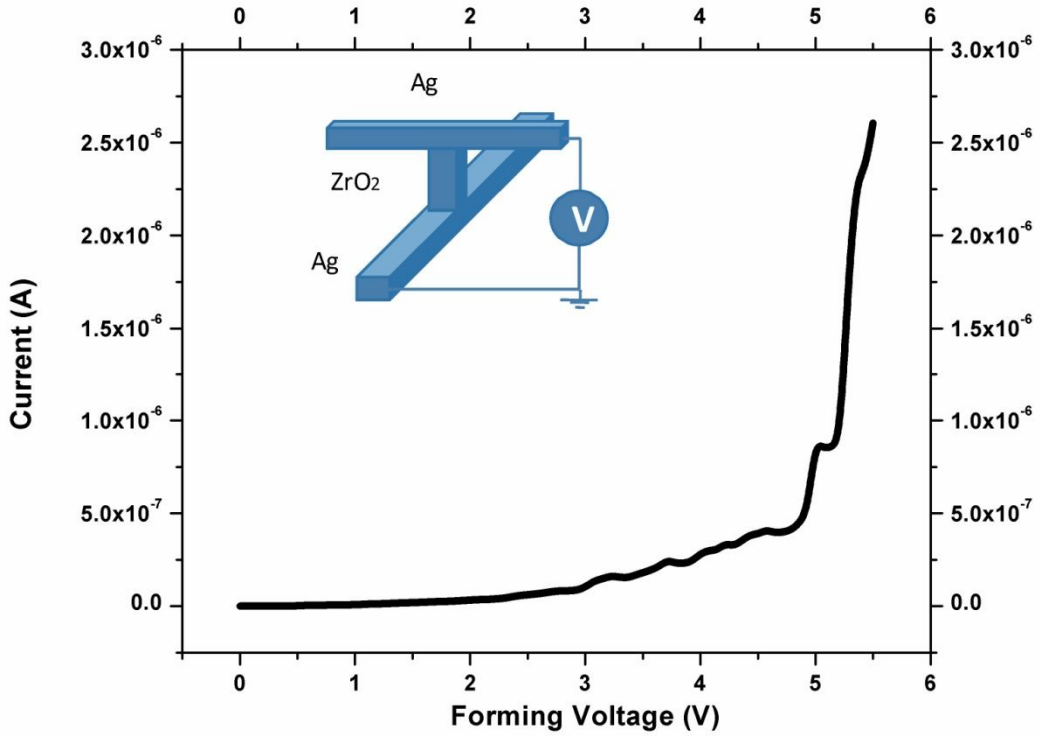

Figure 2.34 The figure shows the forming IV curve of the device. The device was completely electroformed at around +5.5 V. The inset of the figure illustrates the cross-bar structure with its biasing polarity during IV measurements.

Before operating the device in a reversible bipolar resistive switching (BRS) the device was electroformed. The initial forming voltage was applied on the top electrode by sweeping the voltage from 0 V to +6 V without setting any current compliance as shown in figure 2.34. During electroforming process the device started operating in the high resistance state (HRS) or OFF-state with an average resistance of 7.25×10^9 Ω and then fluctuating into low resistance state (LRS) or ON-state from +3 V to +5 V. The complete forming process was observed at around +5.5 V with an average resistance of 1.28×10^7 Ω as shown in figure 2.34.

After initial electroforming process, double voltage sweeps of ± 3 V were applied to the device to observe the bipolar reversible switching as shown in figure 2.35.

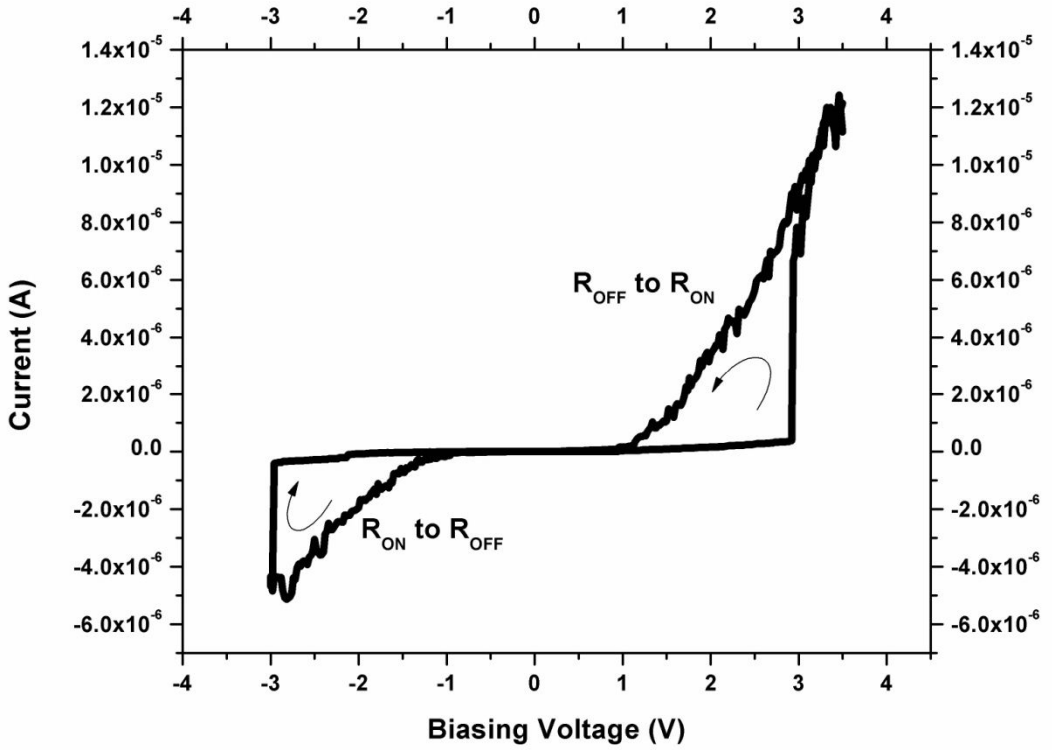

Figure 2.35 One cycle of IV measurement of the flexible memristive device. A double voltage sweep of ±3 V was applied to the cross-bar device. The upper loop shows the SET process and lower loop illustrates the RESET process of the device.

The double voltage sweep was applied from +3 V to -3 V. During the 1st half (+3 V to -3 V) of the voltage sweep the device was in the LRS and in the 2nd half (-3 V to +3 V) of the voltage sweep the device was in the HRS. The resistance of the device during the ON-state was around 5×10^5 Ω and during the OFF-state it was observed to be around 1×10^7 Ω. The reading voltage used to calculate the resistance during the analysis of the above discussed sweep was 1.75 V. The SET process from OFF-state to ON-state was observed at around +3 V while the RESET process from ON-state to OFF-state in the fabricated device was indicated at -3 V. The bipolar reversible resistive switching operation analyzed during the operation of the fabricated device is the indicative of the basic memristive or resistive behavior. The distribution of the ON-state of the device is wider than the OFF-state as indicated in figure 2.35. The positive bias cycle of the pinched hysteresis loop is larger than that of the negative bias cycle.

The robustness of the as fabricated device is shown in figure 2.36. The figure shows the behavior of the device resistance against multiple voltage sweeps. The device was forced over 100 double voltage sweeps. The graph indicates a sufficient large OFF/ON ratio of the device larger than the two orders of magnitude by maintaining a wide gap between its ON-state and OFF-state of the device during its reversible switching operations. The reading voltage for the graph is 1.75 V. LRS is more stable than the HRS of the device.

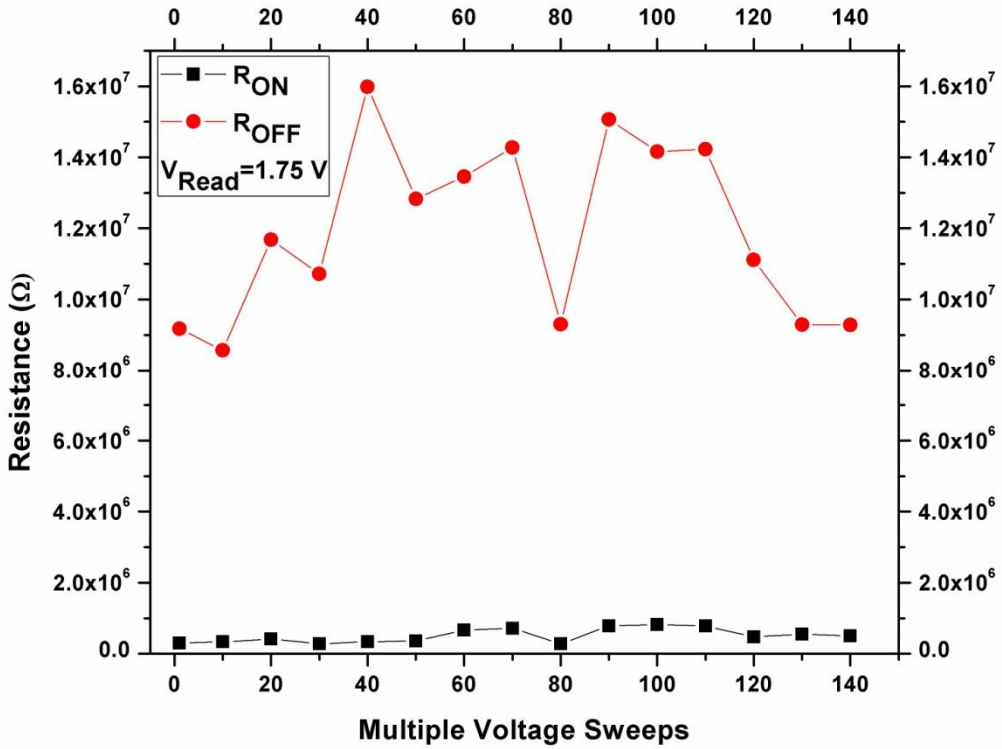

Figure 2.36 Resistance vs multiple switching sweeps graph. The plot indicates a high OFF/ON ratio of 100 : 1. The reading voltage was around 1.75 V for the measurements.

The device could be flexed to examine its robustness and to check its feasibility for the flexible electronics applications. The fabricated device was flexed from flat to almost semi-circle as shown in figure 2.37. The device showed stable bipolar switching operation even over 500 times physical flexes. Over 500 time physical flexes the change in the resistance in the ON-state of the device was observed from around 5×10^5 Ω to 3.6×10^6 Ω and in the OFF-state of the device the resistance change was observed from around 1×10^7 Ω to 3.3×10^8 Ω. The reading voltage of

1.75 V was used to measure the current after each bending state. The as-fabricated device kept its OFF/ON ratio as 1:100 over 500 physical flexes.

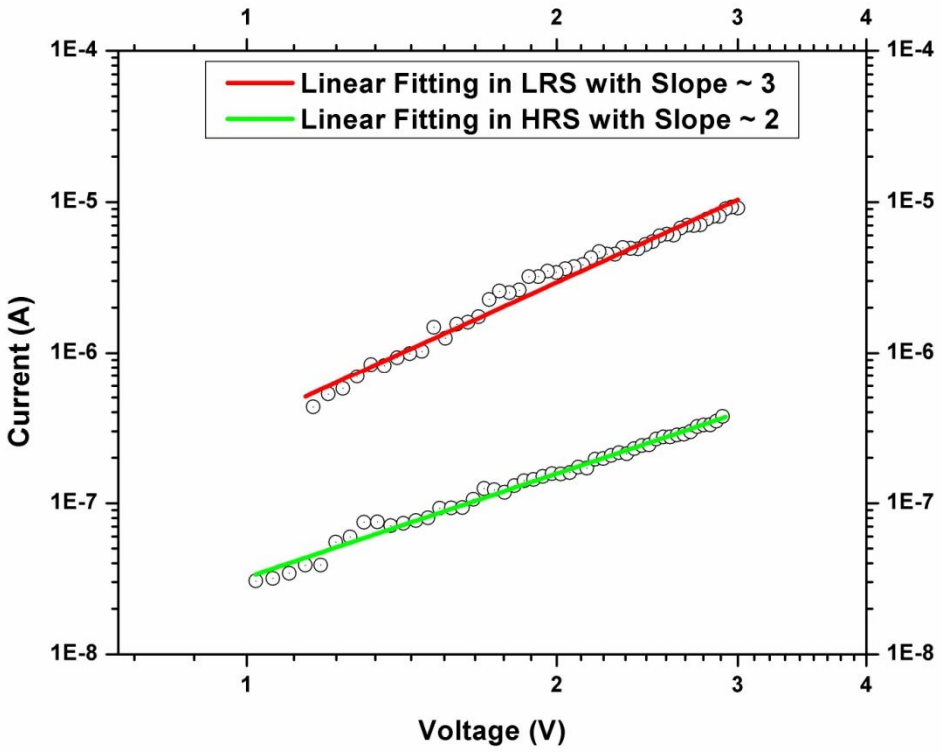

Figure 2.37 IV data and linear fits for the HRS and LRS of the flexible memristive device.

Apart from the need of deep investigation to analyze the switching mechanism, the results presented in the above discussion prove that the current research work provides an alternative to fabricate fully flexible printed ZrO_2 memristor for the flexible electronics applications. So EHD printing process has full potential to be used for flexible memristive devices even at nano-scale by improving the experimental setup.

2.3.4 Current Conduction Mechanism

To find the current conduction mechanism for the HRS and LRS of the device, the IV graph in figure 2.35 has been redrawn in double log scale. The linear lines have been fitted in the IV characteristics for the HRS and LRS of the device as shown in figure 2.38. Some non-linearity appeared because of the non-ideal measurement

conditions. The slopes in HRS and LRS are calculated to be around 2 and greater than 2 (around 3) respectively that shows that the current conduction in the device is dominated by the space charge limited current (SCLC) conduction in the HRS and trap charge limited current (TCLC) conduction during LRS of the device (Bajpaia et al. 2010). The BRS phenomenon in the case of symmetric devices (same top and bottom electrodes) is probably due the formation and rupturing of the multiple conductive paths only at the top interface at different locations not in the entire active layer of the device as indicated in the literature (Jeong et al. 2010) or the BRS phenomenon can be attributed to the change of trap distributions in the top interface layer originated from the motion of oxygen ions due to the biasing voltages (Kim et al. 2011). Further investigation of the switching mechanism of the device is in progress for future work.

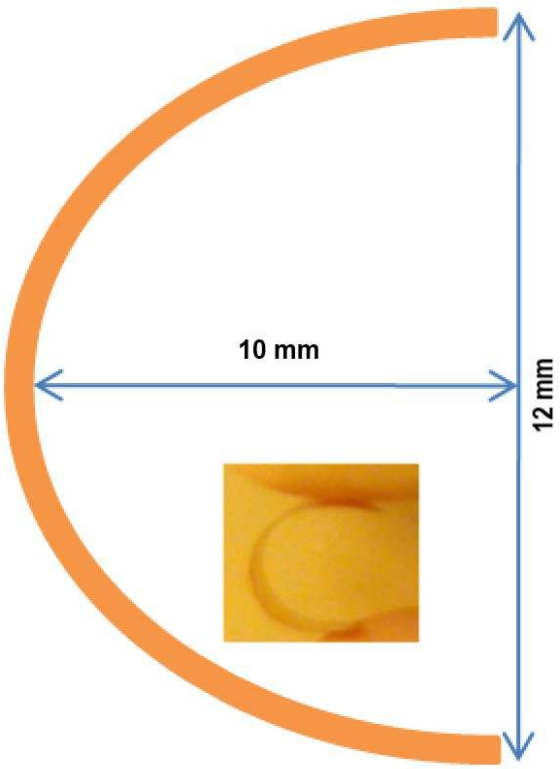

Figure 2.38 Schematic representation (not to scale) and photograph of the bending of the memristive sample.

3. Resistive Switching in Polymers

This chapter describes the resistive switching characteristics in polymer-based sandwich structures. The devices were fabricated using different polymers and were characterized to explicate their resistive switching characteristics. The organic resistive switches have the advantages of simple device structure, low fabrication cost and printability over their inorganic counterparts (Tee et al. 2012, Ling et al. 2008, Paul et al. 2006, Ha and Kim 2010, Ji et al. 2010, and Awais and Choi 2013). Different switching layers including polymeric and non-polymeric materials have been employed to fabricate memristors through different deposition techniques. Polymeric switching layers for the fabrication of the memristor bestow many advantages to the memristors such as cost-effectiveness, room temperature process ability, and mechanical flexibility over their non-polymeric counterparts. Structurally, organic memories or resistive switches can be categorized into four classes: (1) single-layer structure without nanoparticles (NPs) (2) bilayer structure containing two kinds of polymers (3) structure with nanotraps buried in the middle of an organic layer and (4) polymer-NP composite with NP traps randomly distributed throughout the entire host polymer (Ling et al. 2008). Polymer electronic memories have been reviewed in literature, emphasizing the organic material, device structure and the resistive switching phenomenon involved in polymers (Tee et al. 2012 and Ling et al. 2008).

3.1 MEH:PPV based Resistive Switches

Poly[2-methoxy-5-(2'-ethylhexyloxy)-(p-phenylenevinylene] (MEH:PPV) is one of the popular photoactive polymers that is commonly used in the organic light emitting diodes (OLED) and solar cells (Manoj et al. 2003, Ferrance et al. 2010, and Malliaras et al. 1998). MEH:PPV based tunneling diodes have been successfully implemented for the NDR switching effects as reported in the literature (Yoon et al. 2005, Reed et al. 2001, Collier et al. 1999, Lauters et al. 2006, and Thurstans and Oxley 2002). MEH:PPV based NDR switches have also been researched for the alternatives to memory and logic circuits (Reed et al. 2001 and Collier et al. 1999). Due to

enormous interests of the researchers and scientists in the MEH:PPV based NDR devices, a room-temperature deposition technique is being employed to fabricate the MEH:PPV based resistive switches in the current research work. EHDA technique has been employed for the fabrication of the MEH:PPV sandwich layer of the memristor on the indium-tin oxide (ITO) coated polyethylene terephthalate (PET) with a structure of ITO/MEH:PPV/Ag.

Electrohydrodynamic atomization (EHDA) is one of the cost effective room temperature deposition techniques, that promises its feasibility for the deposition of temperature sensitive materials like polymers. In the current work the electrohydrodynamically atomized layer of MEH:PPV on the ITO coated PET for the memristive device has been morphologically characterized with the field emission scanning electron microscope (FESEM) analysis. X-ray photoelectron spectroscope (XPS) analysis of the fabricated layer was also taken to confirm the existence of the polymer. Finally memristive sandwich has been fabricated with a structure of ITO/MEH:PPV/Ag and IV characterization of the memristive behavior has been done in the sandwich of ITO/MEH:PPV/Ag through semiconductor device analyzer.

3.1.1 Experimental Methods

EHDA deposition of the MEH:PPV was done with the help of the experimental setup shown in figure 3.1. The setup contains XY-stage for the substrate movement, light source and camera to observe EHDA phenomenon, ink supply section containing syringe, syringe pump and Teflon tube for ink supply, high power voltage source to supply electric potential, nozzle to deposit the thin layer on the substrate and control unit to monitor and control all the deposition process during the experiment.

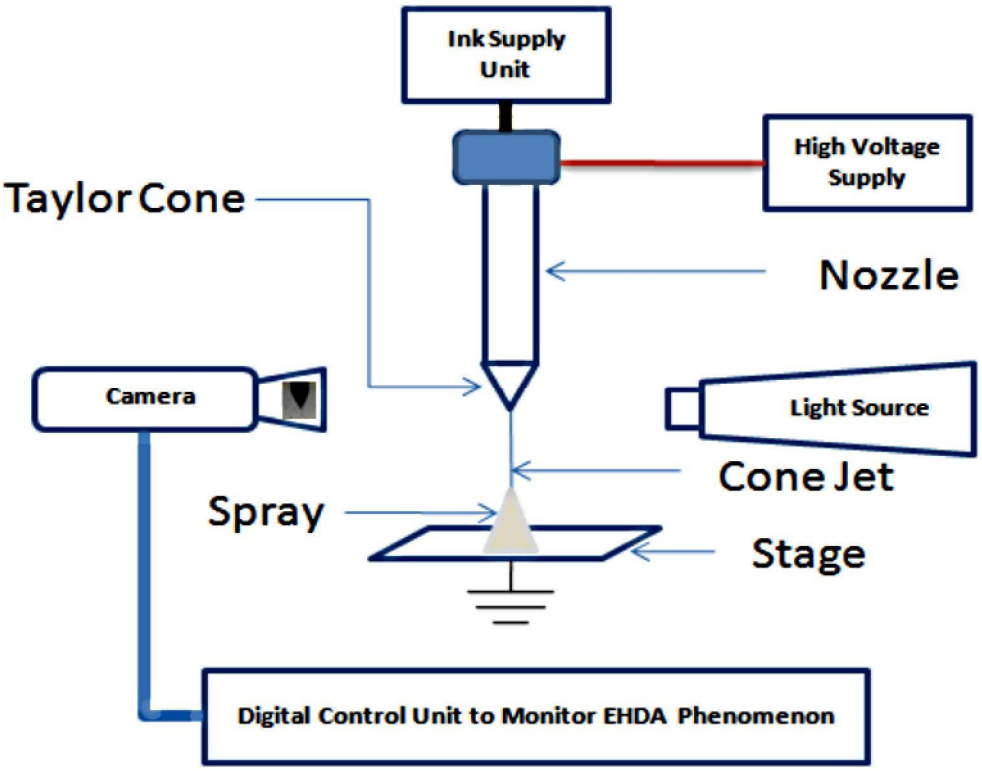

Figure 3.1 Experimental setup for EHDA of MEH:PPV on ITO coated PET.

In-house prepared ink of MEH:PPV (0.3 % by weight) in N,N-dimethyl-formamide (DMF) and di-cholorobenzene (DCB) was filled in the ink chamber and MEH:PPV ink was supplied to the nozzle through ink supply section. Electric potential was applied to the nozzle through the high voltage source. Different modes (dripping, unstable cone-jet, stable cone-jet and multi cone-jet) of atomization were observed as shown in figure 3.2.

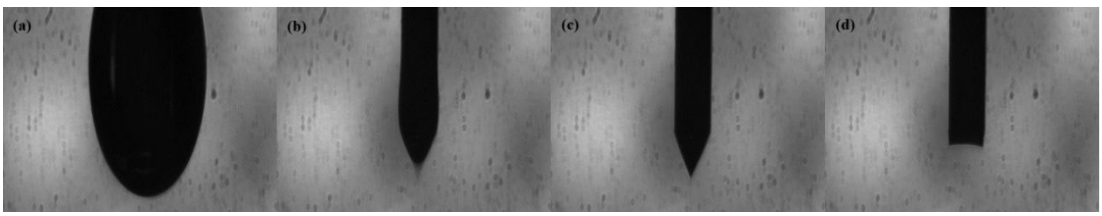

Figure 3.2 Different EHDA modes of MEH:PPV deposition: (a) Dripping (b) Unstable cone-jet (c) Stable cone-jet (d) Multi cone-jet.

Metallic nozzle used for the deposition of the MEH:PPV has the internal diameter of 200 μm and outer diameter of 310 μm. The distance from nozzle to substrate was kept at 4 mm during the experiment. The operating envelope of MEH:PPV ink was

explored with respect to different flow rates and potential differences on the ITO coated PET as shown in figure 3.3.

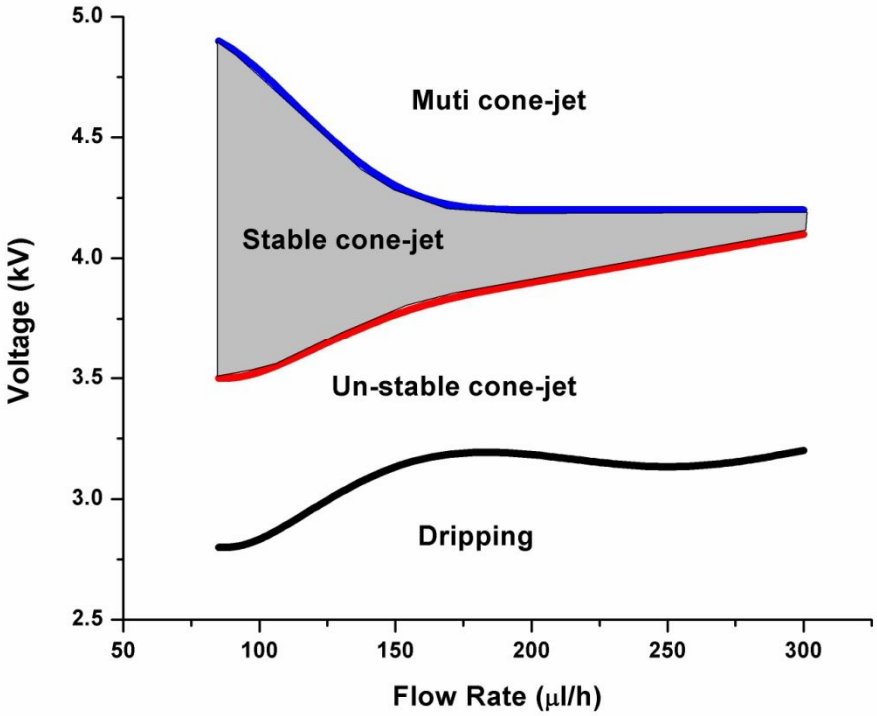

Figure 3.3 EHDA operating envelope for the MEH:PPV deposition on the ITO coated PET with respect to different flow rates and potential differences.

Thin layer of MEH:PPV was deposited on the ITO coated PET under cone jet-mode with flow rate of 100 µl/h and electric potential of 4.3 kV. The MEH:PPV layer was deposited for 5 min. The sample was cured at 110º C for 1.5 h after the deposition process. Finally Ag drop was deposited to complete the ITO/MEH:PPV/Ag sandwich structure.

3.1.2 Layer Characterization of MEH:PPV Resistive Switches

The thickness of the as-fabricated layer of MEH:PPV was measured through film thickness measurement system K-MAC ST4000-DLX and it was found to be 168 nm. The FESEM analysis shows the deposited thin layer of MEH:PPV on the ITO PET through EHDA technique as shown in figure 3.4.

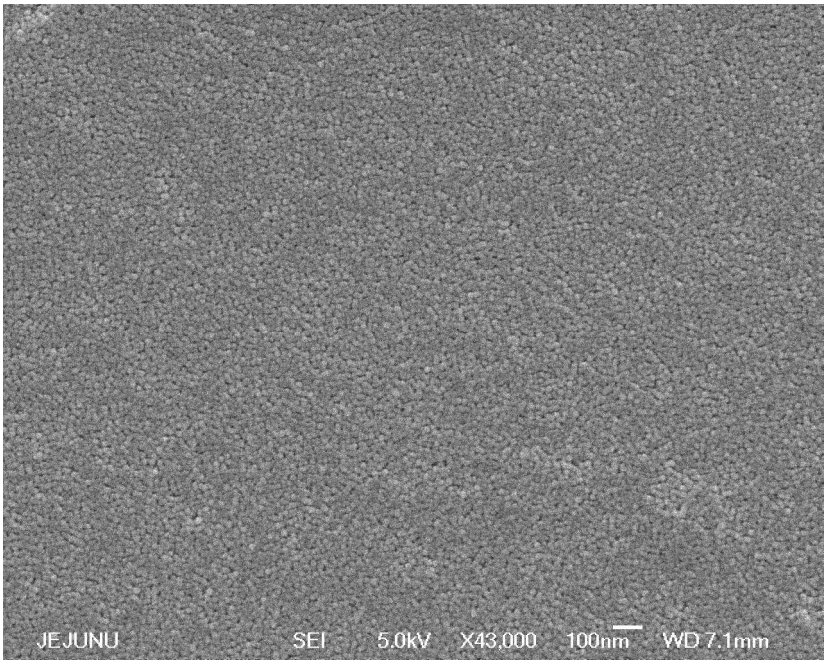

Figure 3.4 FESEM Images of MEH:PPV Film on the ITO coated PET.

Some hill-type structures and minute dots can be seen on the FESEM image, that is because of the preferential landing of the droplets on the substrate. When a strong electric field is created between the nozzle and the substrate eventually the substrate gets oppositely charged with respect to that of nozzle and droplets. The distribution of charge density is not uniform on the substrate surface. This non-uniformity in charge distribution is by virtue of the relative position with respect to the nozzle and local curvature of the substrate surface. Hence the electric field is strong at the concentrated charged areas ultimately droplets are more attractive towards these charged populated areas compared to the others. The preferential landing of the droplets to some specific areas is inherent property of the EHDA phenomena (Muhammad et al. 2012). XPS spectra confirms the presence of MEH:PPV polymer as shown in figure 3.5. The prominent peaks of C and O elements were observed in the graph and can be attributed to C 1s and O 1s respectively.

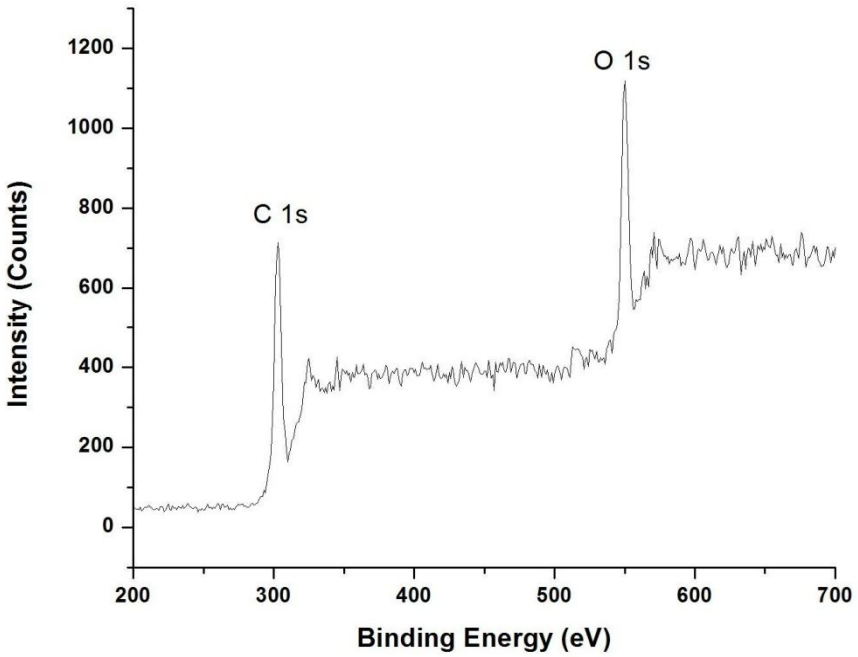

Figure 3.5 XPS spectra of MEH:PPV Film on the ITO coated PET.

3.1.3 Resistive Switching Characterization

The electrical characterization was done with an agilent B1500A semiconductor device analyzer for the as-fabricated memristive switch with a structure of ITO/MEH:PPV/Ag. During all the measurements the top Ag electrode was forced with the applied potential and bottom ITO electrode was grounded. Bipolar voltage was applied as biasing voltage for its characterization from + 5 to – 5 V and then – 5 to + 5 V with a current compliance (CC) of 10 mA. The CC was applied to avoid the break down in the switching layer of MEH:PPV.

I-V measurement of the ITO/MEH:PPV/Ag NDR device is shown in figure 3.6.

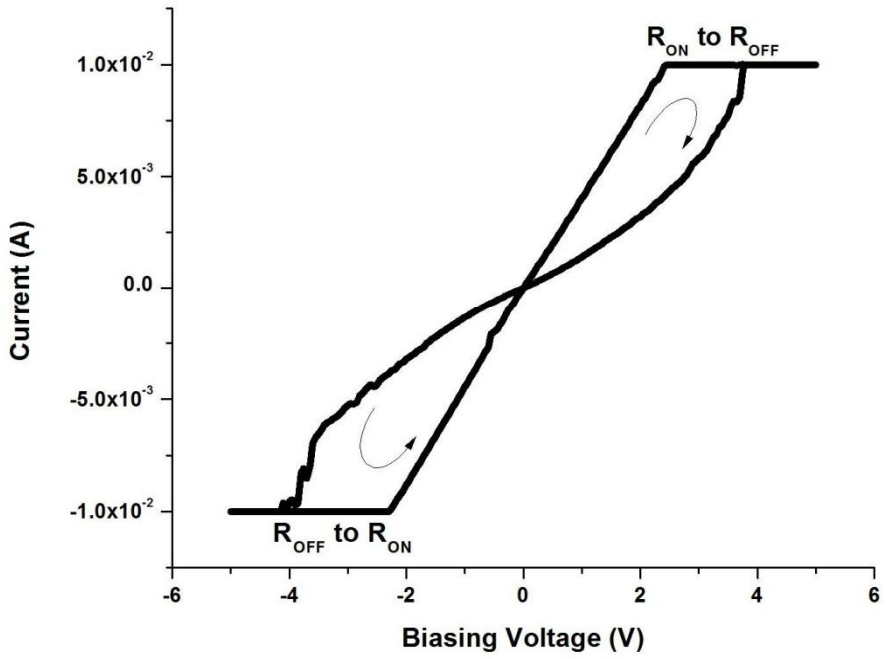

Figure 3.6 IV curve of the ITO/MEH:PPV/Ag sandwich device in linear scale.

On the application of the biasing voltage the sample started operating in the high resistance state (HRS). During positive to negative voltage sweep, the memristor kept its HRS unchanged around - 3.8 V and the sample changed its state from HRS to low resistance state (LRS) at around - 4 V. During negative to positive voltage sweep the memristor kept its LRS state unchanged until + 4 V. At + 4 V the switch changed its LRS into HRS. After going through the complete cycle of biasing voltage the memristor was in LRS. Here it can be noticed that on both sides of the polarity the graph passes through zero current that defines the memristive behavior as evident from the semi-log graph as shown in figure 3.7.

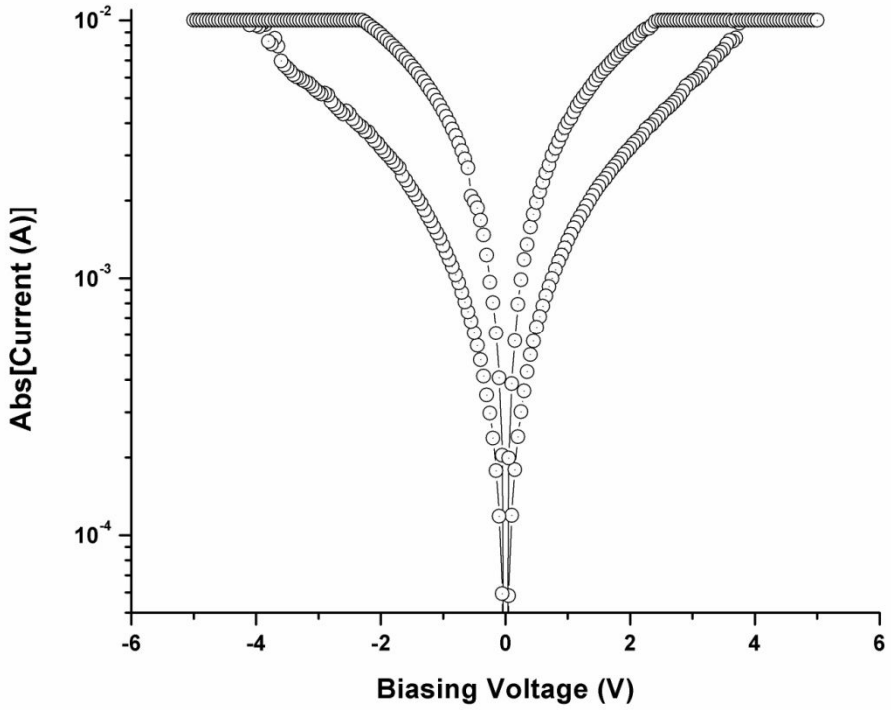

Figure 3.7 Semi-log graph of the IV curve of the ITO/MEH:PPV/Ag sandwich device.

During the LRS/ON/high state the resistance of the MEH:PPV based memristor was found to be 249 Ω and during the HRS/OFF/low state the resistance was calculated to be 714 Ω. The reading voltage used to calculate the resistance of the switch was 1 V. The resistance of the OFF state of the switch is almost two times higher than that of the ON state that concedes a sufficient ground to distinguish between the two states of the fabricated NDR switch. Normally the OFF/ON ratio of the single polymeric materials are quite less that could be improved with the mixing of the other polymers or metallic particle (Ling et al. 2008). The memristive devices having small OFF/ON could be implemented in printed electronics in the areas of neuromorphic applications (Verbakel et al. 2007 and Erokhin et al. 2010).

Endurance test of the fabricated device has been depicted in figure 3.8. The robustness of the as-fabricated switch has been checked against 50 biasing voltage cycles. The switch exhibit reasonable endurance against multiple voltage sweep stresses. As noticed in the endurance test, LRS of the fabricated device is more stable

as compared to the HRS. The change in LRS during the endurance test has been noticed from around 241 to 294 Ω and the change in HRS is found to be from 469 to 769 Ω. Voltage of 1 V has been used as reading voltage for the resistance calculation in the graph.

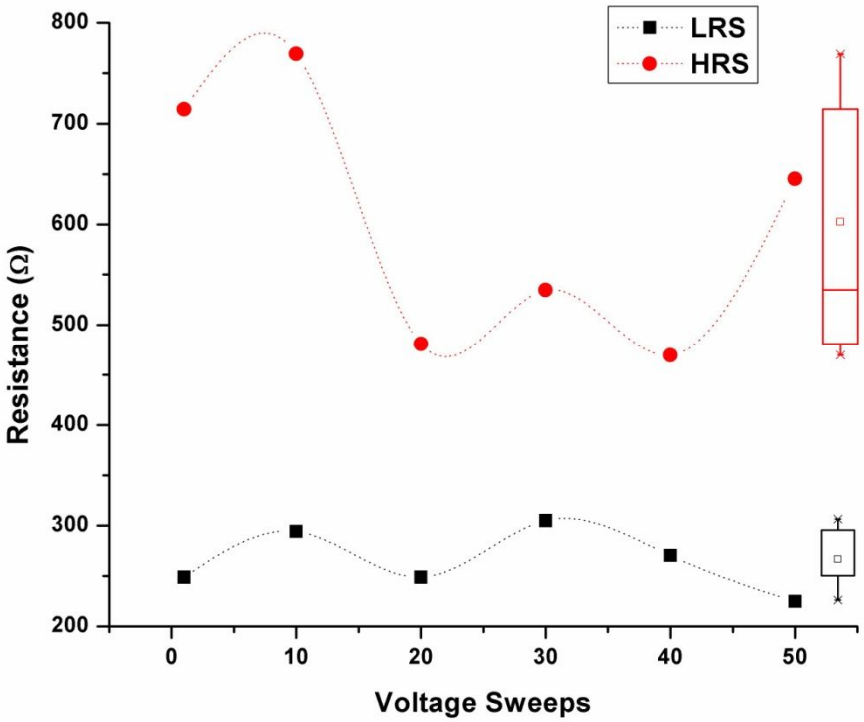

Figure 3.8 Endurance test of the ITO/MEH:PPV/Ag sandwich device with respect to resistance Vs voltage.

The non-volatility of the ITO/MEH:PPV/Ag fabricated device was measured over one and half days, and no prominent resistance change was found during both the states (HRS and LRS) of the device under test. The above discussion and testing leads towards the proliferating applicability of the fabricated device for the next generation printed electronic applications.

3.1.4 Resistive Switching Mechanism in the Fabricated Switches

Switching mechanism in the fabricated resistive switch has been explained with the help of slope fitting in IV graph. The IV graph has been drawn in Log-Log scale for the HRS as shown in figure 3.9. The fitted slope has been shown to be around 1 that

depicts the ohmic conduction during the HRS/OFF state of the device. Figure 3.10 shows the IV graph in log-log scale for the LRS of the device. The calculated slope after fitting the linear line is around 1 that also demonstrates the ohmic mechanism in the fabricated device. Hence both the states of the fabricated device are governed by ohmic conduction. As noticed in the current voltage performance of the fabricated resistive switching device, almost symmetric IV behavior has been elucidated instead of the asymmetric top and bottom electrodes. These symmetric characteristics are ascribed to the bulk conduction instead of the interface conduction. This symmetric bipolar behavior might be due to the electrochemically formation of the carbon conducting channels in the LRS of the device and the dissolution of the carbon conducting paths in the HRS of the MEH:PPV based resistive switch.

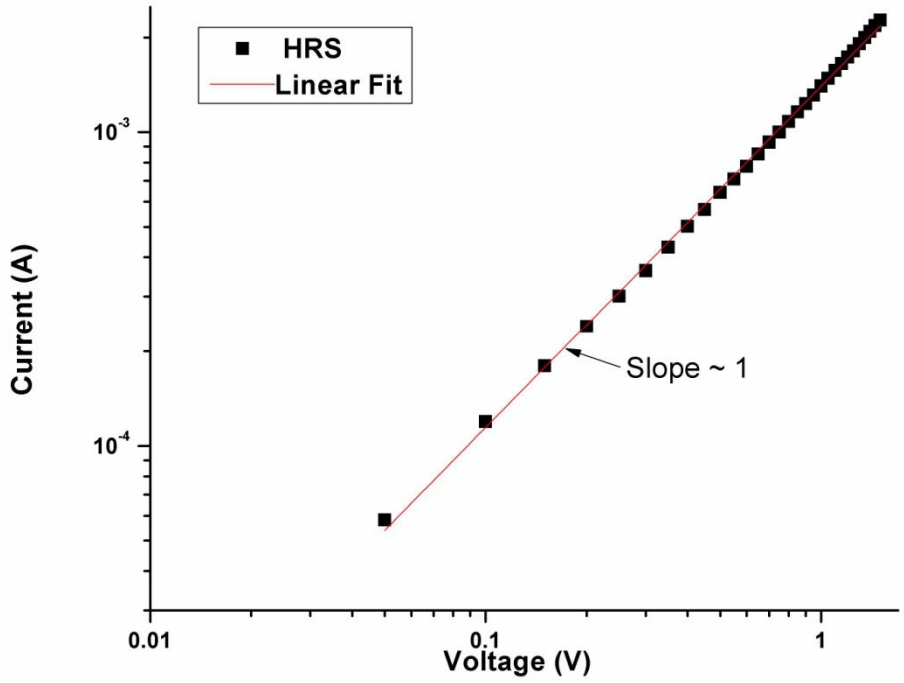

Figure 3.9 IV graph in Log-Log scale of the ITO/MEH:PPV/Ag sandwich device in its HRS.

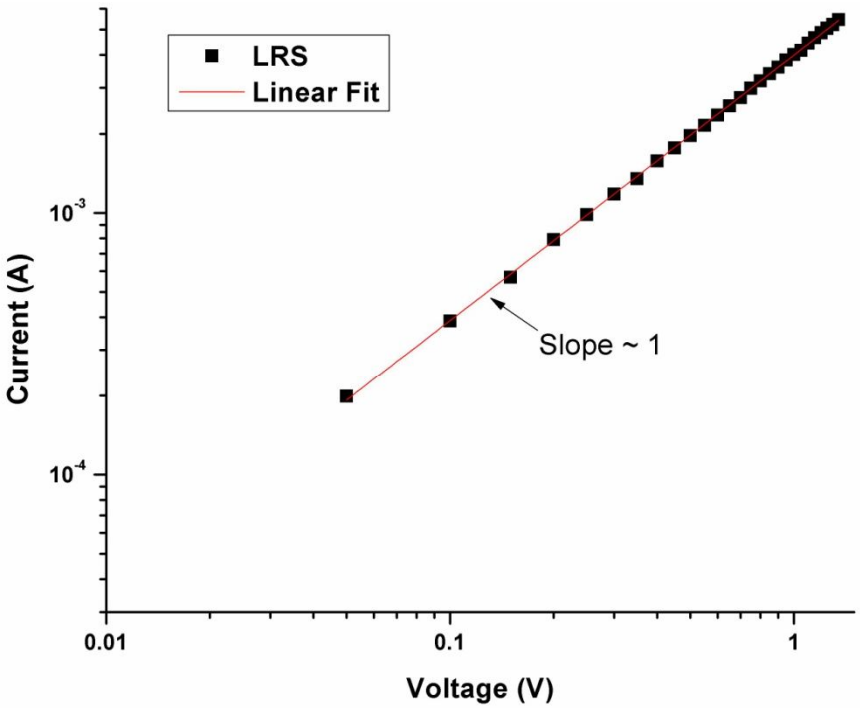

Figure 3.10 IV graph in Log-Log scale of the ITO/MEH:PPV/Ag sandwich device in its LRS.

3.2 PVP based Resistive Switches

Poly(4-vinylphenol)(PVP) is one of the most common polymers being used in dielectric applications for thin-film transistors (TFTs), cross-linking agent applications, and write once read many (WORM) memories and also has been employed in resistive switching memory applications. PVP has shown memory effects after mixing with molecules as the charge-storage medium for resistive random-access memory applications (Paul et al. 2006). PVP was employed in an 8 × 8 WORM memory cross-bar array (Song et al. 2011). High OFF/ON ratio with long retention time was reported for the composite structure of PVP. Thin films of PVP between Al and Au electrodes have been fabricated for WORM memory applications (Mamo et al. 2010).

In the current study, PVP has been used to fabricate organic resistive switches with the simplest sandwich structure of ITO/PVP/Ag. Electrohydrodynamic atomization (EHDA) has been utilized in the current research work to fabricate the thin layer of PVP between two electrodes.

In the current study, the technique is used for fabrication of a thin layer of PVP on ITO-coated PET and the resistive switching properties are reported for the insitu fabricated nanolayer. The layer was characterized using FESEM and XPS analysis and the results confirmed the presence of PVP polymer. Bipolar switching was used to characterize the fabricated ITO/PVP/Ag sandwich structure. Bipolar resistive switching is a kind of inherited switching property of the material in which active material changes its resistance from one state to another state for one direction of voltage sweep, while for the reverse direction of voltage polarity, the resistance of the active resistive material transition again from the second to the initial state. The effect of current compliance (CC) on resistive switching in PVP nanolayers has been demonstrated. The setting of different CCs plays a vital role in the resistive switching of different active materials. In this study, the CC provided stable resistive switching of the fabricated device and granted the window to modulate the resistive switching behavior of the fabricated device regarding its OFF/ON ratio and switching voltage for both polarities. Endurance test and retention time results are reported to confirm the application feasibility of the fabricated device.

3.2.1 Experimental Details

The experimental setup used for the PVP atomization is shown in figure 3.11.

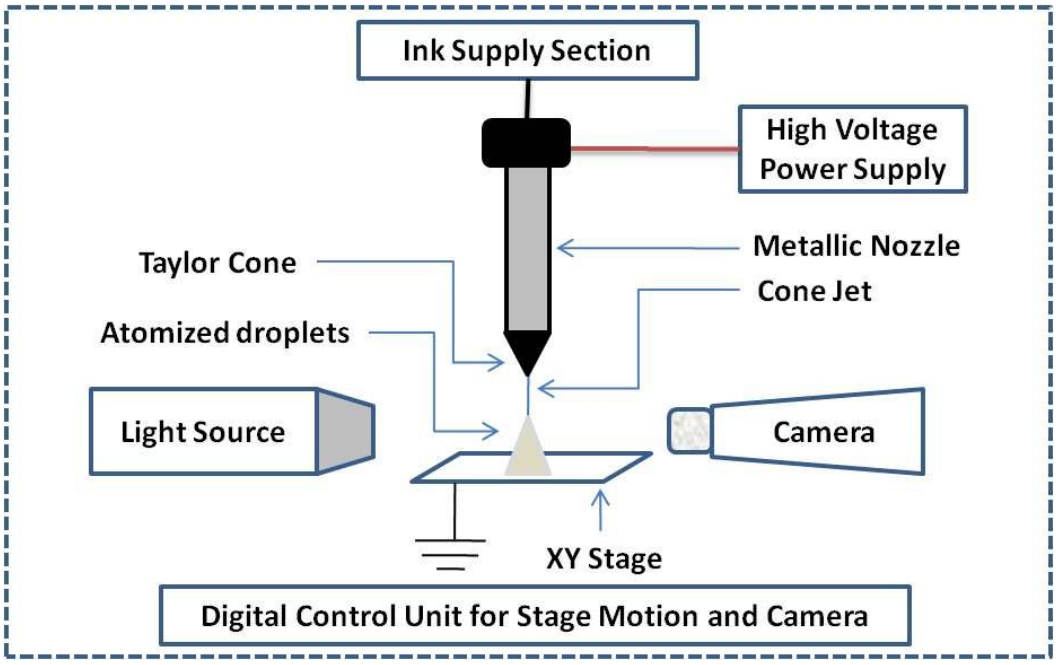

Figure 3.11 Experimental setup for EHDA printing.

The experimental setup includes an X-Y stage, a metallic nozzle, an ink supply section containing a syringe, a syringe pump, a teflon tube, and connectors, a high-voltage power source, a camera to capture all the events during the experiment, a light source, and a digital control unit to monitor and control all the events during the experiment.

PVP (average M_w ~25000) polymer and ITO-coated PET (thickness around 100 μm) were purchased from Sigma-Aldrich. The surface resistivity of the ITO on the PET is 60 Ω/sq with the thickness of 1000 Å. 10 % PVP polymer dispersion was filled in the syringe. The ink was then pumped through a nozzle by a syringe pump. The metallic nozzle was forced with the positive potential and the substrate was grounded during the experiment. Electric stresses were generated between the nozzle and the substrate due to the applied potential. The meniscus appeared at the tip of the nozzle deformed into a conical shape due to the electric stresses between the nozzle and the substrate. Consequently a thin jet was found to emerge at the apex of the cone. The jet was further disintegrated into small droplets by adjusting the distance between the nozzle and the substrate. The stand-off distance was adjusted in such a way that most of the solvent was evaporated during the flight time of the droplets resulting in tiny droplets containing PVP polymers and small amount of solvent left on the ITO-coated PET. The sample was then cured to remove the solvent and to enhance the adhesion of the PVP with the substrate.

The reported sample was deposited by a metallic nozzle having an internal diameter of 110 μm, the flow rate of 100 μl/hr, applied potential of 2.9 kV, and stand-off distance of 1 cm. PVP polymer film on the ITO-coated PET was deposited in 3 passes with the stage speed of 3 mm/s. The deposited sample was cured at 110 °C for 1 hour. Finally circular top contacts with the diameter of around 365 μm to 735 μm were established with Ag conductive epoxy (Circuit Works-CW2400) to complete an ITO/PVP/Ag sandwich structure. The measured thicknesses of the top electrodes were around 32 μm.

The thickness of the deposited layer was measured using a non-destructive thin film-thickness measurement machine (K-MAC ST4000-DLX). PVP nano-layers were electrically characterized with Agilent B1500A Semiconductor Device Analyzer.

3.2.2 Layer Characterization of PVP Resistive Switches

The surface morphology of the prepared sample was characterized through the FESEM analysis. Figure 3.12 shows the FESEM images of the prepared sample in low and high resolution. The FESEM images show very smooth and uniform surface of PVP on the ITO-coated PET substrate. The FESEM images show homogeneous deposition of the PVP layer on the ITO-coated PET substrate through an EHDA technique.

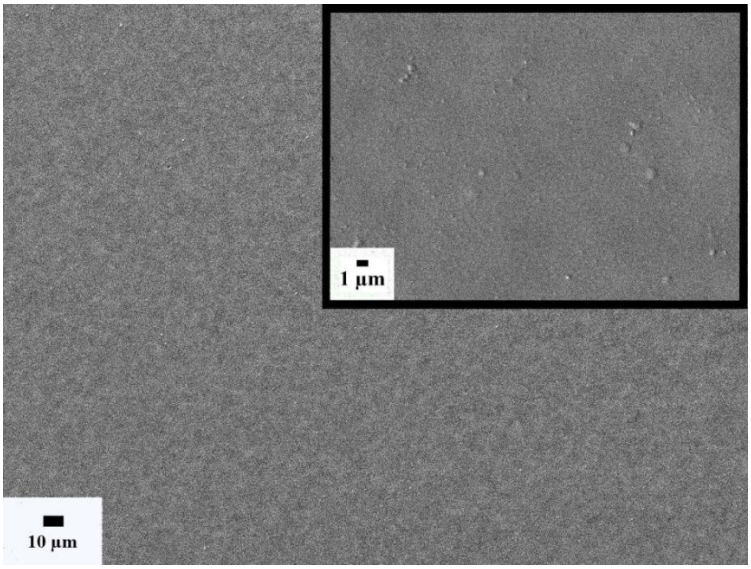

Figure 3.12 FESEM images of PVP film on ITO-coated PET.

The XPS analysis is also given to confirm the composition of the PVP on the ITO-coated PET. Figure 3.13 shows the XPS graph. The graph shows that the prominent peaks are ascribed to C (carbon) and O (oxygen) elements. C 1s peak was observed at the binding energy of 285 eV and O 1s peak was detected at the binding energy of 533 eV.

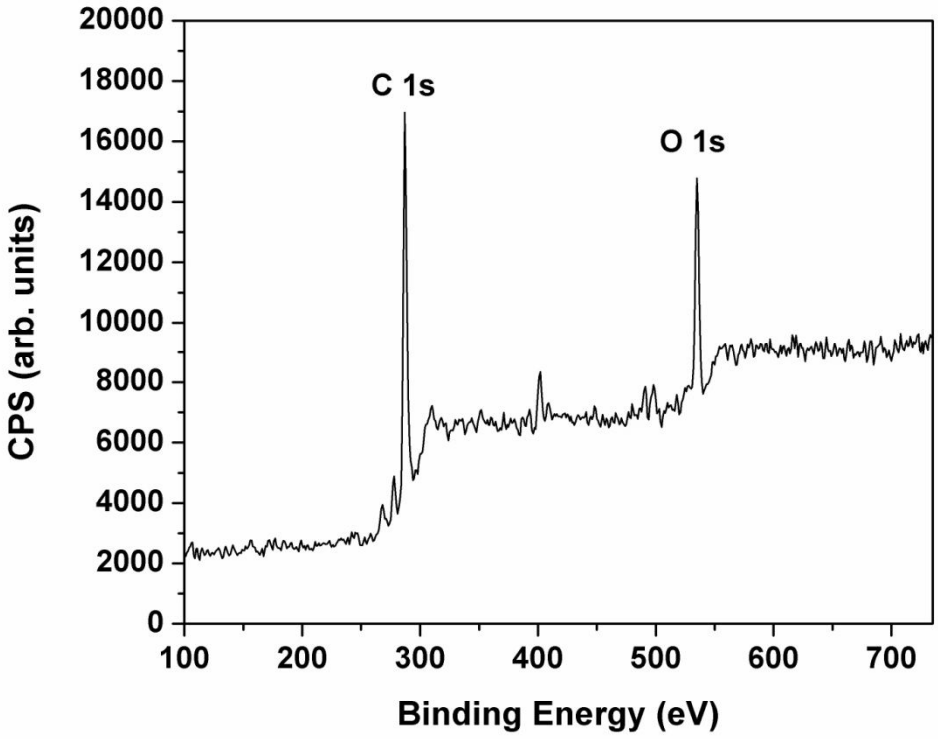

Figure 3.13 XPS analysis of PVP film on ITO-coated PET.

Different atomized PVP samples were taken for the thickness measurement. The average thickness of the fabricated layer was measured to be 110 nm.

3.2.3 Resistive Switching Characterization

To analyze the electrical current-voltage (*I-V*) characteristics of the in situ fabricated ITO/PVP/Ag sandwich, the top Ag electrode of the device was connected to the driving terminal while the bottom ITO electrode was grounded in all the *I-V* measurements.

Initially, the forming voltage necessary for stable resistive switching operation was applied. The electroforming process was performed by applying 0 V to 7 V with CC of 5 mA as shown in figure 3.14. The device started in a high-resistance state (HRS) and electroformed at around 1 V from HRS to a low-resistance state (LRS). The current was limited in the LRS by setting a CC to avoid hard breakdown. The resistance during the HRS/OFF state of the device was measured to be $5\times10^4\ \Omega$ and it was calculated to be $6\times10^2\ \Omega$ during the LRS/ON state.

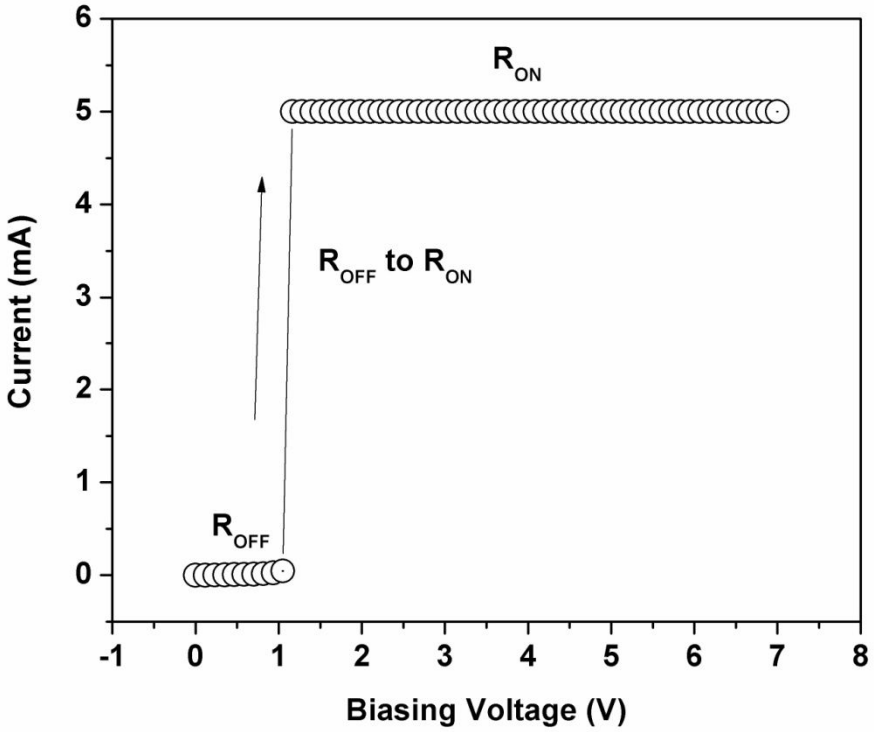

Figure 3.14 I-V curve of the electroforming process of an ITO/PVP/Ag sandwich device with CC of 5 mA.

After performing the electroforming process, double voltage sweeps were used to analyze the resistive switching within the sandwich device. The device was examined from a high CC to a low CC. At the high CC the device did not exhibit remarkable stable resistive switching, but as the CC was lowered, the device showed excellent stable resistive switching behavior.

At CC of 75 nA, a double voltage sweep was applied from +1.5 V to -1.5 V as shown in figure 3.15 a. The device started in the LRS, switched into HRS at around 0.5 V, and remained in the HRS until the application of the reverse voltage sweep at around 1 V. After 1 V the device changed its state from the HRS to LRS. The average resistances in the LRS and HRS were measured to be $1.58\times10^{7}\ \Omega$ and $5.48\times10^{10}\ \Omega$, respectively.

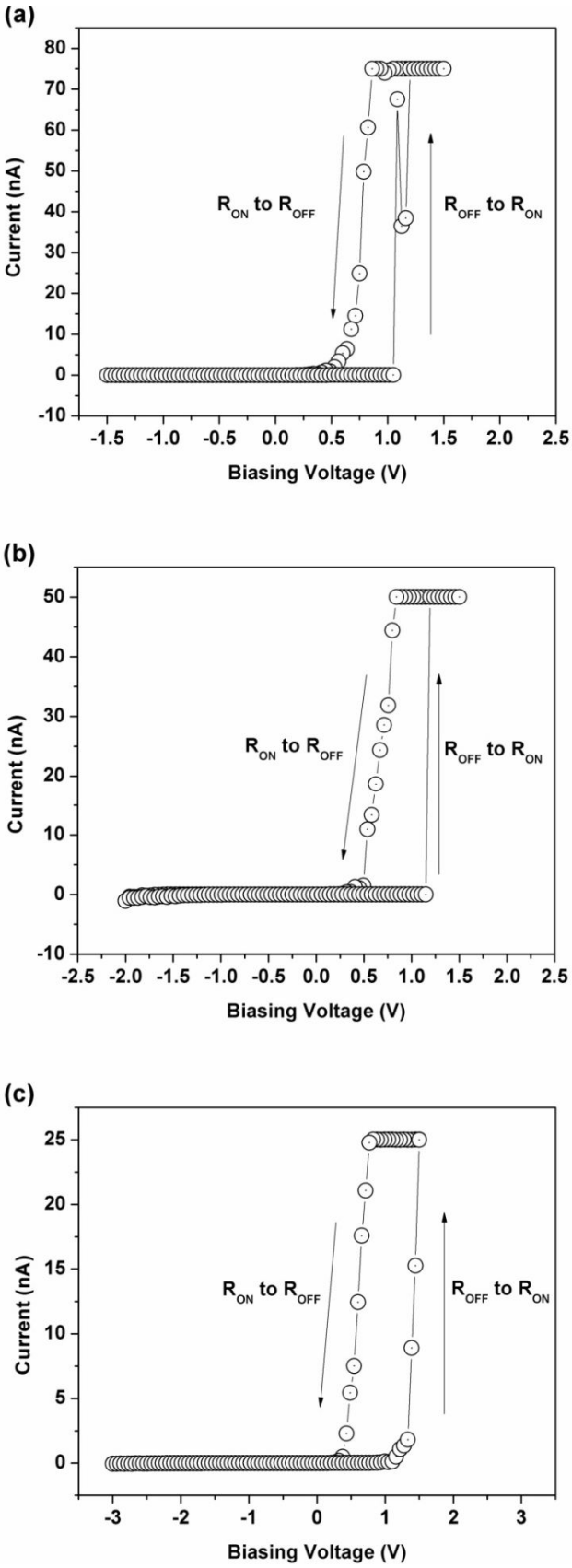

Figure 3.15 I-V curves of an ITO/PVP/Ag sandwich device with different CCs: (a) 75 nA (b) 50 nA (c) 25 nA.

The *I-V* behavior is shown in figure 3.15 b for the case of a 50 nA CC with a double sweeping voltage of +1.5 V to -2 V. The curve is almost the same as in the case of a 75 nA CC. The resistances during the ON and OFF states of the device were found to be $2.39\times10^{7}\ \Omega$ and $5.13\times10^{10}\ \Omega$, respectively.

The *I-V* behavior of the device was the same with a CC of 25 nA as in the previous cases shown in figure 3.15 c. In this case, double voltage sweeping was applied from +1.5 V to -3 V. The average resistances in the LRS and HRS were observed to be $4.65\times10^{7}\ \Omega$ and $2.68\times10^{10}\ \Omega$, respectively.

When the device was driven with increased negative bias, Schottky behavior became prominent, as is evident from figure 3.16 a. When the voltage was swept from +3 V to -7 V with CC of 15 nA, a pinched hysteresis loop appeared showing the *I-V* characteristics of the sandwich device. The behavior of device on the positive cycle was found to remain the same as it was in the previous case but during the negative sweep, the transition from one state to another state also occurred. The transition from a HRS to a LRS occurred at around -6 V and from a LRS to a HRS at around -4 V. During the positive half of the voltage sweep, the average resistances for the LRS and the HRS were $1.15\times10^{8}\ \Omega$ and $1.39\times10^{10}\ \Omega$, respectively while during the negative half of the voltage sweep, the average resistances for the LRS and HRS were $3.72\times10^{8}\ \Omega$ and $7.81\times10^{10}\ \Omega$, respectively. When the CC was set at 13 nA and the same double voltage sweep was used to analyze the *I-V* behavior of the device, the device exhibited almost same behavior as in the case of a CC of 15 nA shown in the figure 3.16 b. The transition from a HRS to a LRS shifted to -5 V and the transition from a LRS to a HRS shifted to around -3.5 V. With the decrease in CC, the *IV* loop on the positive side shortened but the noise disappeared as compared with the previous case of 15 nA. At CC of 15 nA, the average resistances during the positive half of the voltage sweep for the LRS and HRS were measured to be $1.56\times10^{8}\ \Omega$ and $7.48\times10^{9}\ \Omega$, respectively while in case of the negative half of the voltage sweep, the average resistances for the LRS and the HRS were observed to be $4.15\times10^{8}\ \Omega$ and $7.83\times10^{10}\ \Omega$, respectively.

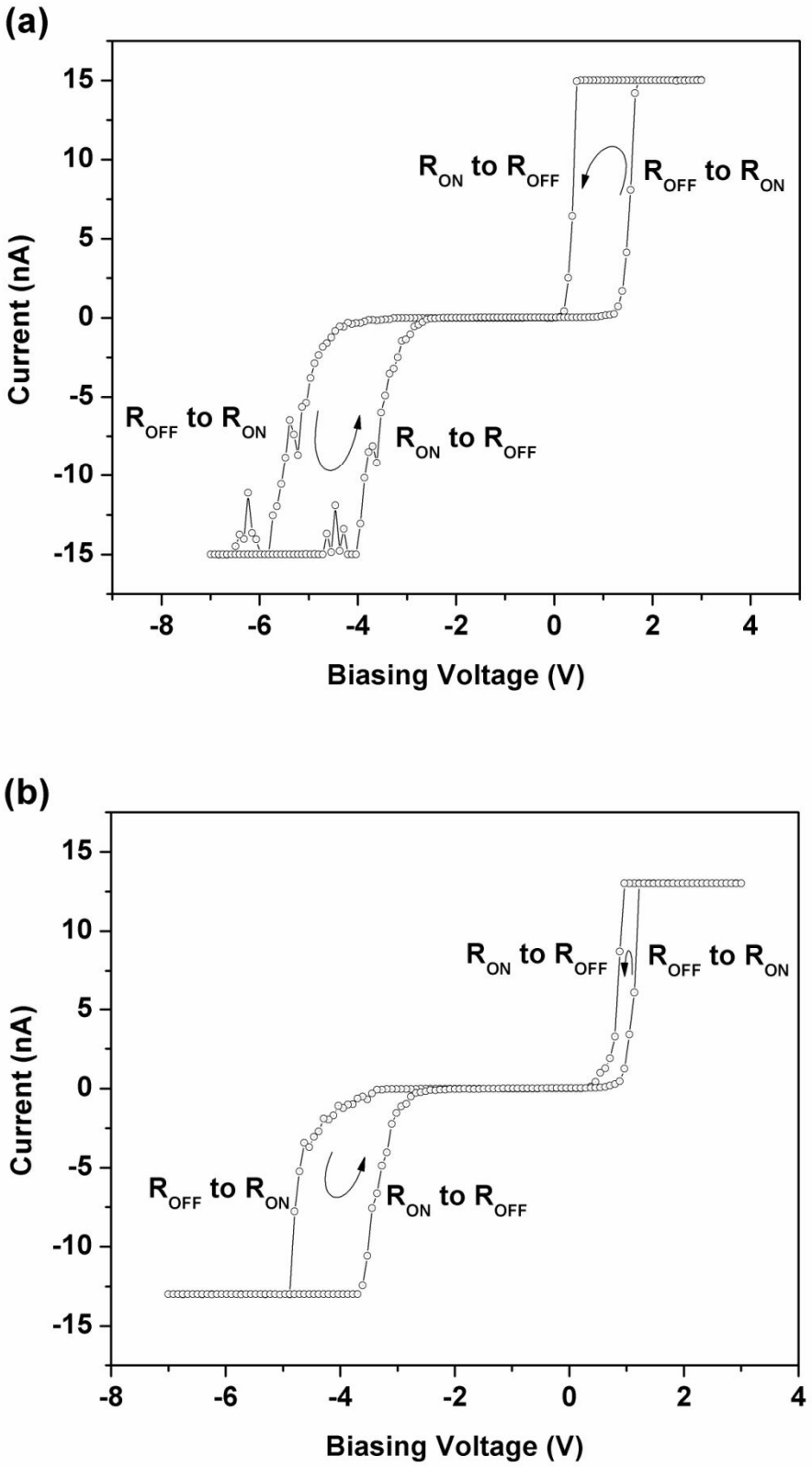

Figure 3.16 I-V curves of an ITO/PVP/Ag sandwich device with different CCs: (a) 15 nA (b) 13 nA.

Figure 3.17 shows the *I-V* behavior of the device at a very low CC of 3 nA. A double voltage sweep of +6 V to -7 V was applied in a case of 3 nA CC. The resulted *IV* pinched hysteresis loop was similar to that appeared in the case of CC of 13 nA. The transition from a HRS to a LRS occurred at -6 V and transition from a LRS to a HRS appeared at -4.5 V. At the very low CC of 3 nA, the average resistances during the positive half of the voltage sweep for the LRS and HRS were $1.08\times10^{9}\ \Omega$ and $1.04\times10^{10}\ \Omega$, respectively while in the case of the negative half of the voltage sweep, the average resistances for the LRS and the HRS were $1.96\times10^{9}\ \Omega$ and $6.66\times10^{10}\ \Omega$, respectively.

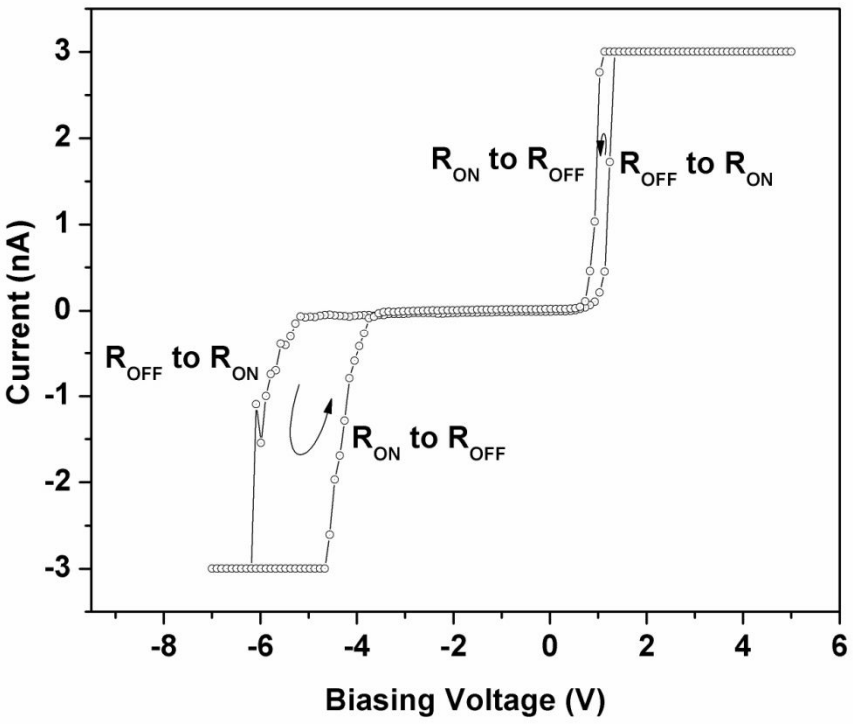

Figure 3.17 I-V curve of an ITO/PVP/Ag sandwich device with CC of 3 nA.

In situ fabricated virgin samples were also analyzed by driving only in the positive cycle (or small voltage on the negative side) of the double voltage sweep without performing electroforming process. When a double voltage sweep was applied from 0 V to +3 V with a CC of 5 nA, the device showed the hysteresis looping behavior consisting of two distinct states, as shown in figure 3.18.

In the forward voltage sweep from 0 to 3 V, the device started operating in a HRS/OFF state, and after reaching a voltage of around 1.6 V, it switched into a LRS/ON state. The average resistance of the device in the HRS was found to be 2.24×10^{11} Ω. In the reverse voltage sweep from 3 to 0 V, the device remained in the LRS unchanged until around 0.5 V. After 0.5 V, the device started a transition into the HRS. The average resistance in the LRS of the device was measured to be 3.92×10^{8} Ω. A sudden transition was observed from R_{OFF} to R_{ON} where a gradual transition was observed from R_{ON} to R_{OFF}.

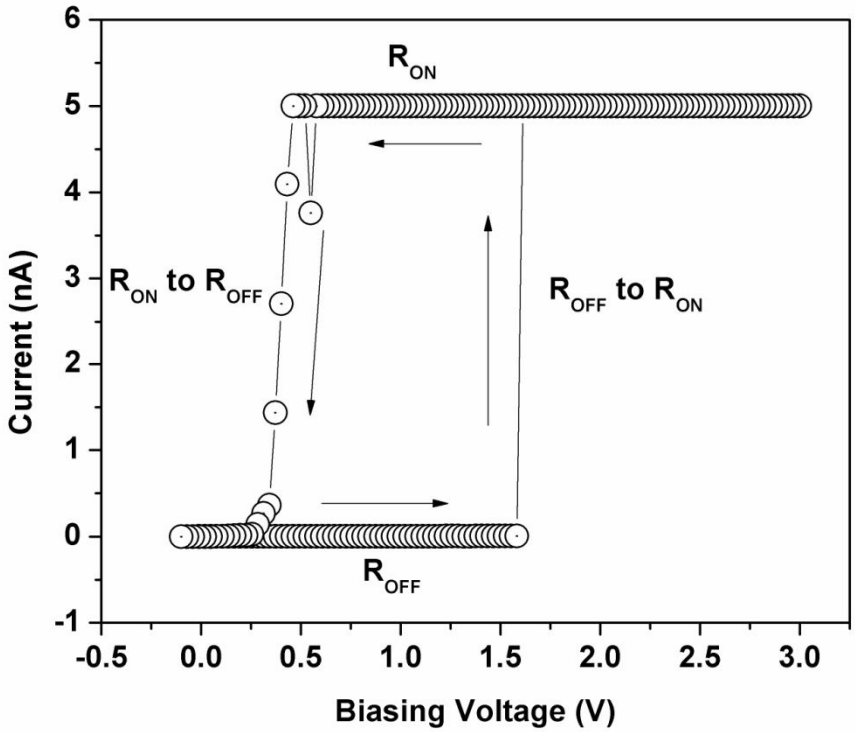

Figure 3.18 I-V curve of a virgin ITO/PVP/Ag sandwich device with CC of 5 nA.

Both the electroformed and virgin samples showed two distinct states according to different CC values. The memory window could be chosen depending upon the sweeping direction and polarity. Resistive switching of the device on the positive voltage polarity side could be observed at low voltages, while on the negative polarity side it took relatively higher voltages. The samples did not show prominent resistive switching at higher CC, in contrast to inorganic resistive switches. Inorganic resistive switches usually exhibit resistive switching behavior at higher CC, while sometimes setting a different CC changes their unipolar resistive switching into

bipolar resistive switching, or vice versa. The fabricated sandwich device has full potential to be implemented in the considered memory application, or as a switching element in electronics applications by setting different CCs.

The endurance of the fabricated switch was tested by applying multiple voltage sweeps. Figure 3.19 shows the endurance test results of the fabricated device with a reading voltage (V_{READ}) of around 0.5 V. Figure 3.19 shows a consistent OFF/ON ratio of more than 100:1. The average resistance during the OFF state was measured to be 2.03×10^{11} Ω and the average resistance during the ON state was calculated to be 1.41×10^{8} Ω.

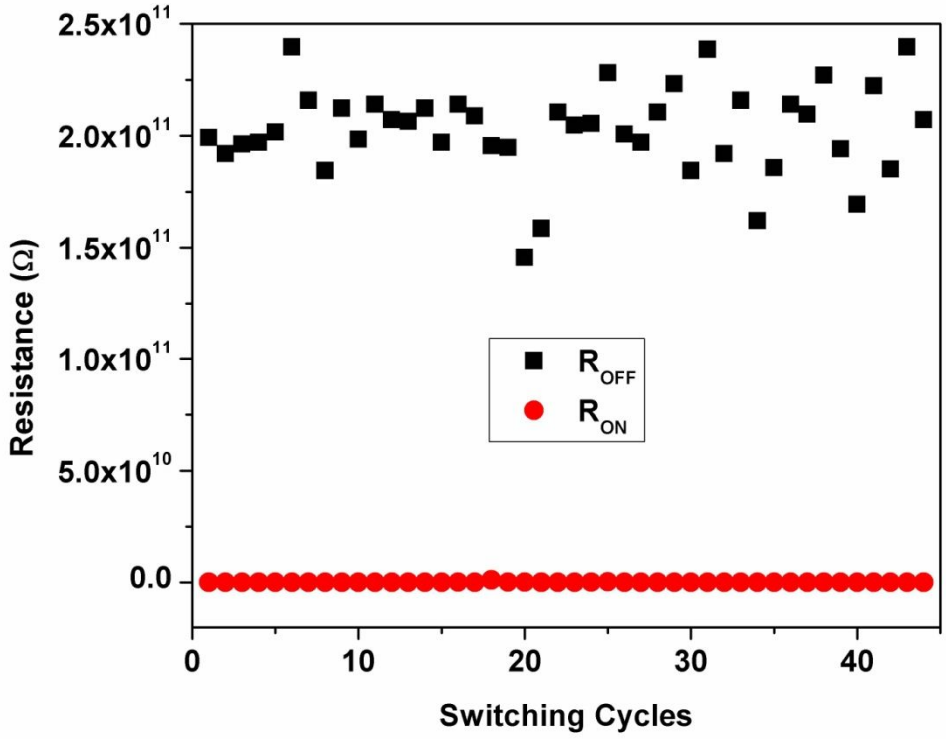

Figure 3.19 Resistance versus voltage sweeps for the fabricated resistive switch.

The retention time of the fabricated memristor was measured to be over 100 min, as shown in figure 3.20. The variation in resistance during both the OFF and ON state was observed to be negligible. The average resistance in the HRS after 100 min was observed to be 1.97×10^{11} Ω, and it was found to be 1.16×10^{8} Ω in the LRS of the device. Although over 100 min, retention time is comparable with the organic resistive switches but the fabricated devices are expected to retain their states unchanged for a longer period of time.

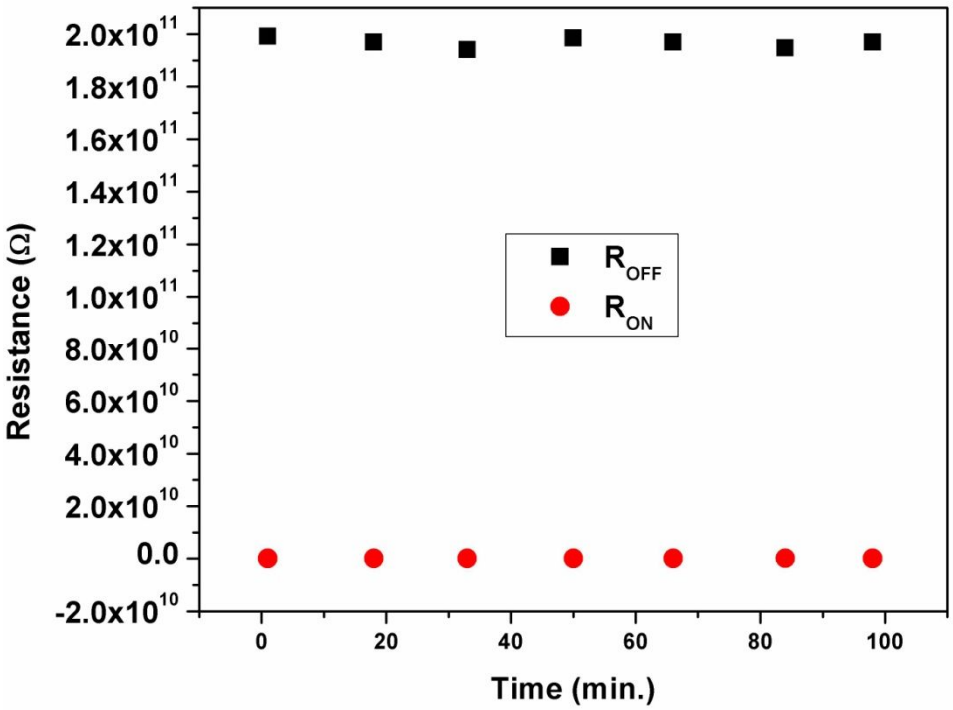

Figure 3.20 Resistance versus time for the fabricated resistive switch.

Twenty-one devices were fabricated during two different experiments. More than 80 % of the devices showed consistent switching behavior with respect to their endurance testing, retention time, and reliability. The fabricated devices exhibited resistive switching behavior irrespective of their device area (top electrode diameter).

3.2.4 Resistive Switching Mechanism in the Fabricated Switches

The resistive switching mechanism in the ITO/PVP/Ag sandwich has been explained using some theories from the literature, supporting the resistive switching in the fabricated sandwich device. On both sides of polarity, Schottky conduction was observed in the fabricated samples. In the positive sweep from 0 to 3 V, the fabricated device showed high resistance inside the PVP layer until 3 V, then suddenly the high resistance turned into low resistance and high current started to flow, limited by the CC. This might be explained by formation of carbon-rich filaments due to local degradation of the PVP layer surrounding the breakdown region, as supported in the literature (Tee et al. 2012, Ling et al. 2008, and Pender and Fleming 1975). The switching phenomenon might also be associated with

formation of metallic bridges by the migration of the top electrode, since Ag is a chemically reactive material (Tee et al. 2012, Ling et al. 2008, and Pender and Fleming 1975). Because ITO is almost inert (stable) in nature, formation of conductive bridges/filaments can only result from local soft breakdown of the switching material or from the reactive electrode. When the polarity was applied in the reverse direction from 3 V to 0 V, the carbon/Ag-rich metallic filaments underwent a rupturing phase. The filaments remained until the voltage dropped to 0.5 V, when suddenly complete rupture of carbon/Ag-rich metallic filaments occurred inside the PVP layer, and the device transitioned into the HRS. Similarly for negative polarity of the voltage source, during the voltage sweep from 0 to -6 V, the device was in the HRS and after reaching 6 V the formation of filaments started to increase, setting the device into the LRS and consequently generating high current limited by the CC. In the reverse direction of polarity, rupturing of the filaments occurred at -3.5 V and the device changed its state from a LRS to a HRS. As noticed, the switching voltage required with negative biasing is higher than that of the positive biasing, which is once more ascribed to the reactive nature of Ag and the inert nature of the ITO electrode. Keeping the ITO bottom electrode at the same potential, during the positive biasing of the Ag top electrode, it took a small voltage to generate the electrical field to obtain soft breakdown for the formation of conductive carbon/Ag bridges, while a sufficiently large voltage was needed in the case of negative biasing of the top Ag electrode to generate the conductive paths. Regarding the Schottky conduction mechanism, positive biasing of the Ag electrode provided forward biasing of the device, whereas negative biasing established the reverse biasing provided that the ITO electrode was at the same electric potential. However, further investigation of the switching mechanism in the fabricated device is needed, the details of which are left for future work.

3.3 PEDOT:PSS based Resistive Switches

Poly(3,4-ethylenedioxythiophene):poly(styrenesulfonate) (PEDOT:PSS) is a conjugated polymer consisted of two polymeric chains: poly(3,4-ethylenedioxythiophene) (PEDOT) and poly(styrenesulfonate) (PSS). PEDOT:PSS has acquired prominent position in polymeric science due to its versatile features of

transparency and conductive in nature with high ductility. PEDOT:PSS has been widely used in a lot of device-based applications such as write-once-read-many (WORM) memories, organic thin film transistors (OTFTs), organic light emitting diodes (OLEDs) and solar cells (Moller et al. 2003, Moller et al. 2003, Sirringhaus et al. 2000, Li et al. 2007, and Peumans and Forrest 2001). PEDOT:PSS has proven its feasibility as a switching layer in the resistive random access memory applications. Polarity independent unipolar resistive switching has been observed in the PEDOT:PSS-based devices (Ha and Kim 2009). Polarity dependent bipolar resistive switching has also been studied in the switching layer of PEDOT:PSS in the sandwiched devices (Ha and Kim 2008). The resistive switching mechanism in PEDOT:PSS based resistive switches has been investigated in both the unipolar and bipolar biasing regimes for the organic non-volatile memory device applications (Ha and Kim 2009, Ha and Kim 2008, Ha and Kim 2010, and Lai and Chen 2011).

By virtue of the massive benefits and interests of the researchers in PEDOT:PSS polymer, the conjugated polymer was used in the fabrication of the polarity dependent bipolar NDR devices in the current research work through electrohydrodynamic atomization (EHDA) printing technique. Atomization of the PEDOT:PSS has been done in our previous work for the solar cell applications (Duraisamy et al. 2012). In the current work, the EHDA was performed to atomized the PEDOT:PSS switching layer on the ITO coated PET for the NDR device applications. The deposited layer of PEDOT:PSS polymer was morphologically characterized through the field emission scanning electron microscope (FE-SEM). Raman spectra was used to analyze and validate the chemistry of the as fabricated PEDOT:PSS polymeric layer. Finally ITO/PEDOT:PSS/Ag(silver) NDR devices were fabricated by deploying Ag metallic contacts. The resistive switching behavior of the NDR devices was analyzed through the semiconductor device analyzer by employing bipolar sweeping voltage. The effect of the current compliance (CC) on the NDR switching of the ITO/PEDOT:PSS/Ag sandwiched structures was examined. The endurance and non-volatility tests were also performed to inspect the application feasibility. Resistive switching mechanism in the fabricated device was explained based upon the redox behavior of PDEOT:PSS material.

3.3.1 Experimental Details

Figure 3.21 shows the EHDA experimental setup for the atomization of the PEDOT:PSS on the ITO coated PET.

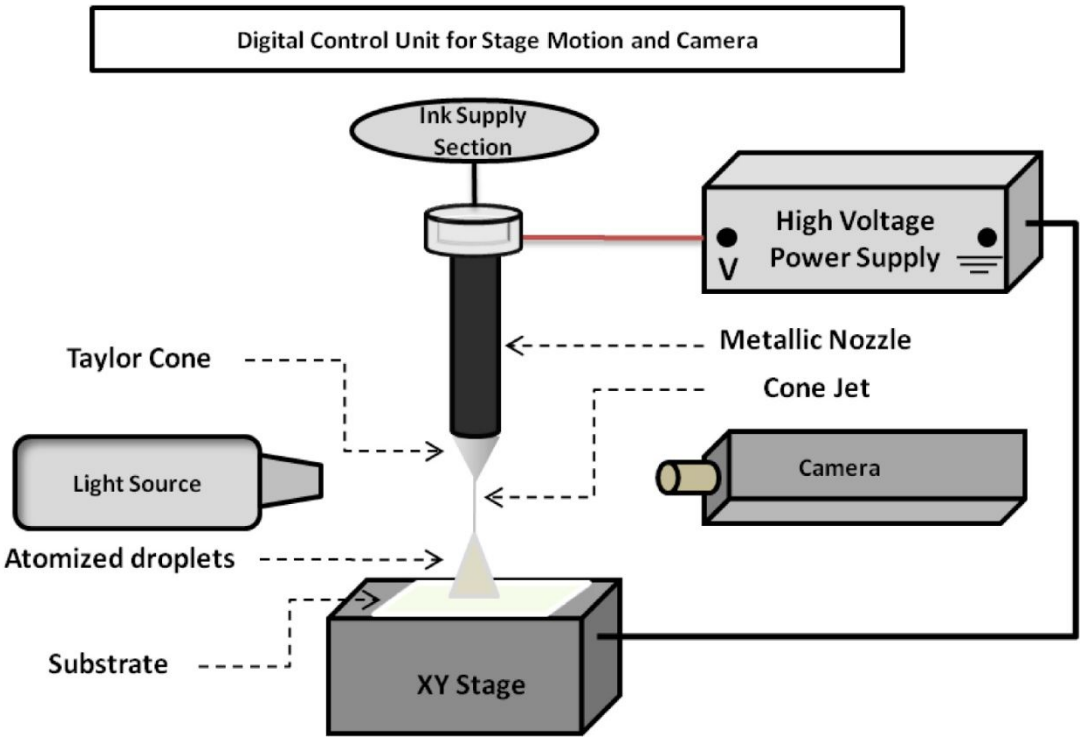

Figure 3.21 Experimental setup for the EHDA of PEDOT:PSS conjugated polymer.

The deposition setup consists of X-Y stage, metallic nozzle with internal diameter of 400 µm and outer diameter of 680 µm, ink supply unit containing syringe, syringe pump, Teflon tube and connectors and high voltage power source. High speed camera and light source are used to monitor all the events during the deposition process. The entire experimental process is controlled through the control unit. Chemically modified PEDOT:PSS ink with isopropanol and deionized water was utilized for the EHDA process (Duraisamy et al. 2012). PEDOT:PDD ink was filled in the syringe that was connected to the syringe pump. Polymeric ink was pumped to the metallic nozzle through Teflon tube by the syringe pump. Under the absence of electric field from nozzle to the substrate only dripping of the conjugated polymer came into happened due to the gravity. When the metallic nozzle was forced with the positive potential through high voltage source and the substrate was grounded, the meniscus appearing at the apex of the nozzle deformed into dripping, micro-dripping,

unstable cone-jet and finally into a conical shape according to the voltage level supplied by the high power source. The conical shape (Taylor cone) appeared because of the electric stress overcome the surface tension of the liquid (PEDOT:PSS ink) and thin liquid jet came out of the Taylor cone. The jet emerging at the apex of the Taylor cone was given a sufficient flight time by adjusting the distance from nozzle to substrate so that it disintegrated into uniform small droplets and collected over the ITO coated PET substrate. During the flight time of the droplets most of solvent evaporated. Further increase in voltage resulted into a multi cone-jet mode of the EHDA process of the PEDOT:PSS ink. All the EHDA modes appeared in the deposition of the PEDOT:PSS ink are shown in figure 3.22.

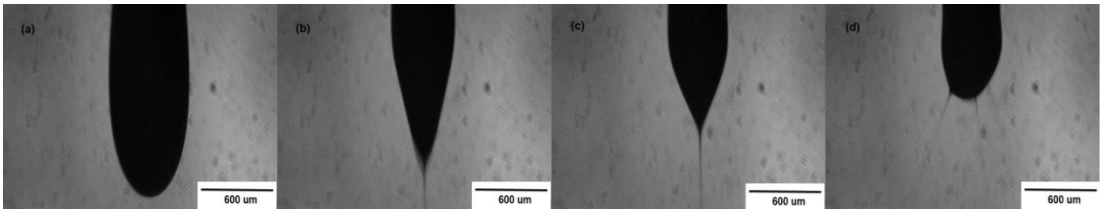

Figure 3.22 EHDA modes of PEDOT:PSS Ink: (a) Dripping (b) Unstable Cone-Jet (c) Cone-Jet (d) Multi Cone-Jet.

PEDOT:PSS operating envelope was also investigated with different voltages and flow rates of the polymeric ink as shown in figure 3.23. The shaped area in the graph indicates the cone-jet mode of the EHDA of PEDOT:PSS ink that is needed to deploy a uniform nano-layer of PEDOT:PSS polymeric ink.

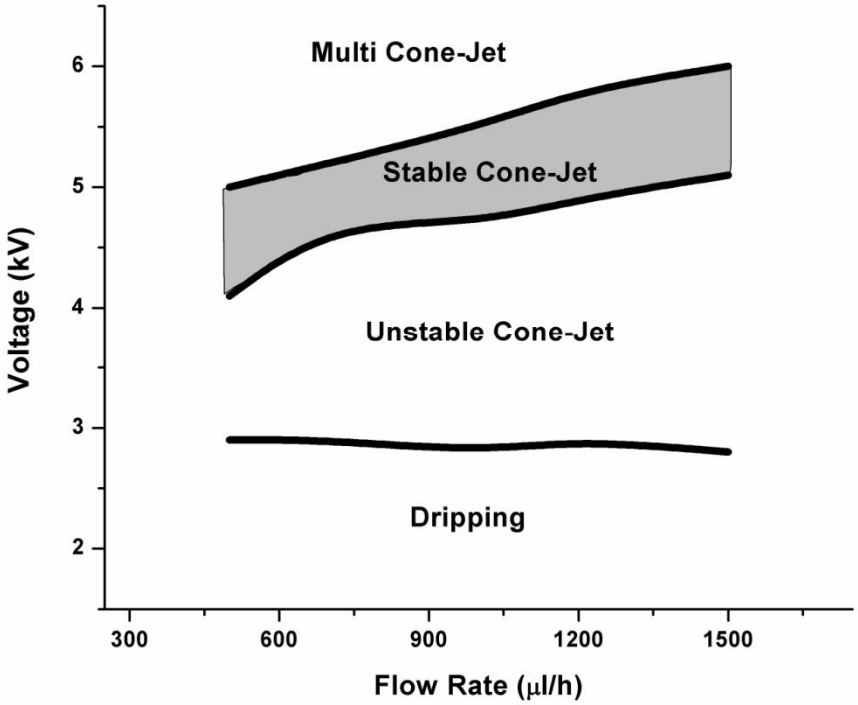

Figure 3.23 Operating envelope of the EHDA of PEDOT:PSS ink.

The reported sample of the PEDOT:PSS ink was deposited in the cone jet mode under the flow rate of 1000 μl/h and with the supply voltage of 5.2 kV in the current research work. The distance from nozzle to substrate was kept at 1 cm. The sample was deposited in a single pass with the substrate speed during the deposition process was kept as 2 mm/s. The deposited sample was cured at 110 °C for 1 h to remove the remaining solvent in the droplets and to achieve a smooth polymeric layer of PEDOT:PSS on the ITO coated PET. To complete the sandwiched structure for the NDR devices, finally Ag drops were deposited on the cured layer of the PEDOT:PSS.

3.3.2 Layer Characterization of PEDOT:PSS Resistive Switches

The reported layer thickness of PEDOT:PSS was measured through film thickness measurement system K-MAC ST4000-DLX and recorded to be 74 nm. The surface morphology of the PEDOT:PSS sample was characterized through the FESEM images taken by SEM, Jeol JSM-7600F. FESEM images of the PEDOT:PSS film on the ITO coated PET in low and high resolution are shown in figure 3.24. As evident

from the FESEM images, very smooth and uniform surface of PEDOT:PSS was deposited on the ITO coated PET substrate through EHDA technique. The hard and soft segments are shown as bright (PEDOT) and dark (PSS) regions respectively (Na et al. 2009). Where PEDOT is the conductive chain and PSS is the insulating chain of the conjugated PEDOT:PSS polymer.

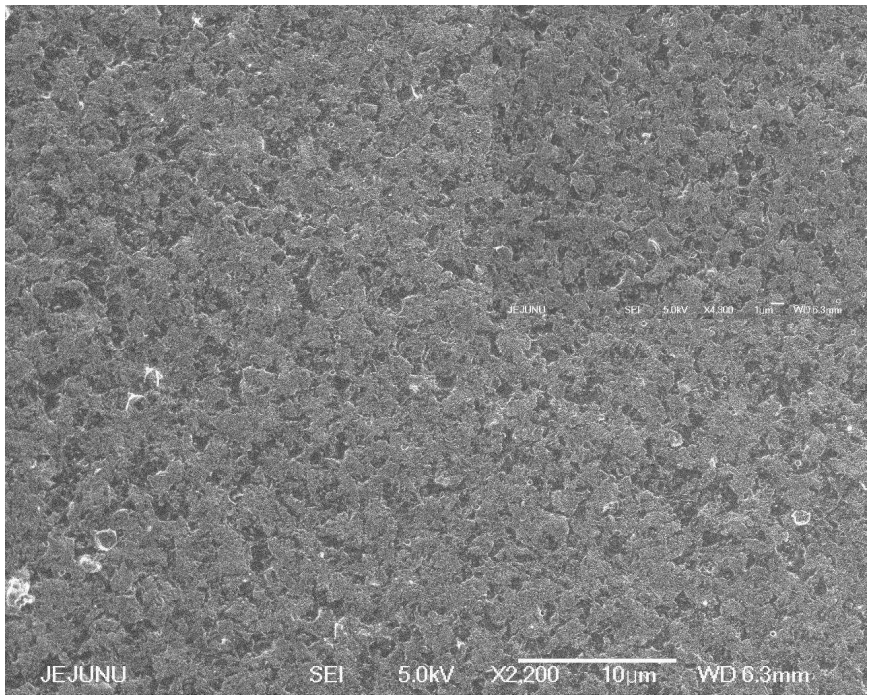

Figure 3.24 FESEM images of the PEDOT:PSS layer on the ITO coated PET.

The chemistry of the deposited sample was confirmed as PEDOT:PSS conjugated polymer through the Raman spectroscopy analysis taken by FT-IR/Raman Spectrometer (IFS 66/S, FRA 106/S) with excitation wavelength of 1064 nm. The Raman spectra validates the presence of the PEDOT:PSS polymer as shown in figure 3.25. In the Raman spectra of PEDOT:PSS, a band with a strong intensity was centered at around 1426 cm^{-1} which corresponds to the symmetric stretching mode of the aromatic C=C band as reported in the literature (Nguyen and Vos 2004).

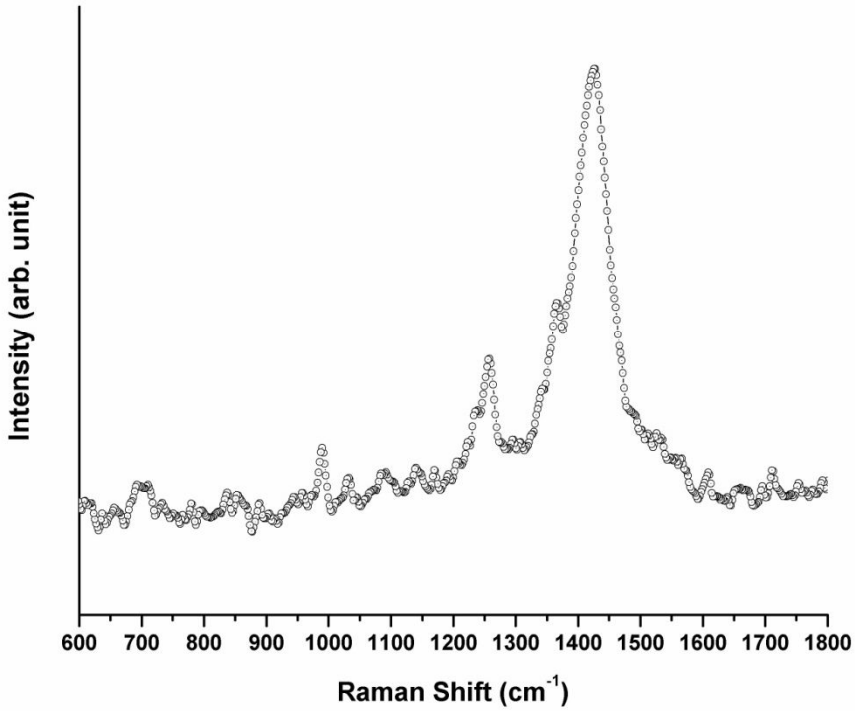

Figure 3.25 Raman spectra of the PEDOT:PSS layer on the ITO coated PET.

3.3.3 Resistive Switching Characterization

Current-Voltage (I-V) characterization of the as-fabricated ITO/PEDOT:PSS/Ag sandwiched device was done with the help of Agilent B1500A Semiconductor Device Analyzer. During the entire process of I-V analysis, the top Ag electrode of the fabricated device was connected with the driving potential while the bottom ITO electrode was grounded.

NDR effects were examined in the ITO/PEDOT:PSS/Ag sandwiched switches by setting different current compliance (CC). The pristine samples of the ITO/PEDOT:PSS/Ag sandwiched structures were examined under different CC to investigate the resistive switching. The samples were forced with the CC of 500 μA, 1 mA, 3 mA, 5 mA, 10 mA, 15 mA and 20 mA. It was found that at low CC the samples did not exhibit resistive switching up to 5 mA but as the CC was set larger than 5 mA the resistive switching within the ITO/PEDOT:PSS/Ag sandwiched devices come into picture as shown in figure 3.26. It was also observed that as setting

the CC larger than 20 mA the hard break down occurred in the fabricated devices of PEDOT:PSS that results in simple ohmic behavior in the PEDOT:PSS nanolayer.

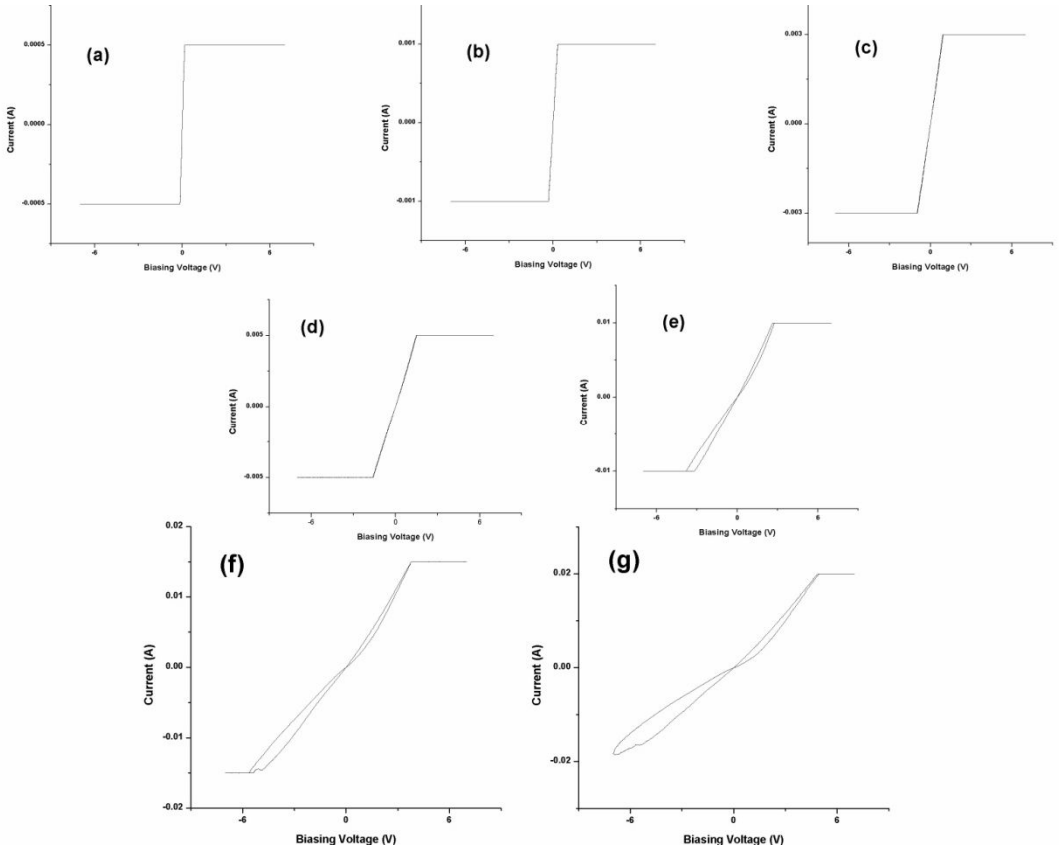

Figure 3.26 I-V analysis of the ITO/PEDOT:PSS/Ag sandwiched device with different CC: (a) 500 µA (b) 1 mA (c) 3 mA (d) 5 mA (e) 10 mA (f) 15 mA (g) 20 mA.

To exempt the PEDOT:PSS resistive switches from hard break down within the nanolayer of PEDOT:PSS, the fabricated switches were operated under the CC of 15 mA and within the voltage of ± 5 V as shown in figure 3.27. Bipolar DC voltage sweep was applied from + 5 V to – 5 V on the Ag top electrode. The I-V behavior of the fabricated device is indicated with arrows in the graph in accordance with the sweeping voltage direction.

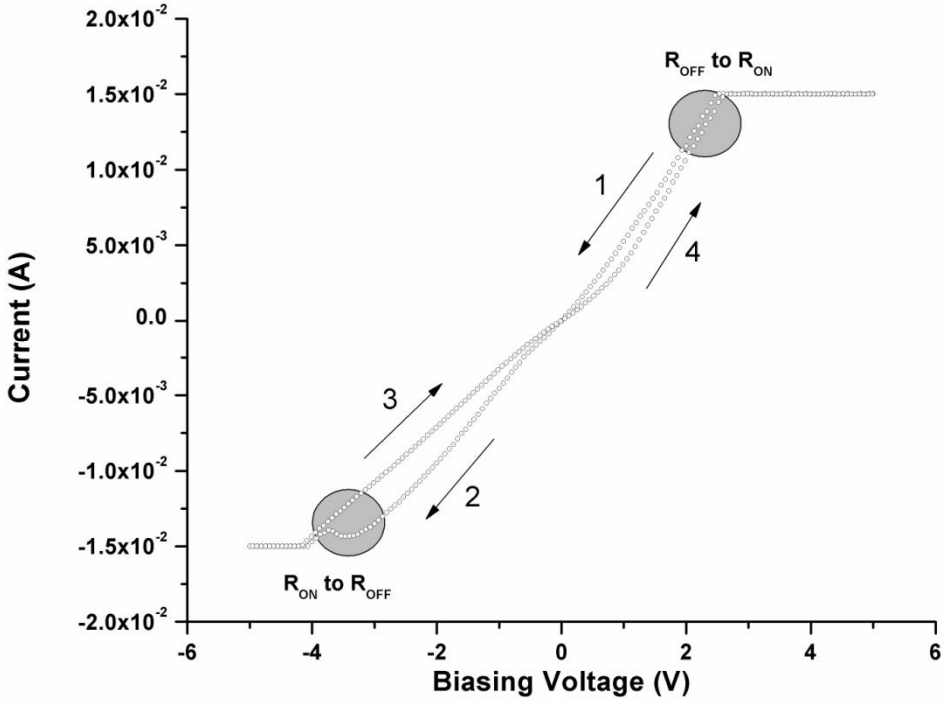

Figure 3.27 I-V curve of the ITO/PEDOT:PSS/Ag sandwiched device with 15 mA CC. The shaded areas denote the setting and resetting of the device. The arrows indicate the sweeping direction of the device.

During the forward cycle of the voltage sweep the fabricated switch started operating in the low resistance state (LRS)/ON-state (R_{ON}) with the average resistance of around 211 Ω. As the voltage reached over – 3 V, the transition from ON-state to OFF-state (R_{OFF})/high resistance state (HRS) occurred called resetting of the device. The reset region is highlighted in the graph with a circular block. The circular region shows NDR characteristics in an I-V trace (-3.25 to -3.75 V) of the fabricated device due to the decrease of current with increase of applied voltage. In the NDR region, the device resistance was translated from a LRS to a HRS. During the reverse cycle of the sweeping voltage, the fabricated device kept its OFF-state unchanged over + 2 V and around + 3 V the device undergoes into the transition phase from HRS to LRS. This is called setting of the device indicated in the shaded circular block in the graph. The average resistance during the OFF-state of the device was observed to be around 266 Ω. The memory window observed in the current work is around 55 Ω that could be widened by deploying the other materials containing metallic nanoparticles into

the PEDOT:PSS layer. The low OFF/ON ratio is required for some specific application like neuromorphic applications. The low resistance in both states of the PEDOT:PSS based resistive switches is due to the conductive nature of the conjugated polymer. The fabricated switch passes through 0 on both directions of the sweeping voltage as shown in figure 3.28 (semilog graph of figure 3.27). The setting and resetting of the device is indicated with the shaded circular blocks in the semilog graph.

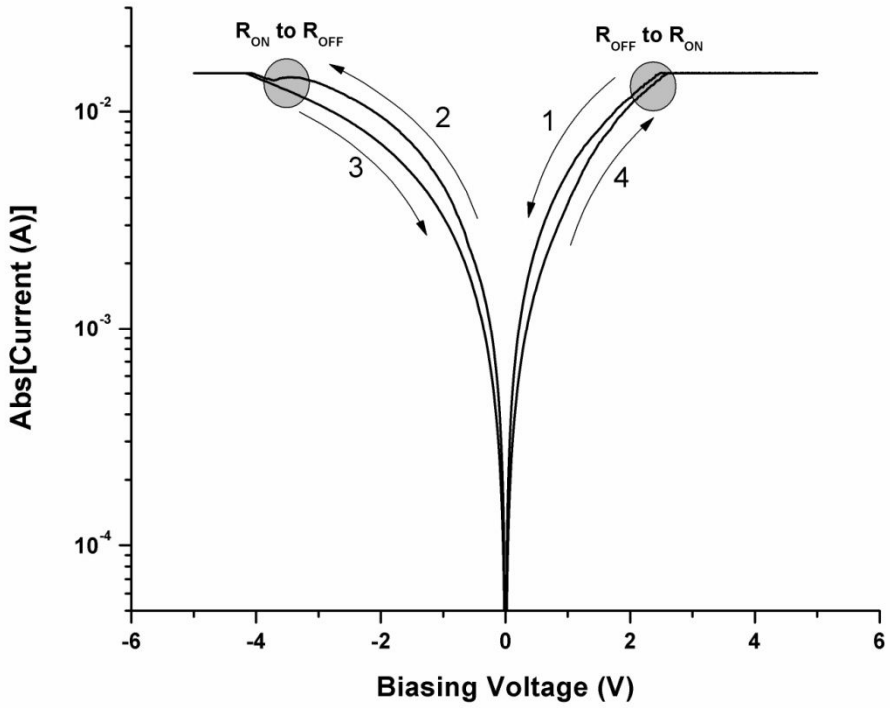

Figure 3.28 Semilog I-V curve of the ITO/PEDOT:PSS/Ag sandwiched device with 15 mA CC passing through 0 on both directions of the polarity. The shaded areas denote the setting and resetting of the device. The arrows indicate the sweeping direction of the device.

High degree of uniformity and robustness was observed against the multiple sweeping voltage stresses in the fabricated switches. I-V behavior of the PEDOT:PSS device is shown for the multiple sweeping voltage over 100 cycles in figure 3.29.

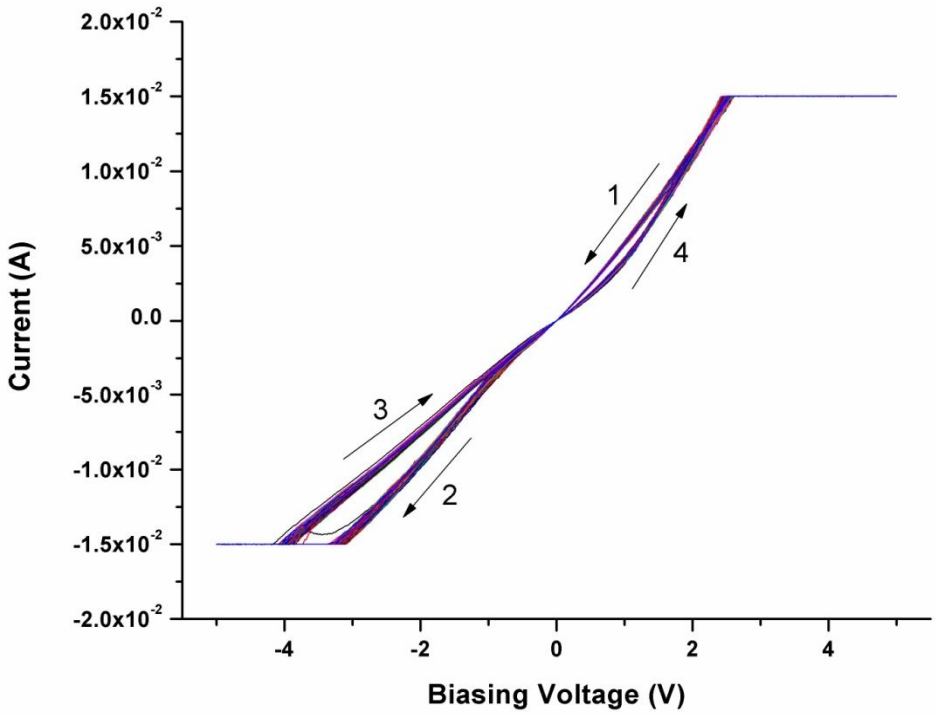

Figure 3.29 Multiple I-V curves of the ITO/PEDOT:PSS/Ag sandwiched device with 15 mA CC over 100 cycles indicate the high degree of uniformity. The arrows indicate the sweeping direction of the device.

Sweeping voltage direction is shown in the graph with arrows. As noticed, the NDR-effect appeared only once in the I-V measurements as shown in the inset of figure 3.29. In fact, this phenomenon is due to the application of CC. The NDR phenomenon appeared only once at some specific CC in the fabricated device. After first I-V trace, the device drew comparatively more current in the subsequent traces. So at a CC of 15 mA, the NDR behavior disappeared in I-V measurements after first I-V trace. During the application of CC, the I-V measurements are changed from voltage driven to current driven mode. When the resistive switch under test attained some specific current amplitude with respect to its switching voltage needed to switch from LRS to HRS, the device switched its R_{ON} into R_{OFF}. Thus, the NDR phenomenon did not come into picture because the semiconductor device analyzer limited the current at its set value (15 mA in figure 3.29). When the CC was extended to some other value, again an NDR effect appeared at that CC as evident from figure 3.26 (f) and (g).

Sweep endurance test is shown in figure 3.30 that depicts the endurance of the fabricated device against multiple sweeping voltages. Over 100 bipolar DC voltage sweeping cycles were applied from + 5 V to – 5 V to check the robustness of the device. The writing voltage for the fabricated device was observed to be +3 V and erasing voltage was observed to be -4 V. The reading voltage (V_{READ}) used for the graph is – 2 V.

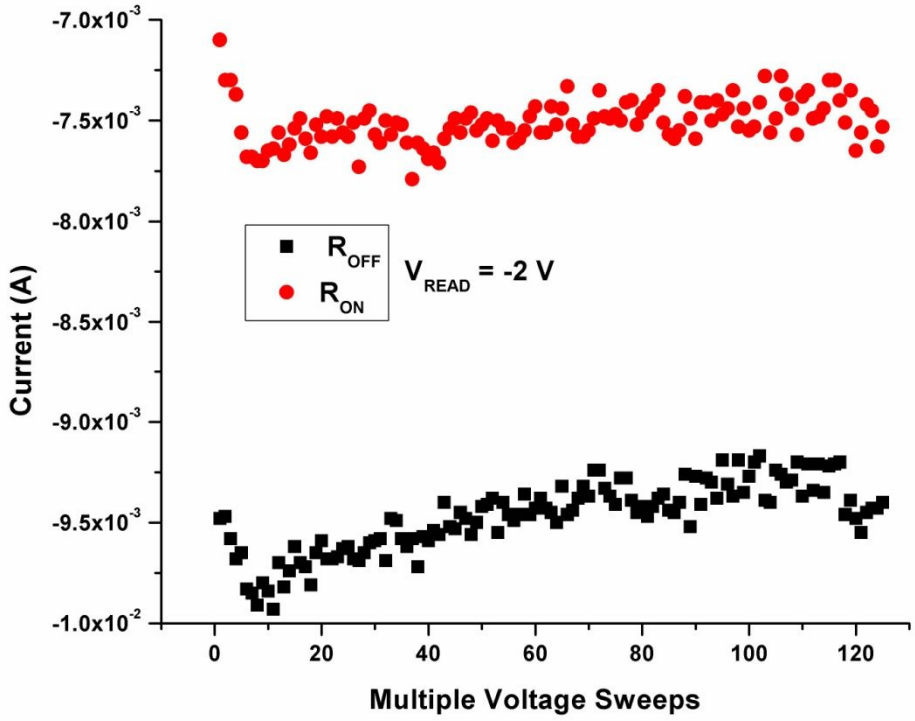

Figure 3.30 Sweep endurance test for the ITO/PEDOT:PSS/Ag sandwiched device at a reading voltage (VREAD) of -2 V over 100 cycles.

The graph shows sufficient margin between two states of the device that is necessary to distinguish ON and OFF-states during the application phase of the sandwiched device. As noticed, an uptrend was observed in the endurance graph that might be attributed to the inherited traps present in the PEDOT:PSS film due to the printing process. These traps were filled after biasing the sample at some sufficient number of sweeps. The sample was tested at around 400 voltage sweeps and it was observed that the mentioned uptrend disappeared at around 90 voltage sweeps.

The retention test of the device was performed over 2500 s. The device kept its state unchanged over 2500 s as shown in figure 3.31. The reading voltage (V_{READ}) used for the retention test is same as in endurance test as – 2 V.

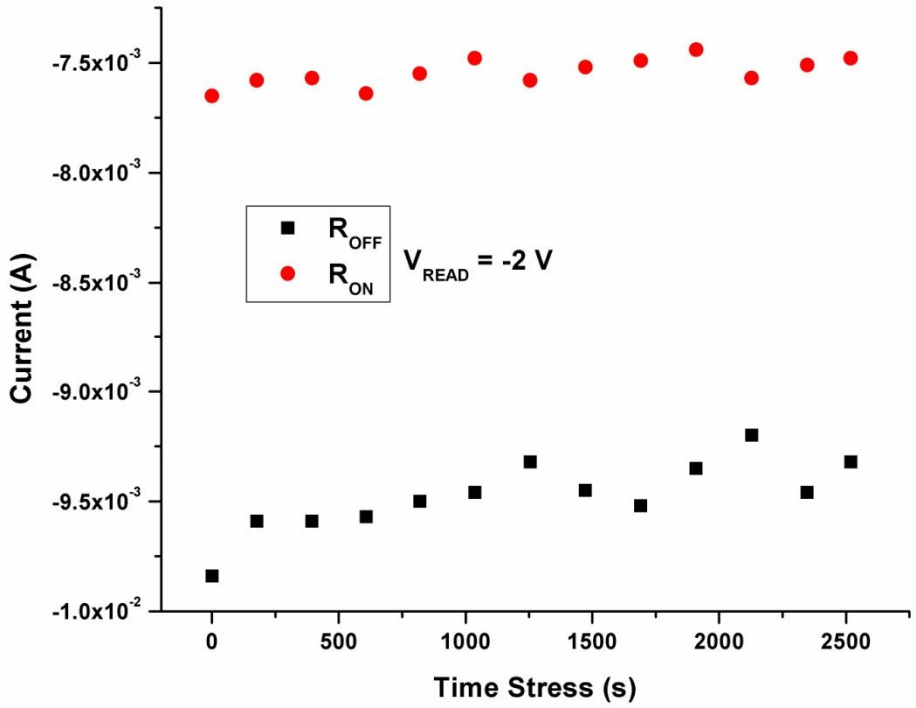

Figure 3.31 Current Vs time stresses graph for the ITO/PEDOT:PSS/Ag sandwiched device at a reading voltage (VREAD) of -2 V over 2500 s.

3.3.4 Resistive Switching and Current Conduction Mechanisms in the Fabricated Switches

The resistive switching mechanism in the electrochemical metallization resistive switching devices could be attributed to the migration of Ag atoms into the PEDOT:PSS film due to the reactive nature of Ag metal. The switching characteristics are also attributed to the trapping and detrapping of Ag atoms at the organic layer but NDR switching mechanism in the PEDOT:PSS based resistive switches is believed to be the redox behavior of the PEDOT:PSS film as reported in literature NDR switching mechanism in the PEDOT:PSS based resistive switches is believed to be the redox behavior of the PEDOT:PSS film as reported in literature (Moller et al. 2003, Sirringhaus et al. 2000, Li et al. 2007, and Peumans and Forrest 2001). When the positive voltage was applied on the Ag top electrode, the PEDOT

chains of the conjugated polymer oxidized to $PEDOT^+$ chains by the injection of hole-carriers through the top electrode. Consequently, the current paths were build up and setting the device into ON-state. Conversely, when the top Ag electrode was applied with the negative potential while the bottom ITO electrode was grounded, the current paths were destroyed by the injected carriers and setting the device into OFF-state. In the OFF-state of the device, the $PEDOT^+$ chains were reduced to $PDOT^0$ chains. The above suggested switching mechanism in the as-fabricated device was analyzed in the I-V curve with a log-log scale. The current conduction mechanisms were concluded on the bases of slope calculation in a log-log scale. In the positive cycle of the voltage sweep, the device started operating in the ON-state. Because the injection of the carriers was done by the positive potential during the CC-region of the biasing voltage, injection behavior was not observed in the forward direction of the voltage sweep as shown in figure 3.32.

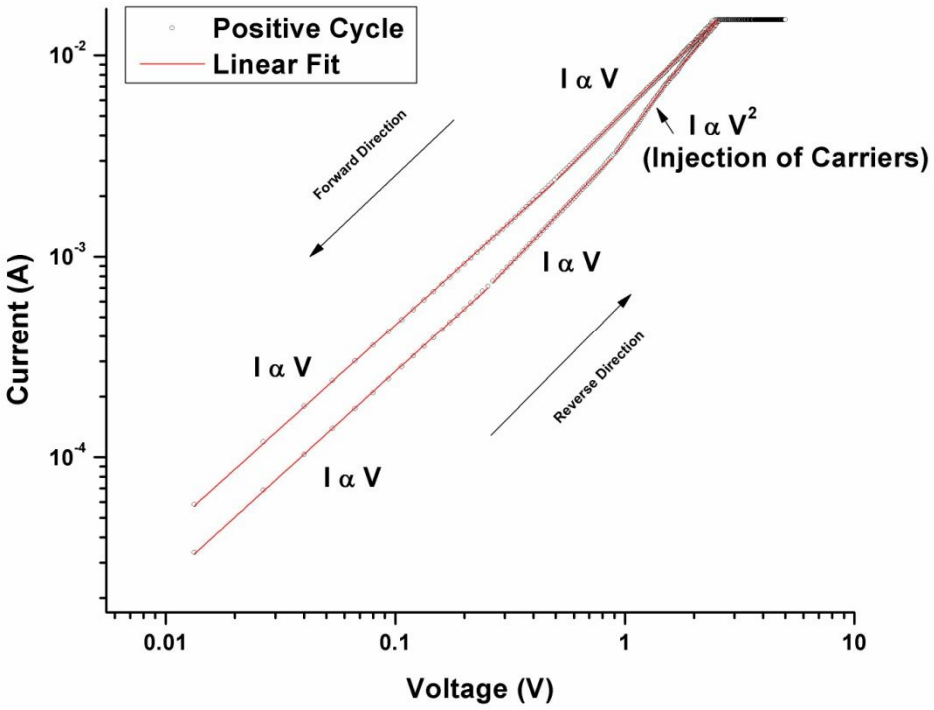

Figure 3.32 Double log I-V graph of the ITO/PEDOT:PSS/Ag sandwiched device in a positive cycle of the sweeping voltage.

During the forward direction of the voltage sweep, the PEDOT chains were oxidized into $PEDOT^+$ chains and current paths were established in the PEDOT:PSS thin film. When the voltage sweep entered into the negative side of the voltage polarity, the device kept its LRS unchanged at around -3 V. Above -3V, the device changed its LRS into HRS due to the injection of carriers by the negative potential as observed in figure 3.33 during the forward direction of the voltage sweep. The injected carriers reduced the $PEDOT^+$ chains into $PEDOT^0$ chains and setting the device into HRS. In the reverse direction of the voltage sweep, the fabricated device exhibited HRS in the negative biasing as shown in figure 3.33.

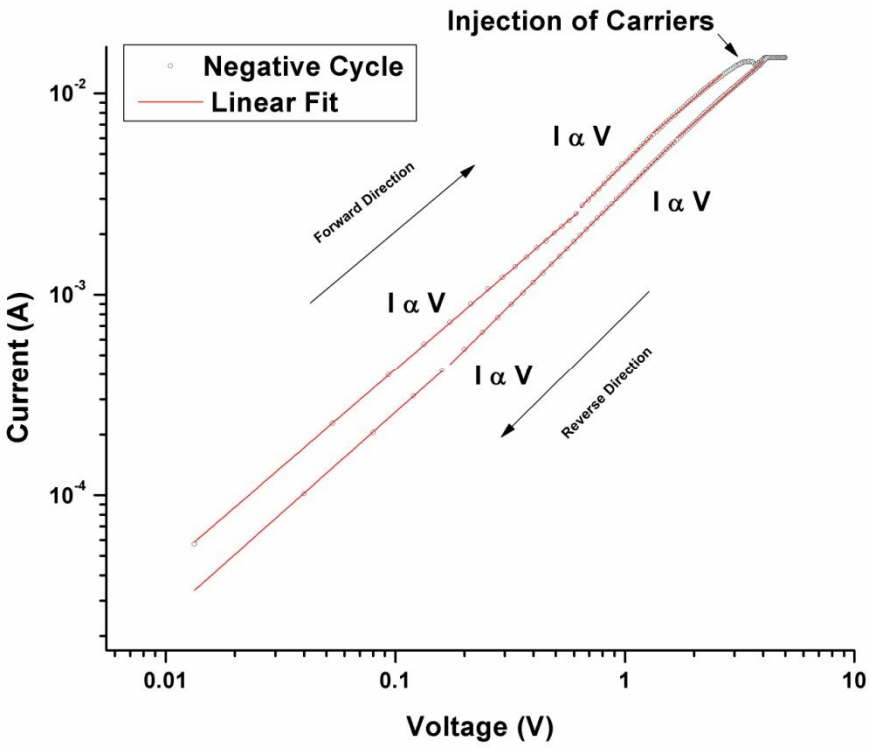

Figure 3.33 Double log I-V graph of the ITO/PEDOT:PSS/Ag sandwiched device in a negative cycle of the sweeping voltage.

When the positive biasing was applied on the top electrode, the device kept its HRS unchanged at around +1 V. Above +1 V, the $PEDOT^0$ chains oxidized into $PEDOT^+$ chains and setting the device again into LRS as observed in the reverse direction in figure 3.32.

It can be noticed in figure 3.32 and figure 3.33 that at lower voltages (below -3 V and +1.5 V) on both sides of the voltage polarity, I-V curve shows linear behavior (I α V) with a slop of 1. So at lower applied voltages, I-V characteristics follow Ohm's law because the density of thermally generated free carriers inside the film is predominant over the injected charge carriers. At higher voltages (above -3 V and +1.5 V) during both the forward and reverse direction of voltage sweep, the current conduction was mainly due to the injection carriers by the top forcing electrode. During the reverse direction of voltage sweep in positive cycle, the I-V curve follows quadratic behavior ($I \alpha V^2$) with a slope of around 2 showing space charge limited (SCL) conduction due to the injection of negative carriers as shown in figure 3.32. While the currents reduces with increasing voltage above -3 V in the forward direction of voltage sweep in negative cycle that shows NDR regime due to the injection of positive carriers as shown in figure 3.33. Ohmic and SCL conductions are bulk dominated mechanisms as reported in literature (Shang et al. 2006 and Shen et al. 2004). Thus the carrier transport mechanism in the fabricated device is bulk dominated inside the PEDOT:PSS film.

3.4 Full Organic Resistive Switches

Metallic electrodes limit the promising feasibility of the organic resistive switches to be employed in electronic industry at their full potential regarding the perspective of organic material advantages. So, engineering of the full organic devices has always been demanded in electronic applications by virtue of their simple device structure, low fabrication cost, printability, and flexibility.

In this research work, the fabrication of full organic resistive switch (FORS) was realized with all of its layers (electrodes as well as switching layer) as organic as opposed to the conventional organic resistive devices in which the electrode-materials were inorganic (metallic or ITO etc). Although hybrid resistive switches (structure containing organic as well as inorganic materials) have been reported in literature but to date, no one has reported FORS devices for resistive switching and memory applications. The fabricated FORS device has full potential to revolutionize the electronics industry by shifting the inorganic/hybrid devices to their organic counterparts. In consequence, the electronic devices would not face fabrication

limitations such as high temperature deposition, high capital cost, lack of printability and flexibility etc. This research work reports the fabrication of FORS devices by spin coating of two polymers: poly(3,4-ethylenedioxythiophene):poly(styrenesulfonate) (PEDOT:PSS) and poly(4-vinylphenol) (PVP) on a polyimide (PI) substrate. PEDOT:PSS is a conjugated polymer consisted of two polymeric chains: poly(3,4-ethylenedioxythiophene) (PEDOT) and poly(styrenesulfonate) (PSS). PEDOT:PSS has been known as transparent and conductive in nature in polymeric science (Duraisamy et al. 2012, Alemu et al. 2012, Kim et al. 2011, and Kymakis et al. 2006). PEDOT:PSS was used as conducting top and bottom electrodes for the FORS fabrication in this study. Poly(4-vinylphenol) (PVP) is another common polymer being used as a dielectric, a cross-linking agent and also has been used as a switching layer in resistive switching memory applications (Paul et al. 2006, Song et al. 2011, Mamo et al. 2010, Liu et al. 2009, and Awais and Choi 2013). PVP was employed as a switching layer between two PEDOT:PSS electrodes for the fabrication of the FORS.

The resistance of the PVP layer, sandwiched between two conducing PEDOT:PSS electrodes, was modulated by the semiconductor device analyzer to elucidate the resistive switching behavior in the fabricated FORS. The robustness of the stable resistive switching was evidenced through stressing the device with multiple voltage sweeps. Resistive switching mechanism was described in the fabricated FORS devices. The current conduction behavior governing the device resistance was concluded based on slopes calculation in the double logarithmic graphs. The current conduction mechanisms were validated through physical current conduction laws. The suggested resistive switching mechanism was correlated with the concluded current conduction behavior in the fabricated FORS.

3.4.1 Fabrication of Printed FORS

Chemically modified PEDOT:PSS ink with isopropanol and deionized water (Duraisamy et al. 2012) was used to deposit the top and bottom conducting electrodes. The switching layer between two PEDOT:PSS electrodes was deposited by the PVP polymeric ink purchased from Sigma-Aldrich.

The reported FORS device, as shown in figure 3.34, was fabricated by spin coating process.

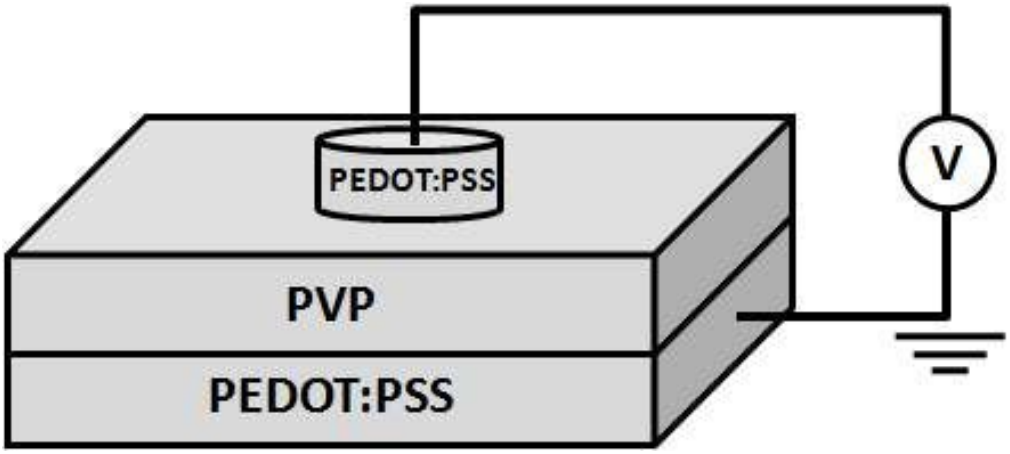

Figure 3.34 Schematic diagram of the FORS device with the sandwich structure of PEDOT:PSS/PVP/PEDOT:PSS.

Initially the bottom electrode was deposited by spin coating the PEDOT:PSS ink on the PI substrate at 700 rpm. The sample was cured at 110 °C for 1 h. After curing process, the sandwich layer was deposited by spin coating the PVP polymeric ink on the PEDOT:PSS bottom electrode at the same parameters listed above. Again the curing of the deposited sample was performed at 110 °C for 1 h. The top PEDOT:PSS electrodes were deposited on the PVP layer by drop casting in a circular shapes with a diameter of around 1500 μm. Finally, the samples were subjected to heat treatment for 110 °C for 1 h.

3.4.2 Layer Characterization of FORS

Cross-sectional image of the fabricated device on the PI substrate was taken by using SEM system (JSM-6700F, JEOL Ltd, Japan) as shown in figure 3.35.

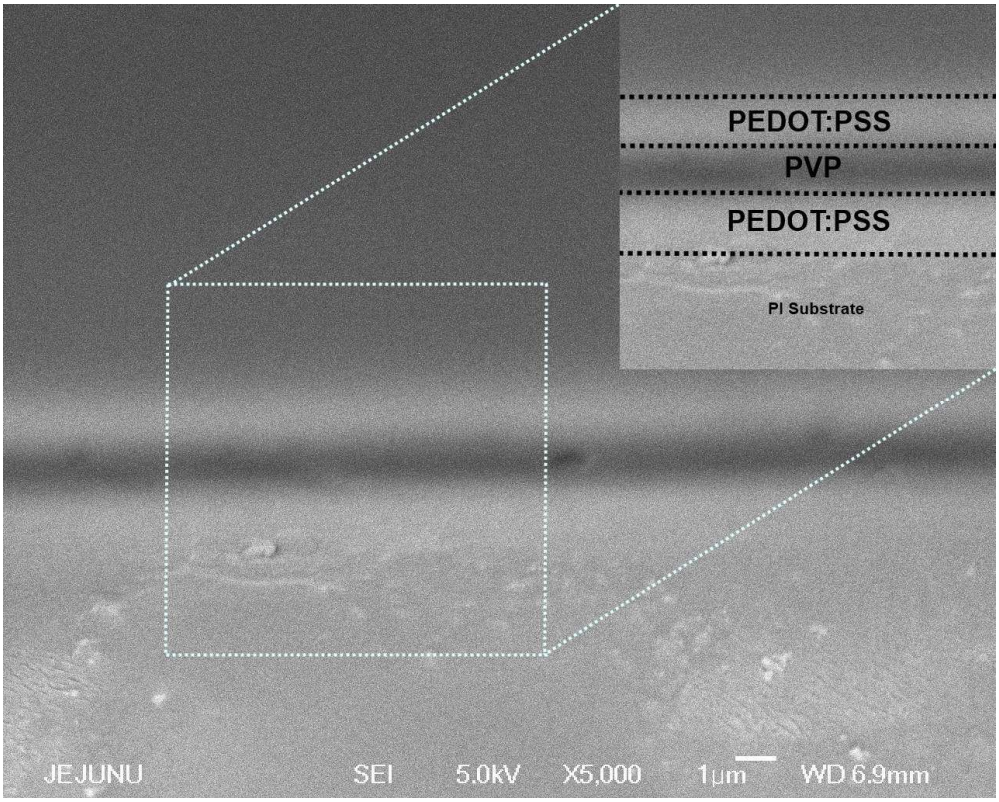

Figure 3.35 Cross-sectional FESEM image of the FORS device with the sandwich structure of PEDOT:PSS/PVP/PEDOT:PSS.

In the field emission scanning electron microscope (FESEM) image, PEDOT:PSS is the first layer on the PI substrate that was used as a bottom electrode. The second layer in the image is the PVP layer on the PEDOT:PSS layer acts as an active layer. The top layer is the PEDOT:PSS layer on the PVP layer serving as a top electrode in the FORS sandwich structure. The thickness of each of the three layers: PEDOT:PSS layer (bottom electrode), PVP layer (switching layer), and PEDOT:PSS (top electrode) is around 1 μm, so the total thickness of the fabricated FORS is around 3 μm as shown in the inset of figure 3.35.

3.4.3 Resistive Switching Characterization

Current-voltage (I-V) measurements of the fabricated devices were performed by an Agilent B1500A semiconductor device analyzer. All of the electrical characterization was done by forcing the top electrode with the voltage source and grounding the bottom electrode. Figure 3.36 shows the I-V measurement of the FORS device.

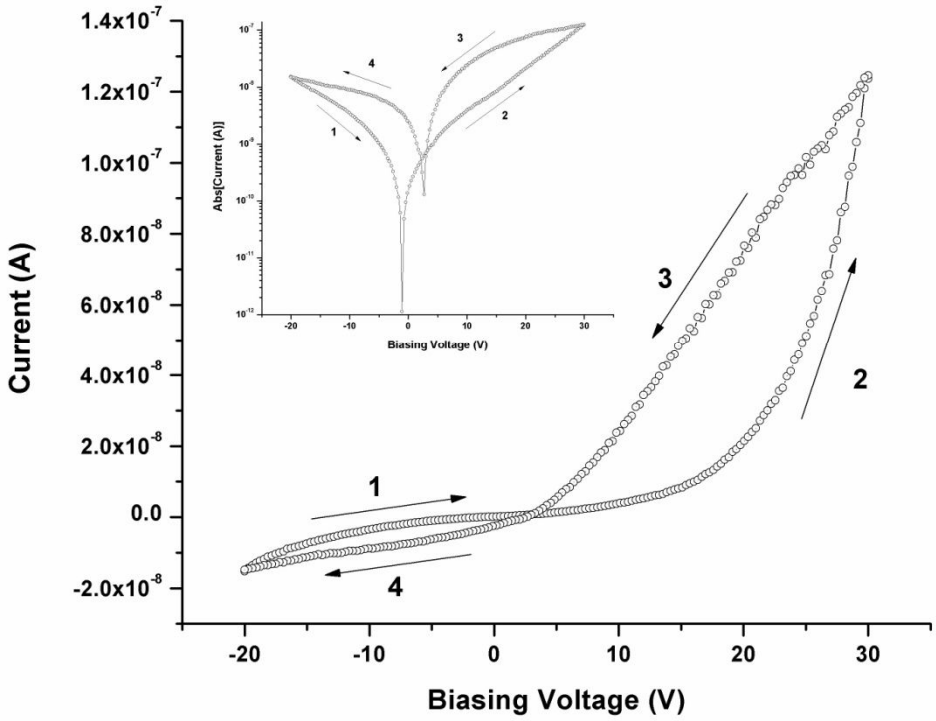

Figure 3.36 IV analysis of the PEDOT:PSS/PVP/PEDOT:PSS sandwich device. The inset shows the semi-log graph PEDOT:PSS/PVP/PEDOT:PSS sandwich device.

I-V curves were obtained by double sweeping the voltage from -20 to +30 V. In the forward direction of the voltage polarity, the device exhibited low conductivity state/high resistance state (HRS)/OFF state. At around +20 V, the device changed its OFF state into ON state/low resistance state (LRS)/high conductivity state. In the reverse direction of the voltage sweep, the device started in the ON state and switched back into OFF state at around -20 V. The exhibited I-V hysteresis with two distinct states can be exploited to use the fabricated FORS for bistable memory applications. It can be noticed that the device offers different memory window on both the positive side and negative side of the voltage polarity. This feature can be utilized to use the fabricated device in two different scenarios. PEDOT:PSS contact is known as an efficient hole injection layer due to its work function (~ 5.1 eV) where as it acts as a high barrier for the electron transport. So, the switching phenomenon in the fabricated FORS could be attributed to the hole injection by the top PEDOT:PSS electrode into the PVP layer and the trapping of mobile carriers (holes) within the PVP layer. As noticed the top electrode was forced with negative

as well as positive polarities, while the bottom electrode was grounded during all the measurements. During the application of negative polarity on top PEDOT:PSS electrode, only small amount of current was flown into the FORS device because PEDOT:PSS is not efficient electron transport material. While in the application of positive potential on top PEDOT:PSS electrode, significant current was flown due to the hole injection role of PEDOT:PSS contact as compared to that of negative potential. So, the discussed phenomenon bestowed different current intensity on both sides of the voltage polarity and produced asymmetric I-V characteristics in the fabricated FORS even though both the electrodes are of same material as evident in figure 3.36. The semi-log graph is shown in the inset of figure 3.36 that shows OFF/ON ratio around 10 : 1 which provides sufficient margin to distinguish between two states. It can also be noticed in I-V curve that there is off-set current for both voltage polarities. This is due to the charge trapping in the polymeric layer as noticed in literature (Kim et al. 2008). In the fabricated FORS device, the carriers were injected through PEDOT:PSS top electrode and were trapped within the PVP layer due to the presence of trap sites in it, that produced off-set effect in the I-V curve. Due to the off-set effect, the current did not drop to zero at zero voltage as noticed in the inset of figure 3.36.

Effect of sweeping rate was checked in the I-V characteristics of the fabricated FORS. It was found that the sweeping rate has no noticeable effect on the I-V characteristics: neither on the switching voltage nor on the OFF/ON ratio. Sweeping rate was defined by the delay time during I-V measurements. The delay time was varied from 10 ms to 100 ms with the voltage step-size of 300 mV. A lower delay time resulted in higher sweeping rate and vice versa. The robustness of the device was tested against multiple voltage stresses, the device performed exceptionally well over 100 voltage sweeps as shown in figure 3.37.

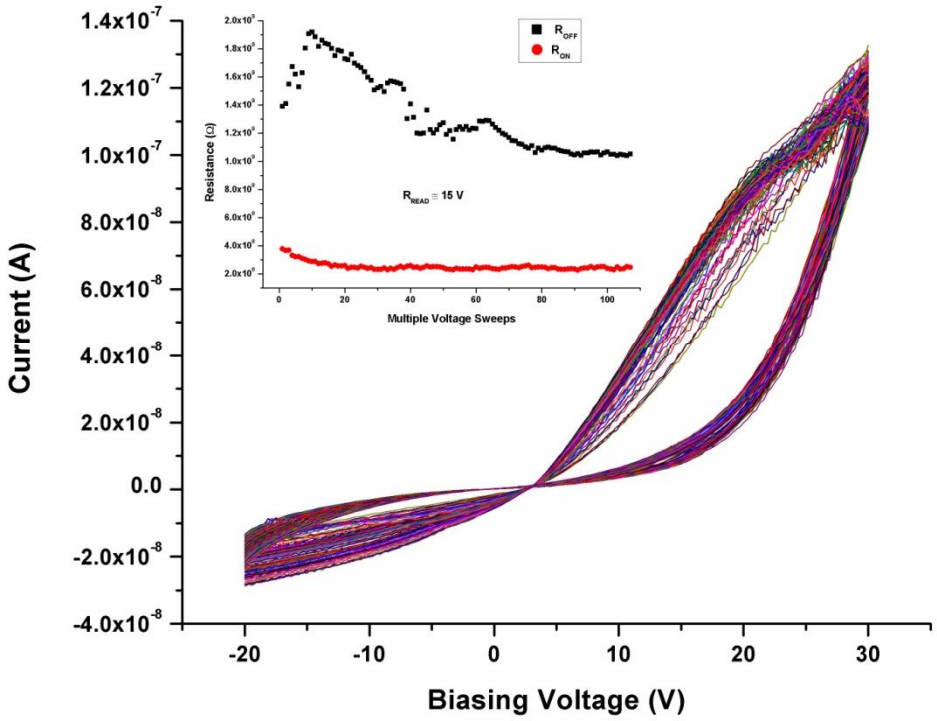

Figure 3.37 Multiple IV curves of the PEDOT:PSS/PVP/PEDOT:PSS sandwich device over 100 cycles. The arrows indicate the sweeping direction of the device. The inset shows the resistance Vs voltage graph for the PEDOT:PSS/PVP/PED sandwich device at a reading voltage (V_{READ}) of +15 V over 100 cycles.

Initially, the resistance of the device in its HRS fluctuated but it settled down after 40 voltage sweeps. It can also be noticed that the LRS is more stable than the HRS throughout the endurance test as shown in the inset of figure 3.37. The fluctuating trend in the endurance test might be attributed to the inherited traps sites and defects created in the PVP film due to the printing process. The fluctuation in I-V curves settled down after 40 voltage sweeps. The average resistances in ON and OFF states of the device were calculated to be 3×10^8 Ω and 1.1×10^9 Ω respectively. The reading voltage (V_{READ}) used to find the OFF and ON state of the device was around +15 V.

The fabricated switch took a large voltage to elucidate resistive switching behavior because of low conductivity of the PEDOT:PSS electrode. The conductive materials having low work functions usually take large voltage for charge injections. This shortcoming could be downplayed by doping the PEDOT:PSS polymer or employing

other techniques to enhance its conductivity (Alemu et al. 2012, Kim et al. 2011, and Kymakis et al. 2006).

5.5 Resistive Switching and Current Conduction Mechanisms in the Fabricated Switches

As noticed in I-V curve of the fabricated FORS device as shown in figure 3.36, the negative polarity on top electrode resulted in a minute current. As compared to that of negative potential, the positive potential on top electrode produced a sufficient high amount of current due to the efficient hole injection role of PEDOT:PSS top electrode. So, the current conduction mechanisms were analyzed only for the positive potential on top electrode.

The current conduction mechanisms in the fabricated FORS were analyzed based on slope calculation by straight line fitting in double logarithmic scale as depicted in figure 3.38, and were supported by the physical laws governing the current conduction mechanism. Four different current conduction mechanisms were suggested underlying bistable resistive switching in the fabricated FORS.

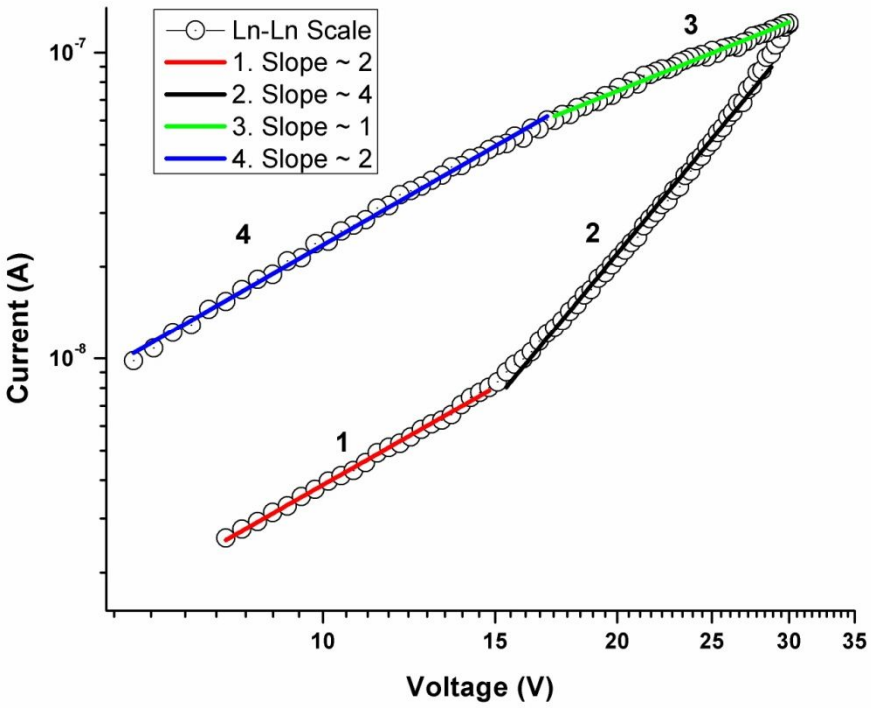

Figure 3.38 Double logarithmic IV graph of the PEDOT:PSS/PVP/PEDOT:PSS sandwich device in a positive cycle of the sweeping voltage indicating different current conduction mechanisms in the forward and reverse direction of the voltage polarity.

In the HRS of FORS device, the conduction mechanism of current is attributed to the space charge limited current (SCLC) conduction up to 15 V (region 1 in figure 3.37). As the holes were injected by the positive potential on top electrode and thereby the accumulation of carriers near the electrode resulted in a space charge buildup. Mutual repulsion among the injected charges limited the further injection of charge carriers into the sample, the resulting current is known as SCLC. Carrier injection electrode (PEDOT:PSS top electrode) is one of the main reasons that arises the SCLC. The injected current in the fabricated sample decreased by several orders due to the presence of traps in the polymer layer (PVP sandwiched layer). The observed phenomenon is quite in line with the reported literature (Ling et al. 2008). The SCLC trap limited regime is controlled by the traps in the PVP layer via thermally activated hopping conduction as reported in literature (Kim et al. 2008, Lampert and Mark 1970, Lin et al. 2007, and Arif et al. 2007). In this regime, the current density is obeyed by the Mott-Gurney law as described below in equation (3.1):

$$J = \frac{9\varepsilon\varepsilon_0\mu\Theta V^2}{d^3} \qquad (3.1)$$

Where ε is the dielectric constant of the switching polymer, ε_0 is the permittivity of the free space, μ is the hole carrier mobility, Θ is the trapping fraction, V is the applied potential, and d is the thickness of the switching polymeric layer.

Once sufficient amount of traps were filled by the mobile carriers, eventually carrier were trapped within the switching PVP polymeric layer. Then, the current in the switching layer was injected due to the trap-charge limited current (TCLC) conduction. Above 15 V (region 2 in figure 3.37) in the HRS of the FORS, TCLC conduction mechanism was found to be the governing conduction mechanism for charge injection into the polymeric layer. In the TCLC conduction, the current increased exponentially and the onset of the trap-filled voltage resulted in the density of traps as observed in literature (Bajpaia et al. 2010 and Brutting et al. 2001). Assuming the trapped hole carrier density >> free hole carrier density, the J-V characteristic is given by the following governing equation (3.2):

(3.2)

Where J is the current density, V is the applied potential, q is the elementary charge, d is the thickness of the material film, μ is the hole carrier mobility, N_v is the effective density of states, ε is the dielectric constant of the material, ε_0 is the permittivity of the free space, H_b is the density of traps at the edge of valance band, and l determines the distribution of traps in the band gap.

In some of the reported literature, an abrupt jump of current by several orders of magnitude was reported after SCLC trap limited regime in the I-V curves which is not considered as normal behavior in SCLC conduction (Kim et al. 2008, Carbone et at. 2005, and Carbone et at. 2006). In contrast to the reported literature, an exponential increase in current was observed after SCLC trap limited regime in the fabricated FORS device that is termed as TCLC conduction.

In the reverse direction of the voltage polarity, the fabricated FORS was operated in the LRS and it was found that the conduction mechanism was dominated by the ohmic conduction (region 3 in figure 3.37) because of the thermal excited mobile carriers hopping from one isolated state to the next as reported in literature (Kim et al. 2008, Lampert and Mark 1970, Lin et al. 2007, and Arif et al. 2007). In this region the current density J can be described by the following governing equation (3.3):

$$J = \frac{qn_0\mu V}{d} \qquad (3.3)$$

Where q is the elementary charge of the carrier, n_0 is the density of free carriers, μ is the carrier mobility, V is the applied voltage, and d is the thickness of the polymeric layer.

In the LRS of the FORS, below 20 V (region 4 in figure 3.38), the fabricated device followed exceptionally well the proportional regime of I to V^2. So, the fabricated FORS device followed trap free SCLC conduction because of the filling of traps through mobile carriers. Trap free SCLC conduction mechanism is usually common after TCLC conduction as reported in literature (Kim et al. 2008, Lampert and Mark 1970, Lin et al. 2007, and Arif et al. 2007). So, the current was injected in the

switching layer of PVP during the LRS of FORS due to the trap free SCLC conduction mechanism.

Based upon the above analysis, the fabricated FORS exhibited reversible resistive switching in the forward direction of the voltage polarity in the HRS of device due to the transition from trap-limited SCLC to TCLC conduction mechanism, and then in the reverse direction of the voltage polarity during the LRS of device from ohmic current conduction to the trap-free SCLC conduction mechanism. So overall, the fabricated FORS exhibited the reversible resistive switching effects due to the transition from the trap-limited SCLC (during HRS) to the trap-free SCLC (during LRS). The non-ideal measuring conditions and more than one current conduction mechanisms involved for charge injection into the PVP polymeric layer ultimately led to the existence of some non-linearities in the perfect line fitting of both the HRS and LRS of the fabricated FORS.

4. Executive Summary

This chapter concludes the discussion of the thesis by providing the summary of chapter 2 and 3 in this thesis.

4.1 Chapter 2

Chapter 2 deals with the fabrication of the ZrO_2-based resistive switches on an ITO-coated PET, glass and PI substrates.

4.1.1 Fabrication of Printed ZrO_2 Resistive Switches on ITO-coated PET

Electrohydrodynamic atomization (EHDA) has been used in this research work to deposit an active layer for the printed resistive switch (memristor). A thin liquid jet of solution containing ZrO_2 (Zirconium Dioxide) nanoparticles was generated through a metallic capillary with a constant flow rate under the electrical forces. Liquid jet was further disintegrated into small droplets, containing nanoparticles, under the influence of electrical stresses and were collected on the ITO coated PET (Polyethylene Terephthalate) to form uniform layer of ZrO_2 nanoparticles. A smooth thin film was observed with an average thickness of 67 nm. Resistive (memristive) behavior was observed in the deposited thin film with ITO (Indium-Tin Oxide) as a bottom electrode and Ag as a top electrode. Bipolar reversible resistive switching was analyzed by setting different current compliances. Results reveal that EHDA has full potential to fabricate the active layer in resistive switches for printed electronics.

4.1.2 Resistive Switching Mechanism in the Fabricated Switches on an ITO-coated PET

This research work analytically demonstrates the resistive switching mechanism in the printed Ag/ZrO_2/ITO structures. The switching between two states (OFF and ON) is attributed to the modulation of ohmic contact into opposite schottky barriers follow-on from the electrochemical dissolution of the Ag filament from the weakest point near the ITO electrode during the transition from ON to OFF state and alteration of the schottky barriers into an ohmic contact consequential from the

reformation of the Ag filament during the transition of OFF state into ON state. Physical current conduction governing laws verify the concluded transition between ohmic contact and schottky barriers.

4.1.3 ZrO_2 - Resistive Switches on Glass Substrate

This research work demonstrates the promising feasibility of electrohydrodynamic (EHD) printing technology for the fabrication of a crossbar resistive switch (memristor) through the patterning of ITO as a bottom electrode and Ag as a top electrode. An ITO/ZrO_2/Ag sandwich exhibiting reversible resistive switching (memristive) behavior has been demonstrated on a glass substrate. A physically layer-wise, electrical current-voltage (IV) characterization was done for the device fabricated using EHD printing. The device dimensions achieved in the current research were around 100 μm × 100 μm. The as-fabricated device showed a high ON/OFF ratio greater than 100000 : 1 with multiple operational voltages less than ± 10 V. The measured retention time of the fabricated device was over 3 days. Results reveal that the current research work provides for the fabrication of a relatively low-cost memristive device with reversible resistive switching properties.

4.1.4 ZrO_2 - Resistive Switches on Flexible Substrate

Electrohydrodynamic (EHD) printing technique has been deployed to fabricate flexible printed resistive (memristive) switch in a Metal-Insulator-Metal sandwich structure of Ag/ZrO_2/Ag on a polyimide substrate under normal room conditions. The top and bottom electrodes were deposited through the jetting of EHD printing and the active layer of ZrO_2 between two electrodes was deposited through the atomization of EHD printing process. The achieved dimensions of the printed device were around 100 μm × 100 μm with the thickness of the bottom electrode, switching layer and top electrode were around 230 nm, 680 nm and 420 nm respectively. The fabricated device showed stable bipolar memristive switching behavior around ± 3 V. The reversible resistive switching behavior was measured with the high OFF/ON ratio of 100 : 1. The device kept on exhibiting memristive characteristics after being physically flexed over 500 times that shows its viability for flexible electronics applications.

4.2 Chapter 3

Chapter 3 describes the fabrication of polymer-based resistive switches with printing technology.

4.2.1 MEH:PPV based Resistive Switches

Poly[2-methoxy-5-(2'-ethylhexyloxy)-(p-phenylenevinylene](MEH:PPV) based organic memristor (Memory Resistor) has been fabricated on the Indium-Tin Oxide (ITO) coated Polyethylene Terephthalate (PET) substrate by the Electrohydrodynamic Atomization (EHDA) technique. Thin jet containing MEH:PPV polymer was generated through a capillary under electrical stresses. The jet was broken into small droplets by adjusting the distance from nozzle to substrate and collected over the substrate under normal room conditions, consequently a high quality layer of MEH:PPV was achieved with an average thickness of 168 nm. The layer was morphologically characterized by Field Emission Scanning Electron Microscope (FESEM) analysis. X-ray Photoelectron Spectroscope (XPS) analysis was also carried out to confirm the chemistry of the deposited material. Electrically, ITO/MEH:PPV/Ag fabricated memristor was found to be switchable between high state and low state between ± 4 V. The research work provides the memristive behavior in electrohydrodynamic atomized layers of MEH:PPV to be used for the next generation printed electronics application.

4.2.2 PVP based Resistive Switches

Resistive switching in organic resistive switches fabricated with a sandwich structure of indium tin oxide (ITO)-coated polyethylene terephthalate (PET)/poly(4-vinylphenol) (PVP)/silver (Ag) is reported. A single layer of PVP was used as an active layer in the sandwich structure between the two electrodes. The active layer of the polymer was atomized with the electrohydrodynamic atomization technique on the ITO-coated PET. The film thickness of the PVP polymeric layer on the ITO-coated PET was measured to be 110 nm. The surface morphology was characterized by field emission scanning electron microscopy and the purity of the film was examined by x-ray photoelectron spectroscopy analysis. Electrical current-voltage (*I-V*) measurements confirmed the memristive behavior of the sandwich device. The

effect of the current compliance (CC) on resistive switching in the fabricated sandwich structure was also explored. The PVP-based organic resistive switch showed a CC-dependent OFF/ON ratio and memory window. Resistive switching memory effects were prominent at low CC up to nanoamps. The as-fabricated device was operated with low operational voltages for both polarities with OFF/ON ratio greater than 100:1. The robustness of the fabricated memristor was checked with multiple voltage sweeps, and the retention time is reported to be over 100 min.

4.2.3 PEDOT:PSS based Resistive Switches

Polymeric negative differential resistive (NDR) switching was explored based on the sandwiched structure of indium titanium oxide (ITO) coated polyethylene-terephthalate(PET)/poly(3,4-ethylenedioxythiophene):poly(styrenesulfonate)(PEDOT:PSS)/silver(Ag) through electrohydrodynamic atomization (EHDA) printing technique. A nanolayer of PEDOT:PSS was being atomized on the ITO coated PET through EHDA technique with the average thickness of around 100 nm. The deposited layer of PEDOT:PSS was morphologically analyzed through field emission scanning electron microscope (FE-SEM) and chemically identification of the sample was carried out through raman spectroscopy analysis. The NDR switching in the fabricated device with the structure of ITO/PEDOT:PSS/Ag was analyzed through semiconductor device analyzer under polarity dependent bipolar sweeping voltage of less than ± 5 V. Effect of the current compliance (CC) in the NDR switching of the fabricated switch has been demonstrated. Multiple resistive switching sweeps were taken to scrutinize the robustness of the fabricated device over 100 cycles. The non-volatility of the as-fabricated device was checked against different time stresses over 2500 s. The switching mechanism is proposed due to the transition between $PEDOT^{+}$ and $PEDOT^{0}$ chains. The current conduction mechanism involved in the PEDOT:PSS based NDR switches is attributed to the ohmic conduction at lower voltages while space charge limited conduction and NRD effects were prominent due to the injection of carriers at higher voltages.

4.2.4 Full Organic Resistive Switches

The research work reported the fabrication of full organic resistive switch (FORS) with the sandwich structure of poly(3,4-ethylenedioxythiophene):poly(styrenesulfonate)(PEDOT:PSS)/poly(4-vinylphenol)(PVP)/poly(3,4-ethylenedioxythiophene):poly(styrenesulfonate)(PEDOT:PSS). The fabricated FORS elucidated reversible bipolar resistive switching behavior at higher operational voltage between -20 V and +30 V. The switching mechanism in the FORS device was attributed to the hole injection through PEDOT:PSS electrode and filling of trap sites in the PVP sandwiched layer by the limited injection. Current conduction mechanisms were concluded and supported by the charge transport governing physical laws. The dominant current conduction mechanism in the fabricated FORS was attributed to the transition from trap-limited space charge limited current (SCLC) conduction to trap-free SCLC conduction mechanism. The robustness of the fabricated FORS was tested over 100 multiple voltage sweeps.

5. Conclusions and Future Work

This chapter describes the conclusions of this thesis and future work.

5.1 Conclusions of the Thesis

5.1.1 Fabrication of Printed ZrO_2 Resistive Switches on ITO-coated PET

Electrohydrodynamic atomization has been successfully deployed to fabricate the active layer of ZrO_2 for bipolar resistive (memristive) switching. ZrO_2 thickness achieved through EHDA is around 67 nm. The fabricated switch could be applied with current compliance from 100 µA to 1 mA and then up to 5 mA. Bipolar resistive switch fabricated in the current work can be used in electrical switching in place of transistors in printed electronics applications. It is successfully demonstrated that EHDA is cost-effective, time saving and direct deposition thin film technique for the active layer of resistive switches at normal room temperature and pressure.

5.1.2 Resistive Switching Mechanism in the Fabricated Switches on an ITO-coated PET

Analytic study has been performed to investigate the switching mechanism in the Ag/ZrO_2/ITO resistive switches fabricated through EHDA printing technique. The high state of the device is achieved owing to the formation of the Ag filament in the ZrO_2 layer and low state is attained through the electrochemical dissolution of the Ag conductive bridge. The switching from LRS to HRS of the device is attributed to the modulation of the ohmic contact into two opposite schottky barriers and vice versa in the transition of HRS to LRS. Finally the concluded conduction mechanisms are validated by straight lines fitting in IV curves of the device both in its low as well as high states.

5.1.3 ZrO_2 - Resistive Switches on Glass Substrate

A relatively low-cost, fabrication friendly and low-power resistive switching (memristive) device was fabricated with EHD printing at normal room conditions. Ag as a top electrode and ITO as a bottom electrode were deposited through EHD jetting. The device was fabricated with device dimensions of 100µm × 100µm.

Further reducing the nozzle diameter and improving the stage speed could achieve nanoscale dimensions. The fabricated device showed a high ON/OFF ratio greater than 100000 : 1. The researched device has full potential for neuromorphic applications due to incremental change in its resistance and for non-volatile memory applications.

5.1.4 ZrO_2 - Resistive Switches on Flexible Substrate

EHD printing, an alternate fabrication process, for the flexible memristor or resistive switch has been demonstrated for the MIM structure of Ag/ZrO_2/Ag on a PI substrate to show its memristive behavior. A high degree of smoothness and uniformity was observed in all the three layers of the device as evident from the FIB image. The device fabricated with purposed technique could be operated within low operational voltage of ±3 V. The as-fabricated device exhibited high OFF/ON ratio of two orders of magnitude. SCLC and TCLC conductions were observed to be the governing current conductions during the HRS and LRS of the fabricated device respectively. Finally the resistive switch also demonstrated reversible resistive switching over 500 times physical flexes to prove its utility in the flexible electronics applications.

5.1.5 MEH:PPV based Resistive Switches

Fabrication of the MEH:PPV based printed memristive device though EHDA technique has been demonstrated. The achieved thickness of the MEH:PPV for the switching layer of the memristor was 168 nm. The FESEM image shows smooth and uniform surface morphology of the deposited layer. IV characterization of the fabricated device promises the memristive behavior in the sandwich structure. The switching mechanism in the fabricated device is attributed to the ohmic conduction during high and low states of the ITO/MEH:PPV/Ag sandwich. Endurance test and non-volatility of the fabricated sandwich device has been examined as well for its application feasibility and found to be satisfactory.

5.1.6 PVP based Resistive Switches

ITO/PVP/Ag sandwich devices were fabricated with the simplest structure amongst the organic resistive switches by using a cost-effective EHDA technique. The influence of the CC on the resistive switching in the ITO/PVP/Ag sandwich was

demonstrated. The fabricated devices have the potential to be operated at low CC on both sides of the voltage polarity. Setting of a lower CC results in better resistive switching in the fabricated ITO/PVP/Ag sandwiches. The fabricated device has the potential to be used as memory or switching element in organic electronics applications.

5.1.7 PEDOT:PSS based Resistive Switches

Negative differential resistive switching effects were demonstrated in the printed organic ITO/PEDOT:PSS/Ag sandwiching device through electrohydrodynamic atomization technique. The modulation of the resistive switching in the fabricated device with different current compliance was presented. The device was tested over 100 voltage sweeps for the endurance description. The fabricated device was checked over 2500 s for the retention test. The switching mechanism in the fabrication device was suggested to the formation of current paths due to the redox behavior PEDOT film. The current conduction mechanism in the fabricated device was attributed to the injection carriers at higher voltages (above -3 V and +1.5 V) which caused SCL conduction at positive cycle and NDR effects at negative cycle of the voltage sweep. While Ohmic conduction was prominent at lower voltages due to the thermally generated free carriers inside the PEDOT:PSS film.

5.1.8 Full Organic Resistive Switches

Bistable resistive switching effects were demonstrated in the FORS with the sandwich structure of PEDOT:PSS/PVP/PEDOT:PSS. Robustness of the fabricated device was scrutinized over 100 voltage sweeps. Four different current conduction mechanisms were found and analyzed through slope calculation. Overall the fabricated resistive device exhibited bistable resistive switching in the transition of trap-limited space charge limit current conduction during the OFF-state of the device to the trap-free space charge current conduction during its ON-state.

5.2 Future Work

ZrO_2 based resistive switches were fabricated by printing technique on different glass, ITO-coated PET and flexible substrates but there integration with the exiting CMOS

technology is still an issue for real time printed electronics applications. Conventional CMOS technology is based on three-terminal transistor while the resistive switch is two-terminal device that needs different circuit design strategy. ZrO_2 based resistive switches were still not realized on stretchable substrates that is one of the forthcoming needs in printed electronics applications. Analytical study of the switching mechanism in ZrO_2 based resistive switches with different electrodes' materials is still left for some potential applications where specific material-electrodes are mandatory.

Organic resistive switches were fabricated based on different organics switching materials. FORS devices were also realized with all the layers in the fabricated device as organic materials. But the switching voltage and OFF/ON ratio is still an issue. Fabrication of FORS devices were done only with the structure of PEDOT:PSS/PVP/PEDOT:PSS material. To date, FORS devices were not fabricated with other polymer materials combinations. That shortcoming in the fabricated device needs some work with respect to the electrode material with high conductivity. Realization of the organic-resistive switches on stretchable substrates will also add-on the advantages of the organic resistive switches over their inorganic counterparts.

References

Akinaga and Shima, Proceedings of the IEEE 98, 2237 (2010)

Alemu et al., Energy Environ. Sci. 5, 9662 (2012)

Arif et al., Phys. Rev. B 75, 195202 (2007)

Asamitsu et al., Nature 388, 50 (1997)

Awais and Choi, J. Electronic Mater. 42, 1202 (2013)

Awais and Choi, Jpn. J. Appl. Phys. 52, 05DA05 (2013)

Awais et al., Microelectron. Eng. 103, 167 (2013)

Awais et al., Thin Solid Films (2013)

Bajpaia et al., Synthetic Metals 160, 1740 (2010)

Beck et al., Appl. Phys. Lett. 77, 139 (2000)

Bozano et al., Appl. Phys. Lett. 84, 607 (2004)

Brutting et al., Synth. Met. 122, 99 (2001)

Carbone et at., Phys. Rev. Lett. 95 (2005)

Carbone et at., Eur. Phys. J. B (2006)

Chen et al., Appl. Phys. Lett. 92, 262110 (2010)

Cho et al., Adv. Funct. Mater. 21, 2806 (2011)

Choi and Awais, J. Korean Phys. Soc. 61, 119 (2012)

Choi et al., Appl. Phys. A 106, 165 (2011)

Choi et al., J. of Appl. Phys., 98, 1 (2005)

Chua, Appl. Phys. A 102, 765 (2011)

Chua, IEEE Transactions on Circuit Theory 18, 507 (1971)

Collier et al., Science 285, 391 (1999)

Du et al., ACS Nano 6, 2517 (2012)

Duraisamy et al., Materials Letters 83, 80 (2012)

Erokhin et al., Nano Communication Networks 1, 108 (2010)

Ferrance et al., J Nanopart. Res. 12, 405 (2010)

Guan et al., Appl. Phys. Lett. 91, 062111 (2007)

Guan et al., Appl. Phys. Lett. 93, 223506 (2008)

Ha and Kim, Appl. Phys. Lett. 93, 033 309 (2008)

Ha and Kim, IEEE Electr. Device L. 31, 368 (2010)

Ha and Kim, Jpn. J. Appl. Phys. 48, 04C 169 (2009)

Hackett et al., IEEE Electron Device Letters 30, 7, 706 (2009)

Hartman, Ph.D. Thesis, TU Delft (1998)

Hickmott, J. Appl. Phys. 33, 2669 (1962)

Hong et al., IEEE Electron Device Lett. 31, 1005 (2010)

Jaworek, Powder Technology 176, 18 (2007)

Jayakumar et al., solid state physics, proceedings of the 55th DAE solid state symposium 2012, AIP Conference Proceedings 1349, 257 (2011)

Jeong et al., Nano Lett. 10, 4381 (2010)

Ji et al., Adv. Mater. 22, 3071 (2010)

Jo et al., Nano Lett. 10, 1297 (2010)

Jung et al., Nano Lett. 4, 1225 (2004)

Kavehei et al., 2011 IEEE 54th International Midwest Symposium on Circuits and Systems (MWSCAS), DOI: 10.1109/MWSCAS.2011.6026575, 1 (2011)

Kim and Chun, Phys. Fluids 13, 643 (2001)

Kim et al., Adv. Funct. Mater. 21, 1076 (2011)

Kim et al., Appl. Phys. Lett. 92, 253308 (2008)

Kim et al., Nano Lett. 11(12), 5438 (2011)

Kymakis et al., The European Physical Journal Applied Physics 36, 257 (2006)

Lai and Chen, IEEE Electron Device Lett. 32, 387 (2011)

Lampert and Mark, Current Injection in Solids, Academic Press, New York (1970)

Lauters et al., Appl Phys Lett. 89, 13507 (2006)

Lee and Chen, MRS Bulletin February 37, 144 (2012)

Lee et al., Appl. Phys. Lett. 95, 262113 (2009)

Li et al., Appl. Phys. Lett. 90, 173505 (2007)

Li et al., The Sixteenth Annual International Conference on Micro Electro Mechanical Systems, 2003. MEMS-03 Kyoto IEEE, DOI: 10.1109/MEMSYS.2003.1189839, 674 (2003)

Lin et al., IEEE Electron Device Lett. 27, 725 (2006)

Lin et al., IEEE Electron Device Lett. 28, 366 (2007)

Lin et al., IEEE Electron Device Lett. 28, 569 (2007)

Lin et al., Nanoscale Research Letters 7:187 (2012)

Ling et al., Pog. Polym. Sci. 33, 917 (2008)

Liu et al., Appl. Phys. Lett. 92, 012117 (2008)

Liu et al., Appl. Phys. Lett. 94, 203301 (2009)

Liu et al., IEEE Electron Device Lett. 26, 351 (2005)

Long et al., Appl. Phys. A 102, 915 (2011)

Lu et al., 2011 16th Asia and South Pacific Design Automation Conference (ASP-DAC), DOI: 10.1109/ASPDAC.2011.5722187, 217 (2011)

Malliaras et al., Phys. Rev. B, Condens. Matter. 58, R13 411 (1998)

Mamo et al., Org. Electron. 11, 1858 (2010)

Manoj et al., J Appl. Phys. 94, 4088 (2003)

Miller et al., IEEE Electron Device Letters 31, 7, 737 (2010)

Mitzi, Solution Processing of Inorganic Materials, A. John Wiley & sons, Inc., New Jersey NJ, (2009)

Moller et al., J. Appl. Phys. 94, 7811 (2003)

Moller et al., Nature (London) 426, 166 (2003)

Muhammad et al., Curr. Appl. Phys. 11 (2011)

Muhammad et al., Thin Solid Films 520, 1751(2012)

Na et al., J. Mater. Chem. 19, 9045 (2009)

Nguyen and Vos, Appl. Surf. Sci. 221, 330 (2004)

Park et al., Nature Mater. 6, 782 (2007)

Paul et al., Nanotechnology 17, 145 (2006)

Pender and Fleming, J. Appl. Phys. 46, 3426 (1975)

Peumans and Forrest, Appl. Phys. Lett. 79, 126 (2001)

Poon, Ph.D. Thesis, Princeton University (2002)

Prodromakis et al., 2010 12th International Workshop on Cellular Nanoscale Networks and Their Applications (CNNA), Berkeley, DOI: 10.1109/CNNA.2010.5430323, (2010)

Prodromakis et al., Proceedings of the IEEE CNNA Conference, (2010)

Reed et al., Appl Phys Lett. 78, 3735 (2001)

Samarasinghe et al., Appl. Phys. A-Mater. Sci. Proess. 91, 141 (2008)

Samarasinghe et al., Natural Science 1, 142 (2009)

Sawa, Mater. Today 11, 28 (2008)

Schindler et al., IEEE Trans. Electron Dev. 54, 2762 (2007)

Shang et al., Physical Review B 73, 245427 (2006)

Shen et al., ChemPhysChem. 5, 16 (2004)

Sirringhaus et al., Science 290, 2123 (2000)

Song et al., AIP Conf. Proc. 1399, 855 (2011)

Strukov et al., Nature 453, 80 (2008)

Thurstans and Oxley, J Phys D 35, 802 (2002)

Verbakel et al., J. of Appl. Phys. 102, 083701 (2007)

Wang et al., IEEE Electron Device Lett. 32, 1442 (2011)

Wang et al., J. Phys. D 44, 475102 (2011)

Wang et al., Microelectron. Eng. 91, 144 (2012)

Wang et al., Microelectron. Eng. 88, 1628 (2011)

Waser and Aono, Nat. Mater. 6, 833 (2007)

Waser, Microelectronic Engineering 86, 1925 (2009)

Wu et al., Appl. Phys. Lett. 90, 183507 (2007)

Xu et al., Langmuir 20, 1021 (2004)

Yang et al., Nanotechnology 20, 215201 (2009)

Yoon et al., Appl. Phys. Lett. 87, 203506 (2005)

List of Related Publications

PUBLICATIONS (Journals):

- **ZrO_2 Flexible Printed Resistive (Memristive) Switch through Electrohydrodynamic Printing Process**
  Muhammad Naeem Awais, Hyung Chan Kim, Yang Hui Doh, and Kyung-Hyun Choi
  Thin Solid Films, Vol. 536, Page No. 308, 2013.
- **Resistive Switching in a Printed Nanolayer of Poly (4-vinylphenol) (PVP)**
  Muhammad Naeem Awais and Kyung-Hyun Choi
  Journal of Electronic Materials, Vol. 42, Page No. 1202, 2013.
- **Memristive Behavior in Electrohydrodynamic Atomized Layers of Poly[2-Methoxy-5-(2'-Ethylhexyloxy)-(P-Phenylenevinylene)] for Next Generation Printed Electronics**
  Muhammad Naeem Awais and Kyung-Hyun Choi
  Japanese Journal of Applied Physics, Vol. 52, Page No. 05DA05-1, 2013.
- **Investigation on switching behavior of ZrO_2 thin film for memory device applications**
  Kyung-hyun Choi, Navaneethan Duraisamy, **Muhammad Naeem Awais**, Nauman Malik Muhammad, Hyung-Chan Kim, and Jeongdai Jo
  Materials Science in Semiconductor Processing, 2013 (In Press).
  DOI: http://dx.doi.org/10.1016/j.mssp.2012.12.019
- **Fabrication of ZrO_2 Layer through Electrohydrodynamic Atomization for the Printed Resistive Switch (Memristor)**
  Muhammad Naeem Awais, Nauman M Muhammad, Navaneethan Duraisamy, Hyung Chan Kim, Jeongdai Jo, and Kyung-hyun Choi
  Microelectronic Engineering, Vol. 103, Page No. 167, 2013.
- **Versatile Resistive Switching (Memristive) Behavior in an ITO/ZrO_2/Ag Sandwich Fabricated Using Electrohydrodynamic Printing**

Kyung-Hyun Choi and **Muhammad Naeem Awais**

Journal of the Korean Physical Society, Vol. 61, No. 1, Page No. 119, 2012.

- **Electrospray Deposition of Graphene Oxide Thin Film, its characterization and investigation of its resistive switching performance**

  Maria Mustafa, **Muhammad Naeem Awais**, Ganeshthangaraj Poonia, and Kyung Hyun Choi

  Journal of the Korean Physical Society, Vol. 61, No. 3, Page No. 470, 2012.

- **Fabrication of high quality zinc-oxide layers through electrohydrodynamic atomization**

  Nauman Malik Muhammad, **Awais Muhammad Naeem**, Navaneethan Duraisamy, Dong-Soo Kim, and Kyung-Hyun Choi

  Thin Solid Films, Vol. 520, No. 6, Page No. 1751, 2012.

- **Resistive Switching and Current Conduction Mechanism in Full Organic Resistive Switch with the Sandwiched Structure of Poly(3,4-ethylenedioxythiophene):poly(styrenesulfonate)/Poly(4-vinylphenol)/Poly(3,4-ethylenedioxythiophene):poly(styrenesulfonate)**

  Muhammad Naeem Awais and Kyung-Hyun Choi

  Electronic Materials Letters (Under Review).

- **Resistive Switching Mechanism in the Printed Non-volatile Ag/ZrO_2/ITO Structures**

  Muhammad Naeem Awais, Yang Hui Doh, and Kyung-Hyun Choi

  (Under Review).

- **Negative Differential Resistive Switching in Poly(3,4-ethylenedioxythiophene):poly(styrenesulfonate) Thin Film through Electrohydrodynamic Atomization**

  Muhammad Naeem Awais, Jeong-Dai Jo, and Kyung-Hyun Choi

  Applied Physics A (Under Review).

PUBLICATIONS (Conferences/Workshops/Symposiums)

- **Flexible Memristor Fabrication for Printed Electronics**
  Kyung Hyun Choi, **Muhammad Naeem Awais**, Hyung Chan Kim, and Yang Hui Doh
  *International Conference Microelectronics and Plasma Technology (ICMAP) 201*2. Republic of Korea.
- **Cost-effective Printed Memristor Fabrication and Analysis**
  Kyung Hyun Choi, **Muhammad Naeem Awais**, Hyung Chan Kim, and Yang Hui Doh
  Cellular Nanoscale Networks and Their Applications (CNNA), 2012 13th International Workshop on Cellular Nanoscale Networks and their Applications, Turin, Italy, August 29-31 2012, Pages: 1-4.
- **Memristive Behavior in Electrohydrodynamic Atomized Layers of MEH:PPV for Next Generation Flexible Electronics**
  Kyung Hyun Choi, **Muhammad Naeem Awais**, and Yang Hui Doh
  The 2012 International Conference on Flexible and Printed Electronics (ICFPE2012), Tokyo, Japan.
- **Patterning of Ag Electrode for the Printed Memristor through Electrohydrodynamic Printing Technique**
  Muhammad Naeem Awais, Yang Hui Doh, Ki Rin Kwon, and Kyung Hyun Choi
  Korea Society of Manufacturing Systems 2011 Spring Conference, 2011.4, Page No. 209~210.
- **Deposition of Non-stoichiometric ZrO_2 Thin Film through Electrohydrodynamic Atomization**
  Muhammad Naeem Awais, Nauman Malik Muhammad, Duraisamy Navaneethan, Dong-Soo Kim, Hyung Chan Kim, and Kyung Hyun Choi
  NANO KOREA 2011 Symposium. Republic of Korea.